Appraising the Suitability of a Hybrid Piston for Internal Combustion Engines and its Fatigue Characteristics

A Thesis in Fulfilment of Master of Philosophy in Mechanical Engineering

By

Ugochukwu Gregory Unamka

Brunel University

Abstract

Automotive engine pistons are not normally expected to be made of plastics or even composites, but before now the latter have been applied to an Over Head Cam follower of an automotive engine. As such this research work sought to demonstrate that the composite Carbon fibre Phenolic composite of the grade used is suitable enough to be employed in a hybrid piston. This work covered three broad areas; Constitutive modelling, Optimization and Fatigue. Numerical/simulation and empirical methods were employed to accomplish the tasks involved. The design of the piston was presented and this design took into account the fact that a composite was involved. A contact analysis was carried out to analyse the stresses arising from the interference of the composite piston skirt and the aluminium cap just in case interference fit is adopted as the method of assembly. Empirical analyses of tubular carbon fibre composite samples as well as carbon fibre Phenolic composite prepregs were carried out to determine the tensile, compressive and flexural capabilities of the materials as the case may be. Young's and Shear modulus values as well Poisson's ratio values were deduced leading to the establishment of the constitutive model of the composite's lamina and consequently that of the laminate for the various samples that were deemed suitable based on the nature of their testing and preparation as well as a piston cap model. With the constitutive models worked out and the piston cap model developed, fatigue analysis of the structure and piston cap followed, and in other to get the best out of the structures or materials and the piston cap optimization followed after which yet more fatigue analysis was done for the optimization outcomes. To a great extent one of the Elastic Modulus values obtained empirically can be said to be sufficiently reliable as its empirical test was simulated numerically and it turned out satisfactory; the maximum stress value from the test was 158.5 MPa while that of the simulation was 158.267 MPa. All the results were almost the same apart from the strain values that were significantly divergent. The adopted Elastic Modulus value of 61049.6757 MPa stemmed from this empirical and numerical analyses and since these two differed only in the strain values and agreed in pretty much in all other the parameters it can be said that this adopted Elastic Modulus value was indeed sufficiently reliable. It also implies that the outcomes of all the other numerical analyses that were carried out with it can be trusted. In the Results and Discussion chapter numerical Crack Propagation was discussed for various crack lengths of a finite element model.

Chapter 1. Introduction/Background.

1.0. Introduction

Composites of varying combinations have been adopted for a wide range of application over the past fifty years up until now for the purpose of tapping the favourable properties of the individual components. The typical property combination is mechanical and chemical for the case of units that are hard and need chemical resistance.

Automotive engine pistons are largely made of conventional materials like steel and aluminium alloys, but a greater use of composites like carbon fibre Polyetheretherketone (PEEK) in recent times is becoming popular. PEEK is mostly used to make piston rings because of its wear characteristics and tribological properties as well. If a reciprocated mass like a piston weighs less it should lead to greater efficiency of the engine it operates in; employing composite materials on a broader scale like using it to form the skirt of a piston would lead to a reduced mass of the piston. So the background of this research is set around appraising the knowledge needed to model such a piston. The objective was to investigate the possibility of employing carbon fibre Phenolic composite in an automotive engine piston. In order to achieve this objective, this work employed carbon fibre Phenolic-composite and an aluminium alloy as the materials for the hybrid piston or the model. Phenolics of grade A or B are good for structural grade systems like the one in question, and possess good tack and drape, excellent high temperature properties, as well a good ablative characteristics, [1]. They are usually employed in aircraft structures, ducts, high temperature furnace chambers, and rocket nozzles. Cure and service temperatures are $325^{o}F$-$375^{o}F$ and $500^{o}F$ respectively, [1]. Composite structures possess great tensile and compressive strength and are the result of the combination of two materials or more to form a structure that has qualities the constituent materials lack. The material with the weakest strength, known as the matrix, is the binding material to the stronger one known as the reinforcement. In many cases the reinforcement is made of fibres. Careful selection of the reinforcement and the matrix as well as their processing or production processes can give manufacturers the opportunity of meeting requirements and specifications of their customers for various applications especially in low stress and high performance applications. Composites manufactured for the automotive

industry or automotive components are developed from non-continuous fibres and are largely for low stress applications, [2].

In general the key properties of a carbon fibre polymer matrix composite structure that can withstand very high temperatures can be found below:

- Low density of about 2.0 g/cm^3, (short, lightweight carbon fibres give a low density of between 1.35 g/cm^3 and 1.55 g/cm^3)
- Operating temperatures of up to 2000°C
- Thermal conductivity coefficient of about 80.5 x 10^{-6}/K,
- Young's modulus E_1 up to 400×10^3 N/mm^2 in the fibre directions,
- Tensile strength X_t up to 3.2×10^3 N/mm^2 in the fibre directions, [3].

Park et al [17] carried out endurance fatigue tests on the named composite in table: 1.1 below over 1.0×10^5 cycles and they found out that its "wear depth of surface" was the same over 6.0×10^5 cycles, with this performance it met their endurance life requirement hence its adoption in their work. They worked on a hybrid model using the two materials whose properties are defined in the tables: 1.1 and 1.2 below.

Mechanical Properties	AL6061 T6	Graphitized T300/AR120 PAN based carbon fibre–Phenolic woven composite
CTE ($\mu\epsilon$/°C), in plane	23.6 (20 °C)	0.8
CTE ($\mu\epsilon$/°C), out of plane	23.6	36
Young's modulus, E_{xx}, GPa	69	61.5
Ultimate tensile strength, MPa	607	417
Poisson's ratio, v_{xy}	0.33	0.34
Shear modulus, G_{xy}, MPa	25.9	19.2
Young's modulus, E_{zz}, GPa	69	14.3

Mechanical Properties	AL6061 T6	Graphitized T300/AR120 PAN based carbon fibre–Phenolic woven composite
Shear modulus, G_{xz}, MPa	25.9	3.35
Thermal Conductivity, W/mK		80.5
In-plane compressive strength, MPa		220
Tensile yield strength, MPa	270	
Operating Temperature		Up to 2000°C

Table: 1.1. Mechanical properties of the Composites and the Aluminium alloy [17].

Lay-up	PAN based		
	Polarized Polycarbonate –PZS	Polarized Polycarbonate - PCS	Polarized Polycarbonate - PQS
Mean, μ	807	842	897
Standard deviation, σ	34.6	33.9	24.5
Scale parameter, θ	822	857	908
Shape parameter, β	29.2	31.1	46.2

Table: 1.2. Parameters of Weibull distribution for composite specimens, S in the abbreviations above indicate that laminates have 12mm thicknesses (PZS ($[0]_{32}$), PCS ($[0/90]_{16}$), PQS ($[-45/0/45/90]_{4s}$).

On the other hand Phenolics in a general sense tend to absorb moisture and consequently swell, the reason being that they have polarised oxygen atoms. This swelling problem can lead to dimensional changes of the piston structure in question if the fluid (coolant or lubricant) contains moisture.

Furthermore this research work employed Ansys, a finite element code for the purpose of analysing the models. The verification of the analysis outcomes was against computed design figures and other established facts.

1.1. Piston Geometry
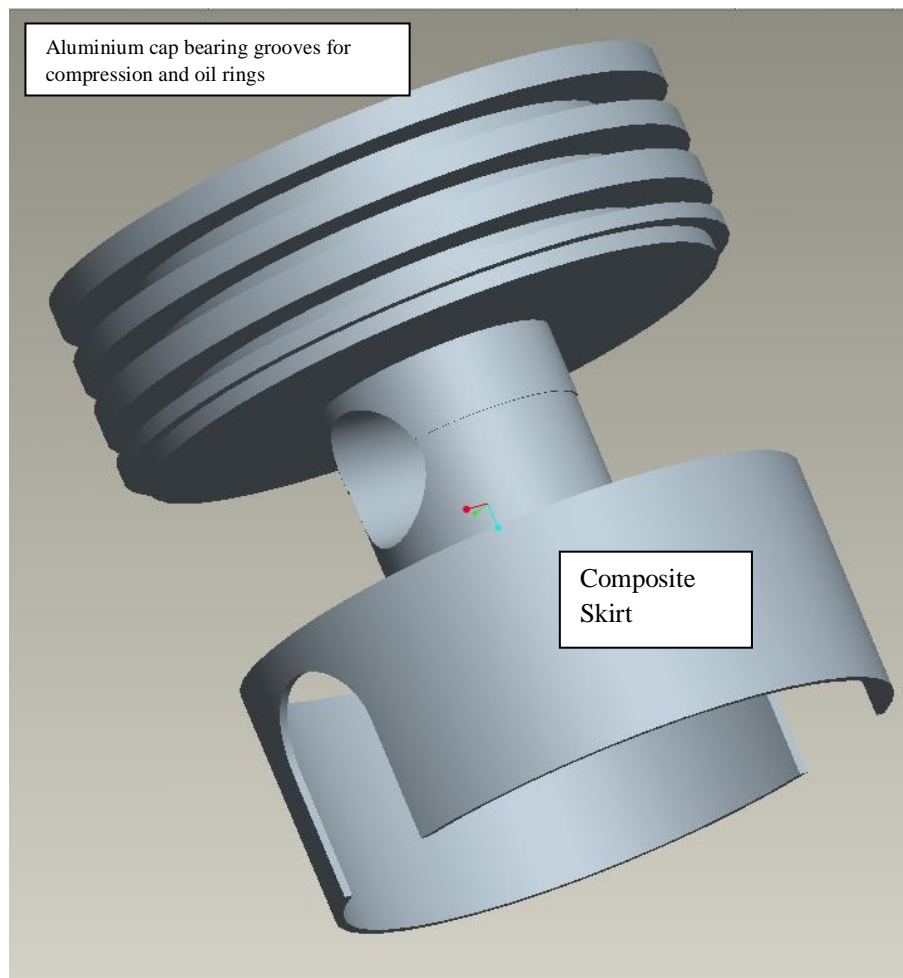
Fig 1.1. Piston Geometry

Pressure

Mandrel

Fabric

Piston Cap

Vacuum Bag
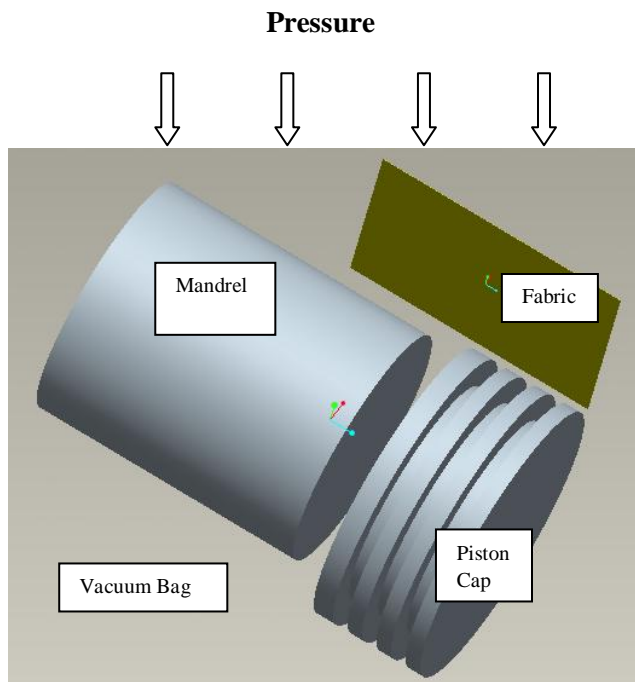
Fig: 1.2a. A pictorial description of the preparation of the hybrid piston

Figures 1.1 and 1.2a above show an attempt to describe a possible form this hybrid composite piston can take. In the fig: 1.1 we have a straight aluminium cap with grooves for the rings on it as well as a provision for the composite skirt to be interference fitted.

Fig: 1.2a shows how the hybrid composite can be fabricated in one piece. A fabric is stacked over the piston cap and the mandrel, and then the desired pressure and vacuum are applied and cured under the desired or required cycle. This co-curing process will produce a hybrid piston that is not interference fitted but co-cured from the composite and aluminium, see fig: 1.2b below. To achieve the figure below the cap with grooves on them is attached to a mandrel, and then the fabric is wrapped round them and pushed into the grooves and then cured. This would result in a hybrid piston that is in one piece. There are merits and demerits in adopting the interference fit or co-curing approaches to fabricate this hybrid piston.
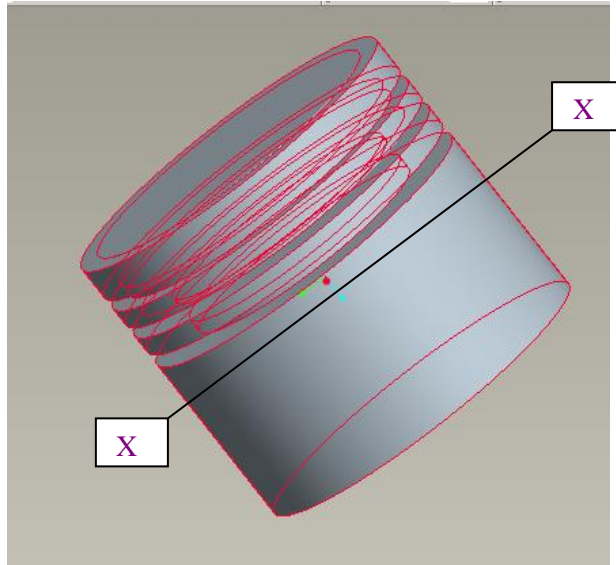
Fig: 1.2b. The picture shows the cross-section X-X where the piston crown ends and skirt begins.

Chapter 2. Literature Review.

2.0. Related Literature

In this chapter some literature are reviewed beginning with experimental papers followed by numerical ones. In some cases one can see the application of the mentioned composites in different components, in others their numerical analysis.

Lee and Lee (2005, p. 26-33) [14] in their paper described the development of an automotive engine hybrid valve lifter made of carbon fibre/Phenolic composite and steel to be employed in the valve of an engine. Effort was made to reduce the mass of the valve lifter so as to achieve better fuel efficiency. The design and manufacture of the composite hybrid valve lifter were equally investigated and addressed based on the operational requirements of the valve lifter. They carried out durability tests and these tests indicated that the hybrid valve lifter was sufficiently durable to undergo the test loads.

Carbon fibre/Phenolic composite was used to make the skirt of their valve lifter because of the good thermal and environmental resistance of the Phenolics matrix.

It is also the reason that the same has been selected for this work. Generally the two projects are about improved functionality (in the light of friction and more), cost, material optimization, and vehicle efficiency, but they differ in that one is about a piston while the other is about a valve lifter.

D. Park et .al (2006, p. 89-98) [18] experimentally investigated the friction and wear characteristics of Phenolic composites under dry sliding and oil lubricated conditions. They noted that the friction and wear characteristics of carbon fibre Phenolic composites are important because of the increasing use of the composite in journal bearing materials. The surface layers of their composite specimen were treated with "nano-sized particles" of carbon black and Polyetheretherketone (PEEK) powder to improve their wear characteristics. They chose the composite in question to work on their hemispherical bearing because of its compressive strength (about 900 MPa) which is larger than the maximum average bearing pressure (over three times this bearing pressure) required in the bushing where this composite would be used. So in effect they had three specimens of the treated composite i.e. the composite treated with carbon black, the composite treated with a mixture of carbon black and PEEK, and the composite without any treatment. The friction coefficients of the

specimens were measured with respect to sliding time, the specimen with carbon black turned out with the lowest coefficient of friction in the dry wear test where as the specimen with the carbon black and PEEK mixture had the lowest coefficient of friction in the oil-lubricated test. This case or work is cited because it makes the case for the use of carbon fibre Phenolics in high temperature sliding applications like in the case of the valve lifter and most of all the automotive pistons.

J. Flock et. al (1999, p. 304-311) [19] had earlier made a case for the use of the fibre in the composite in question, (though they did not exactly set out to do so) which is Polyacrilonitrile (PAN) carbon fibre in high temperature sliding applications. They asserted that high temperature composites have some advantages as regards friction and wear behaviour specifically mentioning PAN carbon fibre Polyetheretherketone (PEEK) composites and their use in journal bearings and piston rings. In essence they investigated friction and wear performance of PAN carbon fibres, pitch based carbon fibres against a 100Cr6 steel counterpart all in PEEK based composites. The pitched based carbon fibres proved to be more superior over the PAN carbon fibres in tribological tests but not as good as the latter at higher pressure. Though equally slightly better than the PAN carbon fibre composite at higher speeds, the fact that it is poor at higher pressure makes it a failed candidate for the work at hand. It has to be noted again that their composite is not carbon fibre Phenolics though its fibre is PAN.

W. S Kuo et. al (2002, p. 989-999) [22] examined three-dimensional carbon/carbon composites for their response under axial compression and transverse shear. In other to assess the failure behaviour they employed a 3D weaving technique, two types of preforms of different bundle sizes of the weaving yarns were used. The PAN based carbon fibre yarns were arranged orthogonally with interlacing loops on the outer surfaces and a Phenolic resin precursor was used to add the carbon matrix.
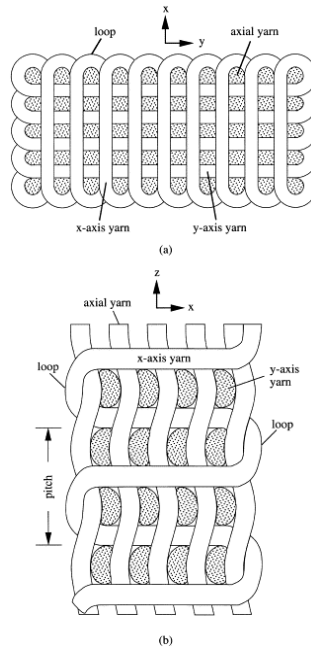
Fig 2.1. Illustration of the yarn structure in the preforms by W.S. Kuo et.al

In this work what is being proposed is a unidirectional 3D fibre yarns arrangement, with no interlacing loops. They are equally more or less woven as the fibre yarns crossover each other. In most of the work reviewed the authors usually do not provide illustrations of the composite structure, model or geometry, what is quite common is the description of the stacking sequence of the constituent laminates which usually is [0/90-0/90]$_s$. This means that the first laminate from the bottom has its principal direction in the zero direction or simply put its fibres are in the same direction as the laminate. The 90 means that the fibres of the following laminate has an angle of 90° lying between their x-axis and the x-axis of the laminate and so on. G. Pitarresi et.al (2005, p. 269-280) [27] discussed the influence of heterogeneity on the qualitative and quantitative determination of the thermo-elastic nature of fibre reinforced plastic composites. Experimental results at the macro scale performed on glass fibre-polyester resin samples were presented to further buttress how the thermo-elastic nature of the "fabric texture pattern and the surface pure resin layer" can be influenced. They then hypothesised that "the surface resin layer behaves as a strain witness towards the laminate" and derived a mathematical model to validate the hypothesis. A. Avila et.al (2005, p. 827-838) [28] pointed out that polymeric composites are largely manufactured by hand lay-up, because of the flexibility it affords. They went ahead to also note that the "mechanical properties are directly influenced by the stacking sequence, fibre volume fraction and morphology, as well as the cure process". They studied the manufacturing process of an E-

glass/epoxy plain weave fabric composite made by hand lay-up. They equally carried out stiffness and strength tests to ascertain the statistical differences caused by the cure processes as well as microscopic analysis to establish the "voids formation rate". In order to capture the rate of defects caused by the curing processes a coupling between macro and micro-mechanical analysis by a "non-dimensional coefficient" was employed. W. Sun et. al (2001, p. 289-299) [20] developed a modelling approach for designing CAD composite unit cells. Their technique was based on a Boolean operation algorithm which involved the "merging and extracting operations" to develop composite unit cells heterogeneously. Their CAD model was seamlessly integrated with their finite element analysis leading to stress and deformation outcomes in the composite unit cells as well as the fibre and matrix. They noted that their modelling technique is capable of capturing the geometry of the designed composite, reinforced fibre architecture and especially material heterogeneity. In the algorithm that actually embodies these operations of theirs, the (M_A)-dominant subtract operation cuts out the fibre element (B) from the matrix (A) to produce a matrix with some cavity, where as the fibre (M_B)-dominant intersect operation forms geometrically added fibre elements. Finally the fibre-dominant Boolean operation joins the matrix with the cavity with the subtracted fibre forming a heterogeneous composite unit cell. In other to model composites in ANSYS the geometry alone is not the crux of the modelling. To do so, the type of element has to be considered carefully as well as the layer configuration, and specified failure criteria. In ANSYS composites are treated as layered composites largely, and much of the illustration is on that basis. The various layers may be of different orthotropic materials as well as different principal direction orientations. It is the fibre directions in these laminates that actually determine the orientation of these laminated layers. To model layered composite materials SHELL99, SHELL91, SHELL181, SOLID46, and SOLID191 elements are available depending on the application and the type of desired results to be calculated. Of interest are the SHELL99, SOLID46, SOLID191 elements.

SHELL99	8-node, 3-D shell element.	Six degrees of freedom per node.	Up to 250 uniform thickness layers, with a side-to-thickness ratio of roughly 10 or greater

SOLID46	8-node, 3-D solid element.	Three degrees of freedom per node.	Up to 250 uniform thickness layers, with a side-to-thickness ratio less than 10.
SOLID191	20-node, 3-D solid element.	Three degrees of freedom per node.	Up to 100 layers per element.

Table: 2.1. Characteristics of the various element types used in analysing composites in ANSYS

In order to determine the state of these laminated layers after some load has been applied one has a choice of three predefined failure criteria or the choice of specifying up to six of these criteria. The predefined ones are Maximum Strain, Maximum Stress, and Tsai-Wu failure criteria. The first two allow up nine failure strains and stresses respectively, the last one also allows up to nine failure stresses but also has room for three coupling coefficients, Modelling Composites, Ch. 12, Ansys Release 9.0 Documentation [21]. P. Rosso and K. Váradi (2006, p. 3241-3253) [23] presented a finite element analysis of a transverse fibre bundle test (TFT) of carbon fibres embedded in a vinylester urethane hybrid matrix. They investigated the evolution of thermal residual stresses due to the cooling phase of the curing process of the model and the subsequent mechanical load transverse to the fibre direction. Using a displacement coupling technique they transferred the boundary conditions from a macro model through an intermediate model to a micro model. They could show that a significant fraction of the total stress that builds up just before failure occurs was as a result of the implicated thermal residual stresses. Detailed and more accurate stress distribution outcomes were obtained from the micro model. These stress distribution results were for areas like the fibre/matrix interface. Using the parabolic failure criterion the experimental data related to the pure matrix was employed to predict time and place of failure initiation. S. Casolo (2006, p. 475-496) [24] presented a macroscopic modelling of in-plane elastic behaviour of composite solids of regular orthotropic make up. Assertions were made that the effect of heterogeneity can be adopted at the macro level by homogenising along the line of a generalised continuum on which specific finite element codes are based. An approach involving a specific rigid element was then proposed as an alternative approach. The work goes further to present the theoretical relationship between the orthotropic Cosserat continuum and the proposed rigid elements. A comparison of the performance of the Cosserat

11

continuum and the rigid element model was carried out using some numerical analyses based on the calculation of their constitutive parameters. The impact of the concentrated load on the composite structure was equally demonstrated. The behaviour of the different materials at the macro-scale could be demonstrated by observing the influence on the strain field maps from the deformation of the vertical and horizontal joints which result from the rotation of the blocks. Pu Xue et.al (2005, p. 69-80) [25] noted that significant in-plane shear deformation and added anisotropy results from thermoforming woven composite panels. In an earlier work they had proposed a new constitutive model for characterizing macro-mechanically the behaviour of a non-orthogonal structure under large deformation. They now "developed a micro- and macro-constitutive model to predict the mechanical properties of woven composites during large deformation based on the microstructure of these composites, i.e., the dimensions of fibres, yarns and unit cell, the material properties of the composite constituents, as well as the orientation of yarns". The modelling approach began with a geometrical characterization of the yarn and the unit cell during a trellising shear deformation. Afterwards they carried a mechanistic analysis on a unit cell to determine the equivalent shear properties of woven composites used in their non-orthogonal model. Meanwhile, a simple and conventional analytical technique was applied to predict the tensile properties of woven composites. This proposed model according to them involving an analytical technique for predicting the tensile properties of woven composites was in agreement with their empirical data. In some kind of validation the models were used to investigate the influence of the geometrical parameters and the material properties on the shear properties of the plain weave composite. S. Nickerson et.al (2005, p. 1993-2008) [26] in their work stated that of great concern is the permeation paths for stored fluids in cryogenic tanks that develop as a result of matrix micro-cracking due to thermal loading. They determined the failure criteria at both the composite (macro-) and constituent (micro-) scale in a bid to determine the most potent analytical techniques for predicting composite damage. At the micro (constituent) scale the parameters were developed using a strain decomposition approach- the multi-continuum theory. J. Munoz et.al (2006, p. 1136-1146) [33] studied the drawbacks associated with using interface elements for fatigue driven delamination cases and proposed some improvements as it concerns the previous work they referenced. They observed some limitations with respect to two key parameters: the number of cycles per increment ΔN and element size Δl in their reference material mentioned above, and these parameters are pertinent to the computational cost of the numerical formulation. They noted that these two parameters are strongly linked in the sense that when a relatively large

interface element is employed the crack growth rate oscillates significantly. This is true as this is the case observed in this work as well as in their reference material. The numerical formulation from their reference material was extended to include cyclic loads with a non-zero minimum value. In the final analysis they proposed a simplification of the mixed mode fatigue driven delamination growth. In this definition the ΔD_f avoids the discontinuities in the definition of the stress-displacement relationship caused by the discontinuity of γ_c a component of the ΔD_f expression. Figiel and Kaminski (2003, p. 1865-1873) [34] presented a computational model of the delamination of a two-layer boron/epoxy–aluminium composite laminate subjected to cyclic loads, mechanical and thermal. The numerical fatigue delamination problem was solved using the linear elastic fracture mechanics theory through finite element method. The fatigue delamination growth was investigated and predicted by applying cyclic compressive shear and periodic temperature loads then plotted the numerical approximation of the curves representing stress and temperature variations against fatigue cycle number. This work is quite pertinent to this one because the finite element code employed-Ansys is common to both works. The geometry was quite simple hence tips were taken in modelling the geometry in this work. In all these experiments and simulations some of them were linear or nonlinear, elastic or elastic-plastic respectively as the case maybe. Linear Elastic Fracture Mechanics (LEFM) is said to treat the materials as isotropic and having linear elastic deformations. Going by this assumption, the stress fields near crack tips are estimated using the elasticity theory, and if the stresses around the crack tip area exceed the material fracture toughness, the crack will yield [35]. In Linear Elastic Fracture Mechanics, the available formulas are largely for plane stresses and plane strains, related with the three basic modes of loadings on a cracked body, which are opening, sliding, and tearing. If inelastic deformation is small compared to the size of the crack-small scale growth, then LEFM becomes a valid approach to analysing the problem. Large areas of plastic deformation may occur before the crack grows; Elastic Plastic Fracture Mechanics (EPFM) should be employed in such a case. The LEFM analysis can be described simply as follows:

The stress field near a crack tip depends on the location, the loading conditions, and the geometry of the sample or object; this is based on linear elasticity theories.

$$\sigma_{ij}^{Tip} \equiv \sigma_{ij}^{Tip}\left(Location, Loading, Geometry\right)$$
$$\equiv \sigma_{ij}^{Tip}\left(r, \theta, K\right)$$

r and θ are the location using the polar coordinate system and the loading and geometry terms can be sub-parameters of the parameter *K*, known as the *stress intensity factor*.

$$K \equiv K\left(\sigma^{Loading}, Geometry\right)$$

In actual sense the stress intensity factor *K* can be calculated with reference to the stress field at the crack tip and related with the established fracture toughness of the material for any possible disparity.

To obtain the fracture toughness of a material-normally material specific, experiments have to be carried out.

$$\sigma_{ij}^{Toughness} \equiv \sigma_{ij}^{Toughness}\left(Material\right)$$

In the case of fracture toughness the stress intensity of the material is known as the critical stress intensity factor K_c and material specific as well.

$$K_c \equiv K_c\left(Material\right)$$

The stress intensity factor *K* should be less than or must not exceed K_c.

$$K < K_c$$

Furthermore near the crack tip of an isotropic linear elastic material the stress fields can be expressed in terms of $1/\sqrt{r}$ and a function of θ and *K* the scaling factor as well the Stress Intensity Factor:
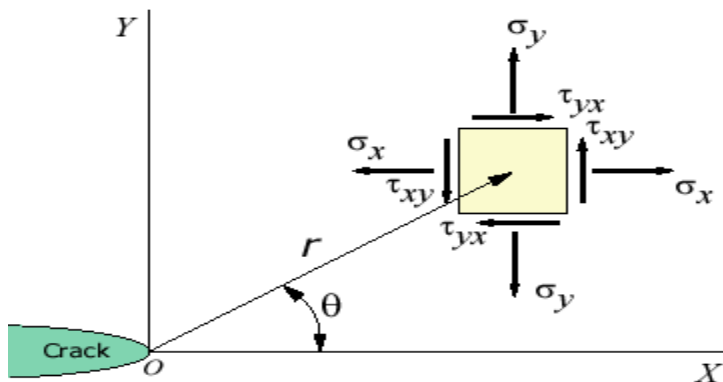

Fig. 2.2. Diagram expressing the crack tip singularity

$$\lim_{r \to 0} \sigma_{ij}^{(I)} = \frac{K_I}{\sqrt{2\pi r}} f_{ij}^{(I)}(\theta)$$

$$\lim_{r \to 0} \sigma_{ij}^{(II)} = \frac{K_{II}}{\sqrt{2\pi r}} f_{ij}^{(II)}(\theta)$$

$$\lim_{r \to 0} \sigma_{ij}^{(III)} = \frac{K_{III}}{\sqrt{2\pi r}} f_{ij}^{(III)}(\theta)$$

The three different mode loads can be applied to a crack and are denoted by the superscripts *I*, *II*, and *III*. In all these the maximum stress near the crack tip is of great concern to designers as they may not want it to exceed the fracture toughness. The stress intensity factor *K* is usually expressed in terms of the *applied stresses* σ at $r \to 0$ and $\theta = 0$ as a result of the foregoing equation. Therefore in simple terms the stress intensity factor on a through crack in a regular plate under uniform tension σ is:

$$K_I = \sigma\sqrt{\pi a}$$

a is the one half width of a through crack, as such the entire length is *2a.* In the work of Subramanian and Duncan tensile testing to establish some data for ASTM A285 steel necessary for fracture analysis of Type I and Type II high level waste tanks was carried out. They analyzed the tensile characteristics "as a function of chemical composition, micro-structural features, test temperature, and orientation" [37] as well as the microstructure around the crack tip of their material among other things. They have it that yield and ultimate tensile strength are affected by carbon content through the control of pearlite volume fraction-though not diverse enough in their tests to show significant effects as they said. Other materials that are part of the contaminants like manganese and sulphur affects the fore mentioned properties in different ways. Manganese has negligible effects where as increased sulphur content and temperature decreased them. They observed that the chemical composition had more effect on the J-R curve as against the tensile properties. Their stress-strain curves demonstrated upper and lower yield point phenomenon-Luder type behaviour-an expected behaviour. G. M. Odegard et. al (2003, p. 1671-1687) [38] developed a technique for constitutive models for polymer composite systems that are reinforced with single walled carbon nanotubes SWNT. They noted that the nanotubes are of the 'same size scale' with the polymer molecules and that their interaction at their interface depends greatly on bonding and

local molecular structure. They went further to state that because of the 'small length scales', the polymer chains and the lattice structures of the nanotubes are no longer regarded as continuous as a result the bulk mechanical properties can no longer be determined using the basic micromechanical continuum mechanics methods. Then they proposed and modelled an 'effective continuum fibre' comprising the nanotubes, the polymer immediately around the nanotubes, and the interface between the nanotubes and the polymer employing an 'equivalent continuum modelling' approach. According to them it also facilitates the incorporation of the analyses prediction approach of the bulk mechanical properties with that of different nanotubes orientations, concentrations, and lengths. Kuo and Fang (2000, p. 643-656) [42] processed a powder impregnated Nylon/carbon yarn and used compression moulding for the compaction of the composite. They used two types of fabrics in their work which were '3-axis orthogonal woven and two-step braided' fabrics [42]. The moulding thickness and moulding temperature were varying parameters in the processes and their variations were carried out to determine their "respective effects on the resulting properties'' [42]. The moulding according to them significantly distorted the through-thickness yarns of the woven fabric possibly because of the compression moulding that was employed. They used three point flexure tests to determine the properties of the materials. Their loading curves show non-linearity with the onset of damage; this is the portion of the curves that is wavy just after the linear portion no matter the inclination. They also indicated that one of the parameters noted above i.e. the moulding thickness has an influence on the flexural modulus and strength as well as the damage nature or "mode". They equally carried out microscopic observations to determine yarn geometries in these moulded composites and their damaged or fractured inner recesses. Xue et. al (2005, p. 69-80) [43] integrated a micro/macro constitutive model so as to determine to a great extent the nature of the mechanical properties of composites reinforced by woven fibres undergoing large deformation using the micro-structure of the composite as a basis. They analysed a unit cell to determine shear properties in a non-orthogonal composite or model as well as the yarn and the unit cell "during trellising shear deformation" [43]. At the same time the tensile properties were determined using conventional methods. They verified their assertions against experimental and finite element results and also conducted a parametric study using the determined model. The study was to establish the influence of the "geometrical parameters and material properties" of the composite constituents on the shear properties of a composite with a plain weave reinforcement. The mechanical properties according to them are:

- "Dimensions of fibres
- Yarns and unit cell
- The material properties of the composites constituents
- The yarn orientations" [43].

In their description of the geometry of plain weave architecture with the aid of the diagram below, they described y_1 and y_2 as the top and bottom sinusoidal paths of the warp yarn respectively and y_3 and y_4 as the top and bottom segments of the two weft yarns. It is not clear if these parameters are lengths or points on the model or not. Assuming that y_1 to y_4 is a path and y_2 to y_3 a segment they are s and $w/2$ respectively, as such having them as undetermined variables in equations does not make them any simpler since they can just be substituted with their equivalents s and $w/2$ mentioned above. They went on to say that the size of the value of the expression below can be used to "measure fabric tightness" [43]. The expression is based on the diagram below.

$$\text{Fabric tightness} = \ [(s-w)/s_1]$$

On a closer look it should not be that the tightness stemming from *s-w* is expressed as a fraction of s_1. *s-w* talks about the gap that is right at the middle of the wave length and as one can imagine if a wide gap exists between the wefts the fabric would not be considered very tight.
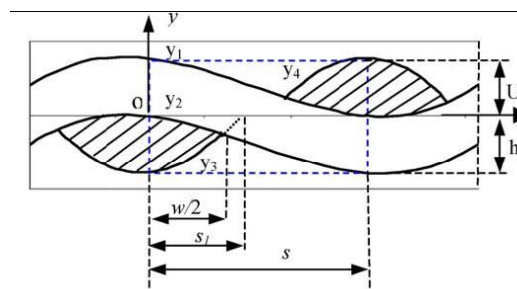

Fig 2.3. Diagram of the representative volume element describing the weft and wavelength of the yarn in work of Xue et. al (2005, p. 69-80) [43].

Kumar et al (2005, p. 66-70) [4] in their work thermo-structural analysis of composite structures carried out "thermo-structural analyses of passive and active hot composite structures considering temperature dependent material properties under thermal and mechanical loads as well as the behaviour of the composite material under thermal, thermo-

chemical and mechanical loads", Kumar et al (2005, p. 66-70). They went on to say that Thermo-structural analysis proves that thermal induced stresses are by far more prominent when compared to stresses due to mechanical loads. Further more in their discussion they noted that "Phenolic resin based bi-directional silica cloth" is the most commonly used composite material for hot structures for the regulation of the exterior wall temperature of nozzle backup structures, Kumar et al (2005, p. 66-70). According to them, a Phenolic composite gets charred once its surface temperature exceeds 700 K and also that the ablation temperature of the carbon Phenolic is 2200 K amongst other things. Their analyses in one case varied some temperature dependent mechanical properties, "modulus, strength and coefficient of thermal expansion along fibre directions with respect to temperature" for the materials Carbon Phenolic, Silica Phenolic and carbon–carbon composites. The tensile strength of Silica Phenolic drops by 80% at the point charring begins when compared to room temperature properties where as for Carbon Phenolic composites it reduces by 66% only. On the contrary according to them, carbon–carbon composite had some increase in strength at heightened temperatures. Silica Phenolic composite had its modulus reduced to about 66% of its value at room temperature and then continues at a faster rate at temperatures higher than 1400 K. The properties of Carbon-Carbon composite "can be treated as constant even up to the elevated temperatures of 2500 K". They have it that the coefficient of thermal expansion (α) for the Silica Phenolic is raised up to 700 K then drops "monotonically when charring starts at that 700 K". That of Carbon Phenolic fluctuated with the increase in temperature. That of Carbon-Carbon depends on the composite make up and room temperature, it fluctuates between negative to positive at heightened temperatures. In another analysis they have it that "a major input data in a thermo-structural analysis is the temperature distribution throughout the structure and its variation with time for the entire range of operation". And they obtained the distribution by carrying out a heat transfer analysis. They also carried out a thermo-structural analysis for thermal loads generated through transient heat transfer and thermo-mechanical loads, Kumar et al (2005, p. 66-70).

Chapter 3

3.0. Methodology.

An extensive review of literature was carried out as can be seen in the chapter above. This work lies in three broad areas: Constitutive modelling, Optimization and Fatigue. To accomplish the task involved in these areas, numerical/simulation and empirical methods were employed. Over the years of this research work, finite element analyses were carried out on various finite element models to determine the various stresses and strains, initially the mechanical properties used in these analyses were those in table:1 from the work of Park et. al [17]. In later stages Monte Carlo simulations were also used on Microsoft Excel to do some of the 'What If' simulations, the Solver application was used in solving the Optimization problems also on Microsoft Excel. The empirical data obtained from the experiments in a bid to determine the constitutive model as well as the fatigue limits were also analysed on Excel. In the first section below the methodology used to determine the Piston cap characteristics is presented and in the subsequent ones the relevant methodologies used are described.

3.1. Description of Specimen's Mechanical Properties and Functional Requirements.

The piston is expected to be a hybrid one made of <u>aluminium alloy AL6061 T6</u> for the piston crown and <u>PAN based carbon fibre–Phenolic woven composite</u> for the skirt. Their respective coefficients of thermal expansion are:

$$\alpha_{pc} = 23.6 \text{ X } 10^{-6} \text{ 1/K} - \text{piston crown}$$

$$\alpha_{ps\text{-}in} = 0.8 \text{ X } 10^{-6} \text{ 1/K- piston skirt-in-plane,}$$

$$\alpha_{ps\text{-}out} = 36 \text{ X } 10^{-6} \text{ 1/K- piston skirt out of plane;}$$

Since the cylinder or sleeve is made of the same material with the piston crown.

$$\alpha_{cyl} = 23.6 \text{ X } 10^{-6} \text{ 1/K}$$

The bending stress in the piston crown σ_b is

$$\sigma_b = p_{za} (r_i/\delta)^2 \quad (1)$$

Where

$$r_i = D/2 - (s + t + \Delta t) \quad (2)$$

If the piston crown is to be reinforced by stiffening ribs, therefore the compression stress at the cross-section x-x (see fig: 1.2b) where the piston crown ends and the skirt begins is

$$\sigma_{com} = P_{za}/F_{x-x} \quad (3)$$

$$P_{za} = p_{za} F_p \quad (4)$$

$$F_{x-x} = (\pi /4) (d^2_g - d^2_i) - n'_o F' \quad (5)$$

$$d_g = D - 2 (t + \Delta t) \quad (6)$$

$$F' = (d_g - d_i) d_o/2 \quad (7)$$

The rupture stress at the above named section is: the maximum angular velocity in idling given as:

$$\acute{\omega}_{id\ max} = \pi n_{id\ max}/30 \quad (8)$$

The mass of the piston crown with rings arranged above the named section is given as

$$m_{x-x} = 0.5 m_p \quad (9)$$

The maximum rupture force is given as

$$P_j = m_{x-x} R \acute{\omega}^2_{id\ max} (1 + \lambda) \quad (10)$$

The rupture force is given as

$$\sigma_r = Pj/F_{x-x} \quad (11)$$

The stress in top ring land comprise of:

Shear stress is given as

$$\tau = 0.0314\ p_{za}\ D/h_l \quad (12)$$

The bending stress is given as

$$\sigma_b = 0.0045 p_{za} \, (D/h_l)^2 \quad (13)$$

The combined stress is

$$\sigma_\Sigma = \sqrt{\sigma_b^2 + 4\tau^2} \qquad (14)$$

Piston specific pressure exerted on the cylinder wall:

$$q_1 = N_{max} / (h_s D) \qquad (15)$$

$$q_2 = N_{max} / (HD) \qquad (16)$$

The piston crown and skirt diameters is given as

$$D_c = D - \Delta_c \qquad (17)$$

$$D_s = D - \Delta_s \qquad (18)$$

Where Δ_c is given as

$$\Delta_c = 0.007D \qquad (19)$$

$$\Delta_s = 0.002D \qquad (20)$$

Diameter clearances in the hot state of the piston crown and cylinder or sleeve as the case may be if the engine is water cooled

$$\Delta'_c = D \, [1 + \alpha_{cyl} \, (T_{cyl} - T_0)] - D_c \, [1 + \alpha_p \, (T_c - T_0)]. \quad (21)$$

$$\Delta'_s = D \, [1 + \alpha_{cyl} \, (T_{cyl} - T_0)] - D_s \, [1 + \alpha_p \, (T_s - T_0)]. \quad (22)$$

3.2. Geometric Modelling.

The Geometries or models were created using Pro Engineer Wildfire as well as ANSYS as the case may be. In the case of those that were created with Pro Engineer they were saved as IGES files choosing the options shells and solids. The Geometries in the Pro Engineer cases were represented wholly; no parts were removed, as they were not very complex ones, in other words they were macro models.

3.3. Element Type.

The Element type that was broadly used in the various analyses is the type is Solid-46 or Brick 8-Node

Element Name	Number of Nodes and Element type	Degrees of Freedom	Thickness description
Solid-46 or Layered 46-Node.	8-node, 3-D solid element.	Three degrees of freedom per node.	Up to 250 uniform thickness layers, with a side-to-thickness ratio less than 10.

Table: 3.1. Description of the Element type broadly used in the analyses in this work, Modelling Composites, Ch. 12, Ansys Release 9.0 Documentation [21].

Programmatically the element type can be specified using the code:

```
/PREP7

!*

ET,1,SOLID45                    | Select First Element Type: Solid45
```

3.4. Material Properties Used.

The Material Properties used are Mechanical/Static and Thermal properties in the same analysis or just the former as the case may be. The steps or Graphic User Interface path goes thus depending on the version of ANSYS being used:

Main Menu > Pre-processor > Material Properties > Material Models > Structural > Linear > Elastic > Isotropic OR Orthotropic

In the window that appears, the Mechanical Properties of the Material is entered against the fields below as the case may be:

    i.   Young's Modulus EX:
    ii.   Young's Modulus EY:
    iii.   Young's Modulus EZ:
    iv.   Poisson's Ratio PRXY:
    v.   Poisson's Ratio PRYZ:
    vi.   Poisson's Ratio PRXZ:

<ol type="i" start="7">
Shear Modulus GXY:
Shear Modulus GYZ:
Shear Modulus GXZ:

In the validation of the tensile test results obtained empirically only EX and PRXY values were used in the analyses. This is so because these validations were carried out in order to replicate numerically what was done empirically; and in those experiments out of plane and share loads were not applied. For the rest of the other properties the GUI path is:

Main Menu > Pre-processor > Material Properties > Material Models > Structural > Thermal Expansion Coefficient > Orthotropic

<ol type="i">
ALPX:

Main Menu > Pre-processor > Material Properties > Material Models > Thermal > Conductivity > Orthotropic

In the window that appears, the Mechanical Property of the Material is entered against the field.

<ol type="i" start="2">
KXX:

Main Menu > Pre-processor > Material Properties > Material Models > Structural > Linear > Density

<ol type="i" start="3">
DENS:

Programmatically the material property can be entered using the code:

```
MPTEMP,1,0                      | Select Material Properties for First Element

MPDATA,EX,1,,x                  | Enter EX Value

MPDATA,EY,1,,x                  | Enter EY Value

MPDATA,EZ,1,,x                  | Enter EZ Value

MPDATA,PRXY,1,,x                | Enter Poisson's Ratio PRXY Value

MPDATA,PRYZ,1,,x                | Enter Poisson's Ratio PRYZ Value

MPDATA,PRXZ,1,,x                | Enter Poisson's Ratio PRXZ Value

MPTEMP,,,,,,,,

MPTEMP,1,0                      | Select Material Properties for First Element
```

```
MPDATA,DENS,1,,x            | Enter Density DENS Value
```

The code above was used to specify the material properties of a composite orthotropically if it has to be isotropic then the code below follows:

```
MPTEMP,1,0

MPDATA,EX,1,,x

MPDATA,PRXY,1,,x

MPTEMP,,,,,,,,

MPTEMP,1,0

MPDATA,DENS,1,,x
```

3.5. Finite Element Model description (Meshing).

Information derived from first principles or from calculation was used to develop three-dimensional models using ANSYS and in some cases Pro-Engineer Wild Fire. The models created in Pro Engineer Wild Fire once imported into ANSYS the 3-D model gets reformed into an Isotropic or Orthotropic Linear model. The Meshing Status varied from one analysis to the other depending on the model in question. In the next chapter that follows the details involved in each mesh case is discussed. Hexahedral/ Wedge and tetrahedral 3D elements were used to mesh the models in most cases; in the latter cases the use of the former was the case. Programmatically the model can be meshed with varying codes one of which is:

```
ESIZE,1,0,                  | Enter Element Size

MSHAPE,1,3D                 | Select Mesh Type

MSHKEY,0

!*

CM,_Y,VOLU

VSEL, , , ,      1          | Select Volume

CM,_Y1,VOLU

CHKMSH,'VOLU'               | Check Meshed volume

CMSEL,S,_Y
```

```
!*

VMESH,_Y1

!*
```

3.6. Boundary Conditions.

This is a condition that has to be met at all parts of the boundary of an area where appropriate differential equations are expected to provide the behaviour of the desired solution. It can also be the physical conditions that were employed or inherent in an empirical test situation or a related case that has to be simulated. Boundary conditions are usually attributes of one or more degrees of freedom (DOF). The nature of the unknown (physical meaning) is fully defined by the related DOF, to which the particular Boundary Condition is associated [45]. In simple terms this is about how the model was restrained. To get the boundary conditions set on the model the GUI path is:

Main Menu > Solution > Define Loads > Apply > Structural > DOF > On Lines or On Area or On Volumes.

Pick all the Lines or Areas or Volumes that are required as the case may be. The exact details of the DOFs can be found in the next chapter for the respective analysis case. Programmatically the model's boundary conditions can be specified thus:

```
/SOL          | Select Solution Processing

!*

/GO

DA,P51X,UZ,x   |Apply Degree of Freedom-DOF in the Z-Direction, Enter Value

FLST,2,2,5,ORDE,2

FITEM,2,x

FITEM,2,-x

!*

/GO

DA,P51X,UX,x   |Apply Degree of Freedom-DOF in the X-Direction, Enter Value

FLST,2,2,5,ORDE,2
```

```
FITEM,2,x

FITEM,2,-x

!*

/GO

DA,P51X,UY,x    |Apply Degree of Freedom-DOF in the Y-Direction, Enter Value

FLST,2,4,5,ORDE,2

FITEM,2,x

FITEM,2,-x

!*

!*
```

3.7. Loading.

Depending on the model and the objective of the analysis in question loads can be applied on lines, areas and volumes. There may also be a need to apply loads in a specified direction like Z, Y or X as in the experiment validation cases. Loads can be structural (Force, Pressure or Moment) or thermal (Temperature). The GUI path is:

Main Menu > Solution > Define Loads > Apply > Structural or Thermal> Force or Pressure or Temperature > On Lines or On Area or On Volumes. Programmatically the load can be applied thus:

```
/SOL

/GO

F,P51X,FZ,x       |Apply Load in the Z-Direction and Enter Value
```

3.8. Analysis Procedure.

Generally in most of the analysis carried out in this work the analysis procedure began with determining the approximate solution to the problem that was entered. In Ansys these problems that need to be solved are formed into partial differential equations or integral ones. In doing so one can specify the number of steps and sub-steps or let it run iteratively. In the latter the equations are solved continuously until a convergence point is found and it begins with an approximation of the solution. The Gaussian, Euler and Runge-Kutta methods are

some of the methods used to integrate the partial differential equations that were not eliminated. Much of the analyses in this work were steady state analysis and in such cases the partial differential equations were eliminated completely.

3.9. Simulation Cases.

In all the simulation cases as it concerns Finite Element Simulations mostly force was varied against displacement and the element edge lengths and types varied widely.

3.10. Experimental Methodology

The initial tensile experimental tests were carried out on roll wrapped tubular carbon fibre composite samples whose external diameter was 5mm and wall thickness 0.5mm and the latter ones were on carbon fibre Phenolic prepregs or fabrics. The tests were carried out to determine the Elastic Modulus, Maximum Stress, Maximum Strain and Maximum sustainable Force values of the samples so that all the other properties can be derived from them. At the point the tubular sample were being used in the experiments the prepregs were not easy to come about, so their tests served as a preparation for further and more relevant tests. The apparatus was an Instron series 9 test rig, see Fig: 3.1 below and in order to carry out the test first of all the program has to be set out on the remote controlled unit- a computer unit- this involved entering the dimensions of the samples and their nature (tubular or flat), the loading speed, scale of the graph to be plotted, humidity, room temperature and more.

Fig: 3.1. Instron series 9 test rig.

After all these the well gripped sample (see Fig: 3.2 and Fig: 3.3 below) is strapped with a device that acquires the elastic modulus of the material-the extensometer, this modulus is dependent on the maximum load or force attained which in turn depends on the time the failure occurs. The time the failure occurs most certainly depends on the strength of the adhesive. This is so because once the adhesive as was the case of the tubular samples fails the load fails to reach or exceed its peak. The adhesive was used to hold the plugs in place so that the tubular samples can be gripped. These tubular samples were really difficult to grip as a result of that varying gripping methods were tried like passing a crosspin through the inserted plugs and in another case split collars were used and kept in place with slip rings and unthreaded bolts.

Fig: 4.7. Roll wrapped carbon fibre composite with mild steel plugs at both ends. It is important to note that the plugs are held in place by some adhesive.

Fig: 4.8. The sample fitted with grips at both ends. The grips are actually split collars that are kept in place by slip rings and unthreaded bolts. See the holes for the bolts.

In these tests the load which was force was varied against displacement and the results that were recorded were then used to derive the constitutive model, and consequently used in solving the optimization as well as in the fatigue analysis.

Chapter 4

4.0. Analysis.

4.1. Design of a petrol engine piston

The equations used in determining the following data was obtained by Kolchin A and Demidov V [32] on the basis of their heat analysis data, speed characteristics and dynamic analyses assumed to be in compliance with existing engines.

Cylinder diameter D	78 mm
Piston stroke S	78 mm
Actual maximum pressure of combustion p_{za} at $n_N = 3200$ rpm,	6.195 MPa
Piston area F_p	477.6 mm^2
Maximum rated force N_{max} at $\varphi = 370^o$	0.0044 MN
Mass of piston group m_p	478 g
Engine speed in idling $n_{id\ max}$	6000 rpm
λ	0.285
Piston crown thickness δ	7.5 mm
Piston height H	88 mm
Piston skirt height h_s	58 mm
Ring radial thickness t	3.5 mm
Ring radial clearance in the piston grove Δt	0.8 mm
Piston crown wall thickness s	5 mm
Top ring land height h_l	3.5 mm
Number of oil passages in the piston n'_o	10

Diameter of oil passages in the piston d_o	1 mm

Table: 4.1. Piston and Engine parameters based on the work of Kolchin A and Demidov V [32]

The piston was a hybrid one made of <u>aluminium alloy AL6061 T6</u> for the piston crown and <u>Graphitized T300/AR120 PAN based carbon fibre–Phenolic woven composite</u> for the skirt, though in the empirical analysis what was analysed was <u>Sigratex Prepreg CP 8014-225-48 PAN based carbon fibre-Phenolic woven composite.</u> Their respective coefficients of thermal expansion were:

$$\alpha_{pc} = 23.6 \text{ X } 10^{-6} \text{ 1/K} - \text{piston crown}$$

$$\alpha_{ps\text{-}in} = 0.8 \text{ X } 10^{-6} \text{ 1/K- piston skirt-in-plane,}$$

$$\alpha_{ps\text{-}out} = 36 \text{ X } 10^{-6} \text{ 1/K- piston skirt out of plane;}$$

Since the cylinder or sleeve is made of the same material with the piston crown.

$$\alpha_{cyl} = 23.6 \text{ X } 10^{-6} \text{ 1/K}$$

The bending stress in the piston crown σ_b is

$$\sigma_b = p_{za} \left(r_i/\delta \right)^2 \quad (1)$$

$$6.195 \ (29.7/7.5)^2 = 97.1 \text{ MPa.}$$

Where

$$r_i = D/2 - (s + t + \Delta t) = 78/2 - (5 + 3.5 + 0.8) = 29.7 \text{ mm. (2)}$$
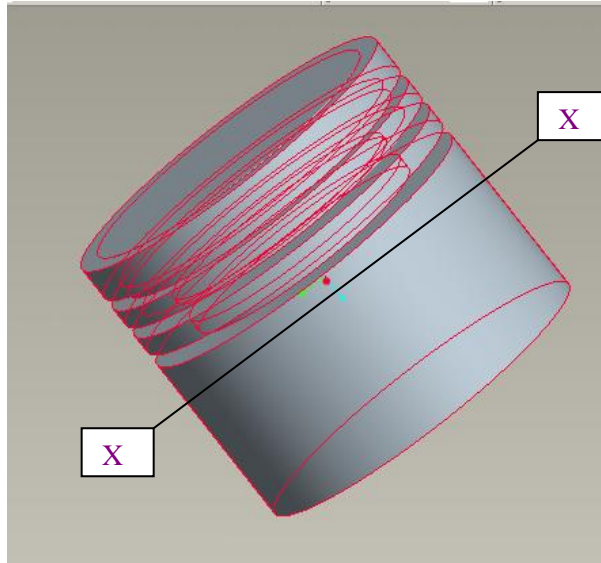
Fig: 4.1a. The picture shows the cross-section X-X where the piston crown ends and skirt begins.

If the piston crown is to be reinforced by stiffening ribs, therefore the compression stress at the cross-section X-X (see fig: 4.1a) where the piston crown ends and the skirt begins is

$$\sigma_{com} = P_{za}/F_{x\text{-}x} \quad (3)$$

$$0.0296/0.00096 = 30.8 \text{ MPa.}$$

Where force at the cross-section X-X is:

$$P_{za} = p_{za}\,F_{p} \qquad (4)$$

$$6.195 \text{ X } 47.76 \text{ X } 10^{-4} = 0.0296 \text{ MN;}$$

$$F_{x\text{-}x} = (\pi/4)\,(d^{2}{}_{g} - d^{2}{}_{i}) - n'{}_{o}F' \quad (5) \text{ --------------}$$

$$= [(3.14/4)\,(69.4^{2} - 59.4^{2}) - 10 \text{ X } 5] \text{ X } 10^{-6} = 0.00096 \text{ m}^{2}; \text{-------------}$$

$$d_{g} = D - 2\,(t + \Delta t) \quad (6) \text{ ----------------------}$$

$$78 - 2 = (3.5 + 0.8) = 69.4 \text{ mm;} \text{ ------------------------}$$

$$F' = (d_{g} - d_{i})\,d_{o}/2 \quad (7) \text{ ------------------}$$

$$(69.4 - 59.4)\,\tfrac{1}{2} = 5 \text{ mm}^{2}$$

The rupture stress at the above named section is: the maximum angular velocity in idling given as

$$\acute{\omega}_{id\ max} = \pi n_{id\ max}/30 \quad (8)$$

3.14 X 6000/30 = 628 rad/s.

The mass of the piston crown with rings arranged above the named section is given as

$$m_{x\text{-}x} = 0.5m_p \quad (9)$$

0.5 X 0.478 = 0.239 Kg.

The maximum rupture force is given as

$$P_j = m_{x\text{-}x}R\acute{\omega}^2_{id\ max}\ (1 + \lambda) \quad (10)$$

$0.239 \times 0.039 \times 628^2\ (1 + 0.285)\ 10^{-6} = 0.0047$ MN

The rupture stress is given as

$$\sigma_r = Pj/F_{x\text{-}x} \quad (11)$$

0.0047/0.00096 = 4.9 MPa.

The stress in the top ring land:

Shear stress is given as

$$\tau = 0.0314\ p_{za}\ D/h_l \quad (12)$$

0.0314 X 6.195 X 78/3.5 = 4.34 MPa

The bending stress is given as

$$\sigma_b = 0.0045p_{za}\ (D/h_l)^2 \quad (13)$$

0.0045 X 6.195 $(78/3.5)^2$ = 13.88 MPa

The combined Stress is

$$\sigma_\Sigma = \sqrt{\sigma_b^2 + 4\tau^2} \quad (14)$$

$$= \sqrt{13.88^2 + 4 \times 4.34^2} = 16.4 MPa$$

Piston specific pressure exerted on the cylinder wall:

$$q_1 = N_{max}/ (h_s D) = 0.0044/ (0.058 \text{ X } 0.078) = 0.97 \text{ MPa.} \quad (15)$$

$$q_2 = N_{max}/ (HD) = 0.0044/ (0.088 \text{ X } 0.078) = 0.64 \text{ MPa.} \quad (16)$$

The piston crown and skirt diameters is given as

$$D_c = D - \Delta_c = 78 - 0.55 = 77.45 \text{ mm} \quad (17)$$

$$D_s = D - \Delta_s = 78 - 0.156 = 77.844 \text{ mm} \quad (18)$$

Where diameter clearance of the piston crown-Δ_c is given as

$$\Delta_c = 0.007D = 0.007 \text{ X } 78 = 0.55 \text{ mm;} \quad (19)$$

And diameter clearance of the piston skirt-Δ_s is given as

$$\Delta_s = 0.002D = 0.002 \text{ X } 78 = 0.156 \text{ mm.} \quad (20)$$

Diameter clearances in the hot state of the piston and cylinder or sleeve as the case may be if the engine is water cooled.

$$\Delta'_c = D \left[1 + \alpha_{cyl} (T_{cyl} - T_0)\right] - D_c \left[1 + \alpha_p (T_c - T_0)\right]. \quad (21)$$

$$\Delta'_s = D \left[1 + \alpha_{cyl} (T_{cyl} - T_0)\right] - D_s \left[1 + \alpha_p (T_s - T_0)\right]. \quad (22)$$

$$T_{cyl} = 383 \text{ K}, T_c = 593 \text{ K}, T_s = 413 \text{ K}, T_0 = 293 \text{ K}$$

In this hybrid piston the Carbon fibre Phenolic composite has a greater coefficient of expansion than the aluminium alloy because of this difference the latter would have some more induced stress. Consequently a net coefficient of thermal expansion would result for the out of plane case if the composite is positioned such that the out of plane direction is parallel to the sleeve or cylinder, which is

$$\alpha_{p\text{-}out} = 36 \text{ X } 10^{-6} \text{ 1/K} - 23.6 \text{ X } 10^{-6} \text{ 1/K} = 12.4 \text{ X } 10^{-6} \text{ 1/K.} \quad (23)$$

The in-plane case is

$$\alpha_{p\text{-}in} = 23.6 \text{ X } 10^{-6} \text{ 1/K} - 0.8 \text{ X } 10^{-6} \text{ 1/K} = 22.8 \text{ X } 10^{-6} \text{ 1/K.} \quad (24)$$

Hence

$\Delta'_{\text{c-in-plane}}$ = 78 [1 + 23.6 X 10^{-6} (383 – 293)] – 77.45 [1+ 22.8 X 10^{-6} (593 – 293)] = 0.1859mm.   (25)

$\Delta'_{\text{s-in-plane}}$ = 78 [1 + 23.6 X 10^{-6} (383 – 293)] – 77.844 [1+ 22.8 X 10^{-6} (413 – 293)] = 0.1087 mm.   (26)

$\Delta'_{\text{c-out of plane}}$ = 78 [1 + 23.6 X 10^{-6} (383 – 293)] – 77.45 [1+ 12.4 X 10^{-6} (593 – 293)] = 0.4276mm.   (27)

$\Delta'_{\text{s-out of plane}}$ = 78 [1 + 23.6 X 10^{-6} (383 – 293)] – 77.844 [1+ 12.4 X 10^{-6} (413 – 293)] = 0.2058 mm.   (28)

4.2. Contact Analysis

In this section, a macro contact analysis of the composite and the aluminium alloy is described using two cylindrical representative volume elements, see Fig: 4.1b below. This sought to illustrate the nature of the interference between the Aluminium alloy and Carbon fibre Phenolic composite as the former expands and cools faster than the composite. The applied load of 210°c is the most attainable temperature at the hottest part of the piston which is the cap area or region; see that there is also the skirt area that extends the most. The inner most cylinder represents the Aluminium alloy and the outer most Carbon fibre Phenolic composite. These volumes were not added, this is not normally the case with pistons or exactly the desired approach. The element types are Brick 8 node Solid-45 and Layered Solid-46, the former was used to define the cylinder that represent the Aluminium alloy though the most appropriate would have been Brick 20 node Solid-95, Layered Solid-46 was used to define the cylinder that represents the composite.
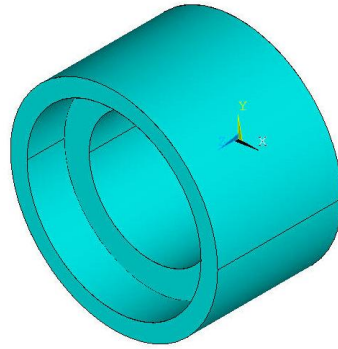
Fig: 4.1b. Two cylindrical representative volume elements that served as the hybrid piston.

In the figure above a load of $210^{\circ}c$ was applied on the external walls of the model which is normally the areas that such a temperature load is most prominent. Lee and Lee [14] have it that the stresses developed by the interference fit is highly localised at the contact interface. This is evident as shown, the maximum Z-component stress occurred at this said interface.
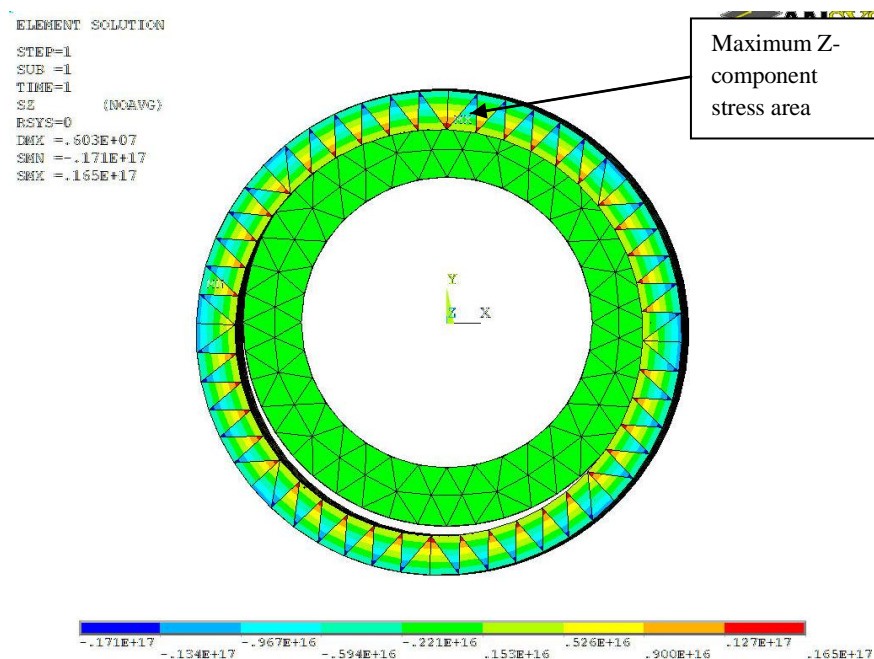

Fig: 4.2. Element solution contour plot of Maximum Z-component stress, whose value is 0.165e+17 Pa, see also that it occurred at the interface region. Notice a very tiny spot of red in the direction of the arrow.

Fig: 4.2 above is the element solution contour plots of the maximum stress of the Z-component. According to Lee and Lee [14] $\sigma_3 = -p_c$, where p_c is contact pressure of the

composite. As can be seen the stress values are largely negative or compressive. See Figs: 4.3, 4.4, 4.5, 4.6 and 4.7 for the deformed and un-deformed edge of the model, deformed and un-deformed model, deformed model Von Mises stress element solution contour plot and the Z-direction element solution contour plot of strain respectively.

Description	Minimum	Maximum
X–component of stress (Pa)	-0.170E+17	0.163e+17
Y-component of stress (Pa)	-0.175e+17	0.164e+17
Z-component of stress (Pa)	-0.171e+17	0.165e+17
Von Mises stress (Pa)	5.833	0.657e+15
Displacement-X component (mm)	-0.163e+7	491797
Displacement-Y component (mm)	-0.179e+7	281338
Displacement-Z component (mm)	-197769	990155
Total strain- X component	-11288	7224
Total strain- Y component	-11880	8951
Total strain- Z component	-5053	9978

Table: 4.2. Element solution stress, strain, Von Mises and displacement values.
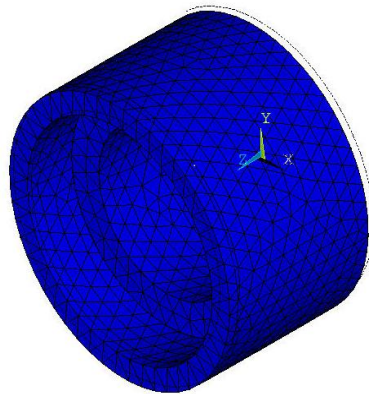
Fig: 4.3: Deformed and undeformed edge of the model
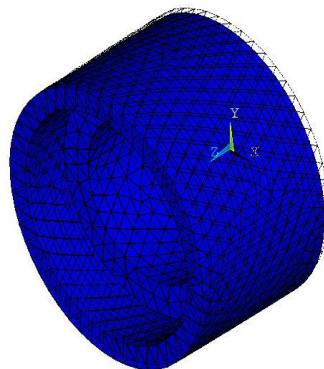
Fig: 4.4. The deformed and un-deformed model
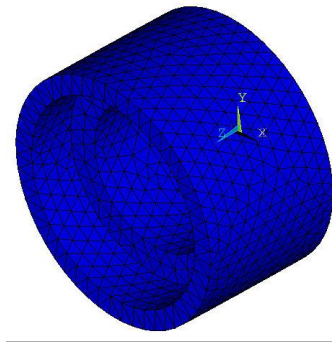

Fig: 4.5. Deformed model
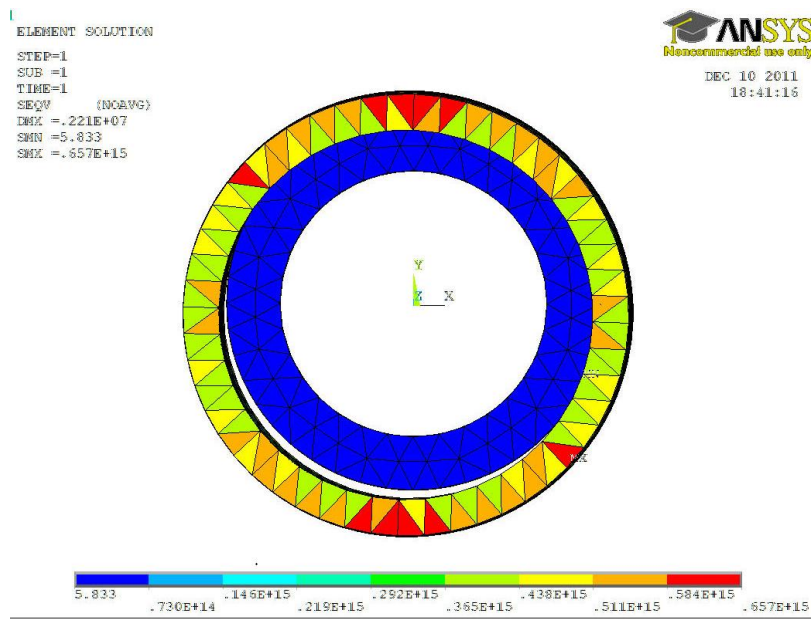
Fig: 4.6. Von Mises stress element solution contour plot for the model.
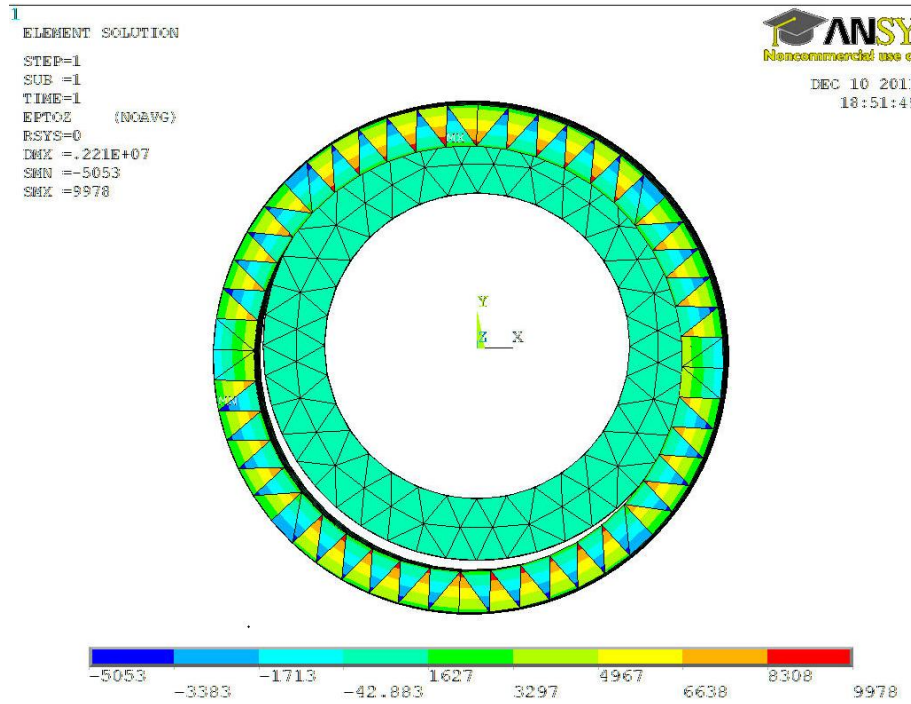
Fig: 4.6a. Strain in the Z-direction contour plot.

4.3. Analysis of the Tubular composite

4.3.1. Objective of experiment

The objective of the experiment was to determine the tensile and compressive capabilities of the material as well as the modulus of elasticity.

4.3.2. Description of experiment and outcomes

The material is a roll wrapped tubular carbon fibre composite whose external diameter is 5mm and thickness 0.5mm, see figs: 4.7 and 4.8 below. The tubular samples were fitted with mild steel plugs so that they can be gripped for tensile load tests. In later cases other plugs made of different materials were used.

Fig: 4.7. Roll wrapped carbon fibre composite with mild steel plugs at both ends. It is important to note that the plugs are held in place by some adhesive.

Fig: 4.8. The sample fitted with grips at both ends. The grips are actually split collars that are kept in place by slip rings and unthreaded bolts. See the holes for the bolts.

The apparatus is an Instron series 9 test rig see (fig 4.9) below. In order to carry out the test first of all the program has to be set out on the remotely controlled unit- a computer unit- this involves entering the dimensions of the sample and its nature (tubular), the loading speed, scale of the graph to be plotted, humidity, room temperature and more.

After all these the well gripped sample is strapped with a device that acquires the elastic modulus of the material-the extensometer, see (fig 4.10) below, this modulus is dependent on the maximum load attained which in turn depends on the time the failure occurs. The time the failure occurs most certainly depends on the strength of the adhesive. This is so because once the adhesive fails the load fails to reach or exceed its peak. The adhesive is used to hold the plugs in place.

Once all are in place and the test is initiated or started from the remote unit the control module attached to the test bench indicates its readiness then the test takes off, see the test rig in fig: 4.9.

Fig: 4.9. Instron series 9 test rig.

Fig: 4.10. The extensometer-device that acquires the elastic modulus can be seen strapped to the test sample. See also the bolt head and the slip ring.

At this time the plot of the graph gradually begins to develop doing so at a ramp rate of 0.5 mm/min. Seven tests were carried out initially in these exercises and as the case may be the plots do not develop in the same manner and rate though the scale of the graph determines this to some extent, see the extensometer in fig: 4.10.

It has to be noted again that during the tensile tests failure occurred when the adhesive bond breaks, as a result of this it can be said that the test depends on the adhesives strength.
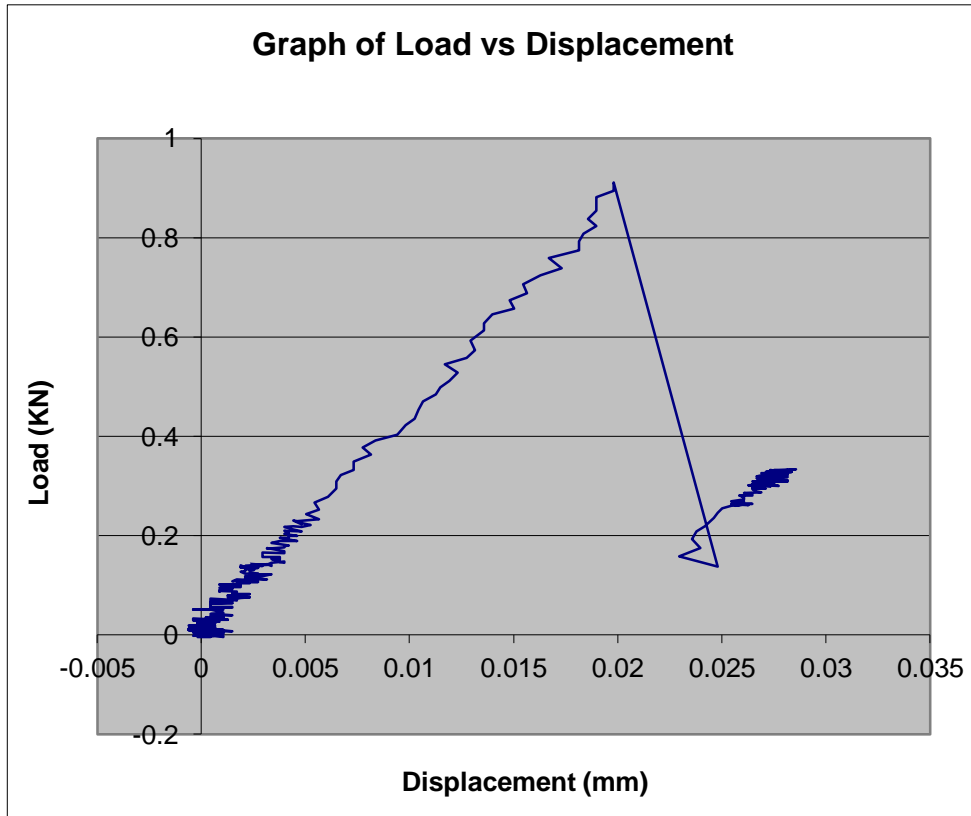
Fig: 4.11. Graph of Load against displacement, the maximum load is 0.91141 KN and maximum displacement is 0.02857 mm. The modulus is 47.1588 GPa.

The graph above in fig: 4.11 was that of the first tensile test, the zigzag scatter of the plot demonstrates what happened during the test. These happened as the load struggled to attain its peak. At the lower part of the plot it was more pronounced as can be seen, but from 0.3KN it seemed to have straightened out. Observing the digital counter on the control module attached to the test rig the part of the plot from 0.3KN seems to have recorded some sort of elongation. The graph below in fig: 4.12 was that of the second tensile test also follows a pattern like the one above in fig: 4.11 though the maximum load and maximum displacement of 0.3788 KN and 0.0089 mm respectively were remarkably lower.

Graph of Load vs Displacement
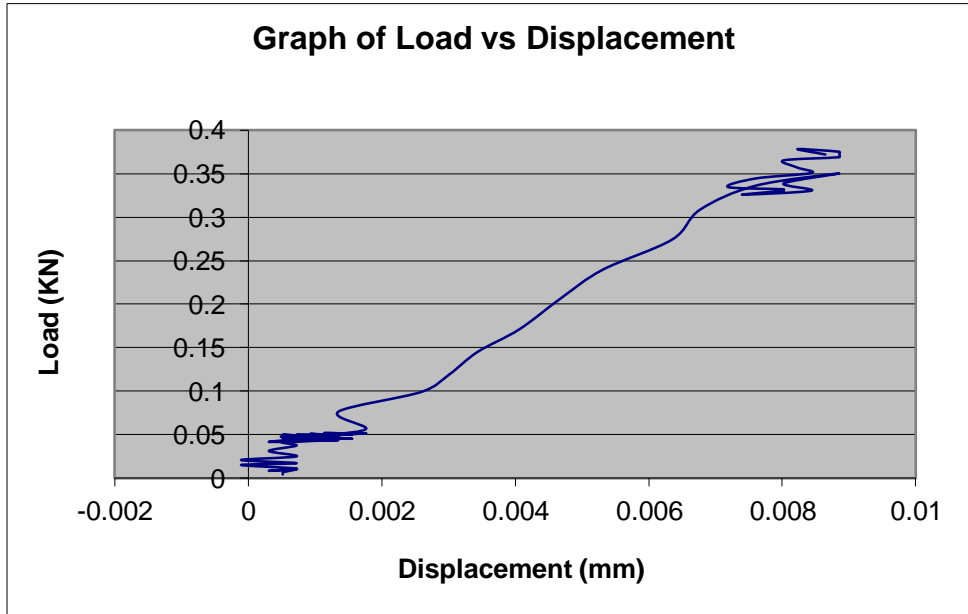
Fig: 4.12. In the test that produced this plot failure occurred earlier than expected, which is also why the point of the plot are scanty relative to the one above. The modulus is 44.432 GPa.

The adhesive in this case was not affected because cross pins were passed through the tubular sample so as the load was gradually applied the cross pin at lower end of the sample-normally where the failure occurs- gradually began to tear away at the wall longitudinally see (fig 4.13) below.

Fig: 4.13. The tubular sample with the cross pin through it.

The decision to use the cross pins came about as a result of the failure of the adhesive at the lower end of the tubular sample. It was thought that these cross pins would hold out longer than the adhesive, but the one at the lower end tore away at the material as carbon fibre composites do not have good shear strengths.

In the third case the maximum load was 0.9014 KN and the maximum displacement 0.01932 mm and with much less data points relative to that of the first plot. In this case what seemed to have happened was that an improvement on the test operation was attained to some extent.
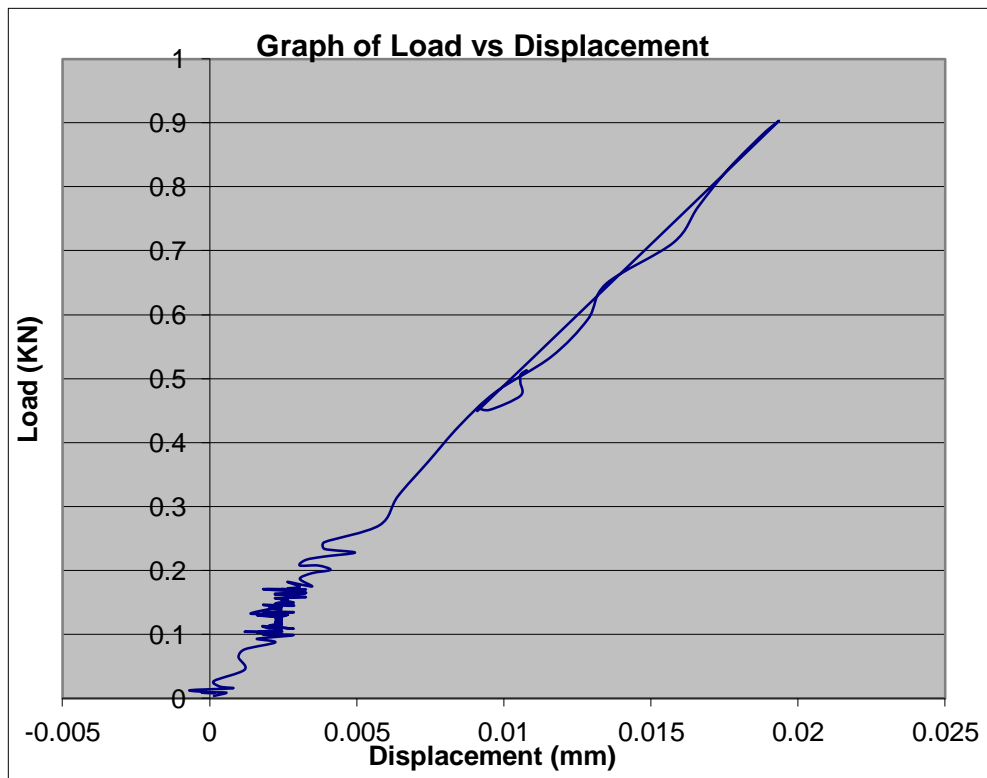
Fig: 4.14. The maximum load and displacement in this graph are 0.9014 KN and 0.01932 mm respectively. The modulus is 47.6696 GPa.

In the fourth case the cross pins were passed through the sample and the mild steel plugs so what can still be seen is still fewer data points but a remarkable larger maximum load of 1.13329 KN and a displacement of 0.02467 mm, see fig: 4.15. One would expect the displacement to be remarkably large as well, but that was not the case as one of the tests above had a displacement larger than it.
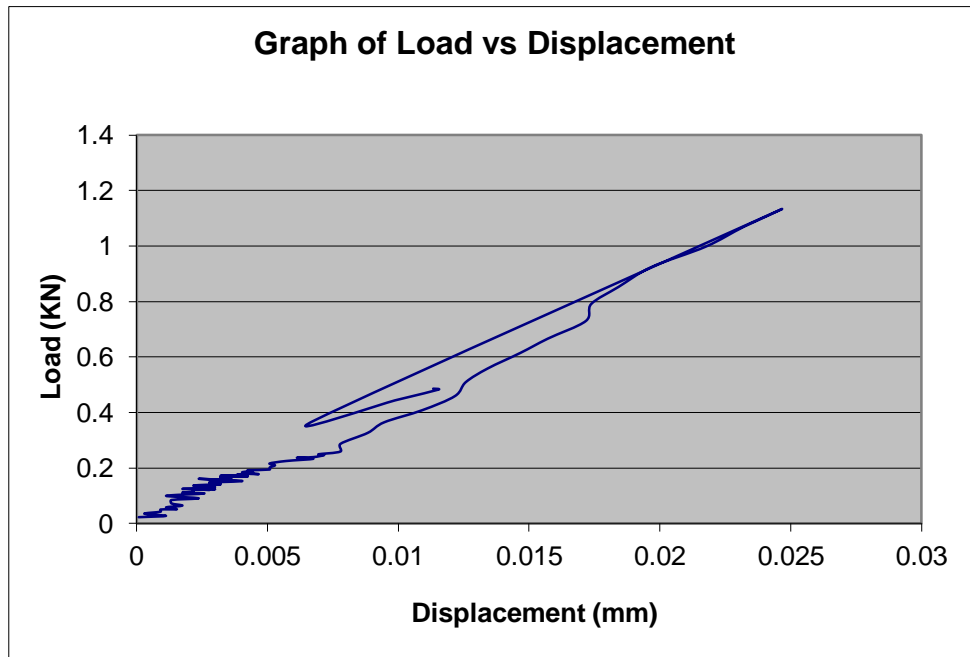
Fig: 4.15. In this graph the test produced a maximum load of 1.13329 KN and a maximum displacement 0.02467 mm. The elastic modulus was 53.9671 GPa.

In the next series of tests compressive loads were applied to the test samples, the first test was carried out with the mild steel plugs on and it produced a maximum load of 1.15753 KN and a maximum displacement of 0.02619 mm, see fig: 4.16.
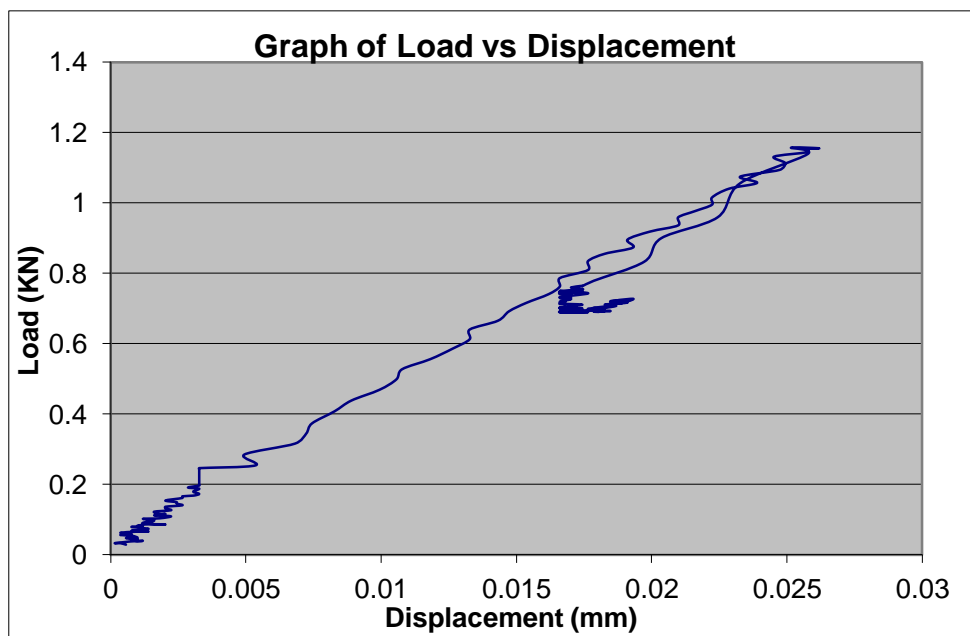

Fig: 4.16. The maximum load and displacement in this graph are 1.15753 KN and 0.02619 mm respectively. The elastic modulus was 45.6805 GPa.

Furthermore in the rest of the remaining tests the mild steel plugs were not used since all doubts had to be cleared as to whether the plugs have been influencing the outcomes of the tests.

The sixth test is one of such tests and in it some more remarkable outcomes were obtained. The maximum load reached was 2.14495 KN and a maximum displacement of 0.06018 mm, see fig: 4.17. These values are far greater than all that had been obtained possibly because of the lack of the plugs and most of all the absence of the adhesive that seemed to have gotten in the way of the tensile tests, by the virtue of their function which is holding the plug in place. The load attained was almost if not 1 KN more than all obtained results so far and the displacement almost 0.04 mm more than any previous one.
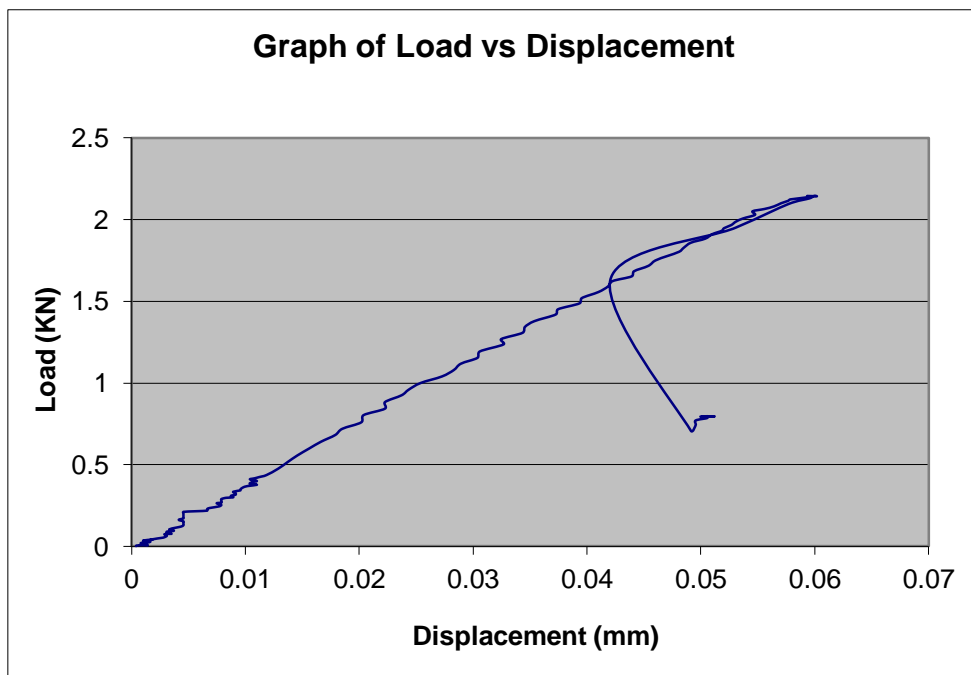

Fig: 4.17. The maximum load and displacement in this graph are 2.14495 KN and 0.06018 mm respectively. The elastic modulus was 35.9389 GPa.

With the high values from this last test whose graph is in fig: 4.17 above one may suspect that this remarkable deviation may be down to some factors. As a result of that the length of the sample was suspected as a factor. Hence a sample of about half the length of all that has been used in the previous tests described above was used in this next test.

What can be seen is a maximum attained load of 1.26163 KN which is quite like all the other maximum loads and a maximum extension of 0.03161 mm.

The length contributed significantly to the attained maximum load as with shorter lengths comes greater stiffness and a greater adaptability and resistance to some stresses associated with compressive and bending loads as the case may be.

Graph of Load vs Displacement
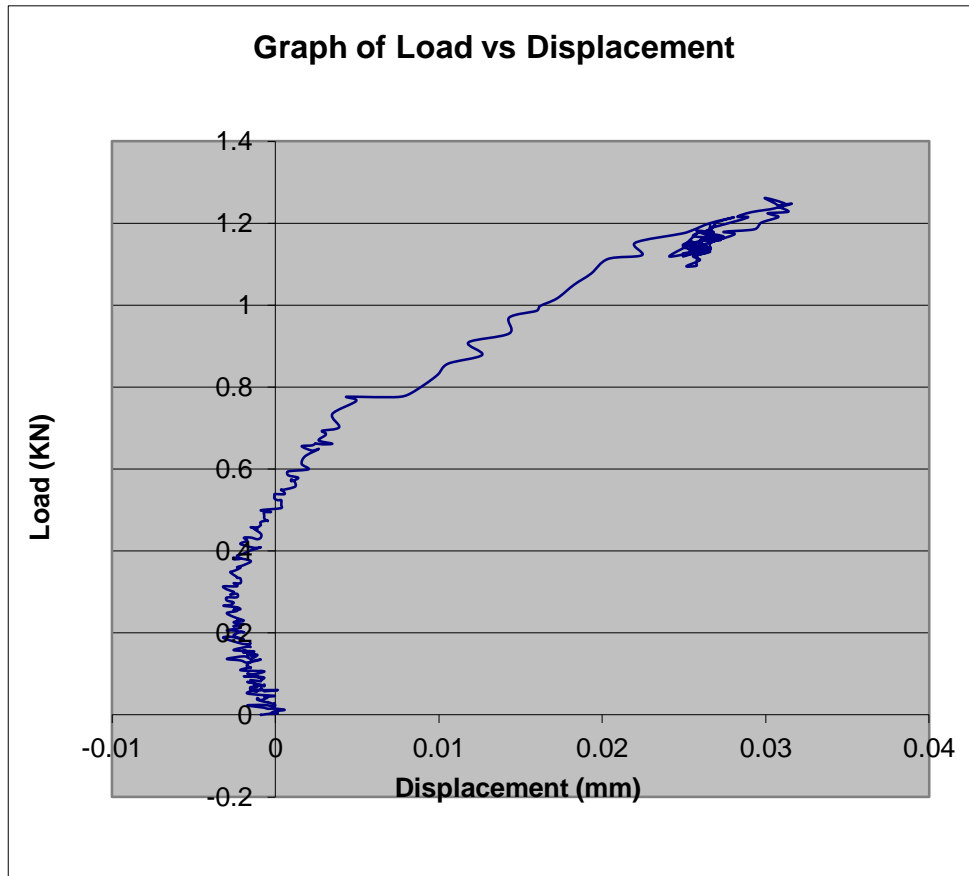
Fig: 4.18. The maximum load and displacement in this graph are 1.26163 KN and 0.03161 mm respectively. The elastic modulus is 39.9124 GPa.

Errors were inherent in the tests above; this largely occurred due to none zero initial values of extension or displacement, see fig: 4.18. They normally do not invalidate the test outcomes. At the end of every test the raw data is immediately available on the CPU or written to its hard drive, but not all the raw data were used in plotting the graphs above. The reason for this among other things is the facts that the tests do not always start at zero readings for the displacement, and these none zero readings-normally negative displacement values- are equally part of the raw data hence the reason to use the ones recorded after the zeros that are positive. At the same time some negative displacement values were still read after the zero value of the displacement recorded. This was owing to some interference that was not exactly externally induced but due to the test rig. As a result of this the data to be used for plotting

the graph was carefully selected such that it included little or no negative displacement values. Kuo et.al [22] described these negative displacement values as representing the displacement needed for the test material to fully contact the test rig or fixture.

The Young Modulus values in table: 4.4 below were read off the extensometer that was strapped on to the test sample. A cursory look tells one that these values relative to the stress, displacements and the maximum loads value are not uniform. In the tensile test cases for the first four tests the test with the largest displacement-0.0203 mm and the largest maximum load 1.133 KN-doesn't have the largest Young modulus. One would normally expect that this test case should produce the largest Young modulus but that was not the case. This non-uniformity is also the case in the rest of the results as well as in the compressive cases.

Test 3 a tensile case had the largest maximum load as well as the largest strain of 0.0016, but test 1-tensile, had the largest maximum load outside the former mentioned above but that was not the case for its strain. All these are largely down to the fact that these test cases were not absolutely the same; in some cases the test sample had just the adhesive held mild steel plugs and the others with cross-pins passing through the sample and the mild steel plug respectively. All these contribute varying factors hence the non-uniformity inherent in the results above.

The reason why we have a Young modulus of the sort we have in test 1 was largely due to the fact that the sample had just the mild steel plug held by some adhesive, and the load was largely on this adhesive, as a result the modulus was largely based on this adhesive. This adhesive by all imagination is expected to produce a modulus of that nature or there about. So as can be seen it has the second largest stress but nearly the least strain and these would produce a modulus of that nature.

4.3.3. Further Experiments

The next test that was carried out was a flexural loading case or a three point test where a pyramid like cast piece exacts the bending load on the sample which lay atop a cast piece. See the set up in the Fig: 4.19 below.

Fig: 4.19. The test set up for the three point test or flexural load test. See the pyramid like cast piece just touching the sample which is lying atop a die piece.

As it is well known carbon fibre composites have poor shear strengths so much was not expected from this test as a result the maximum load attained was 0.10345 KN and a maximum extension of 5.00074 mm. These two values above confirm the samples poor shear strength especially the significantly high extension of 5 mm. See below in fig: 4.20 the sample under load before damage occurred. Much unlike the previous tests discussed above the failure was of the sample and not that of the adhesive so the figures above are most pertinent to the material of the sample.

Fig: 4.20. The sample is under some load is visibly deflecting.

It must also be noted that once the material yielded or reached its yield point failure also took place.

Graph of Load vs Displacement
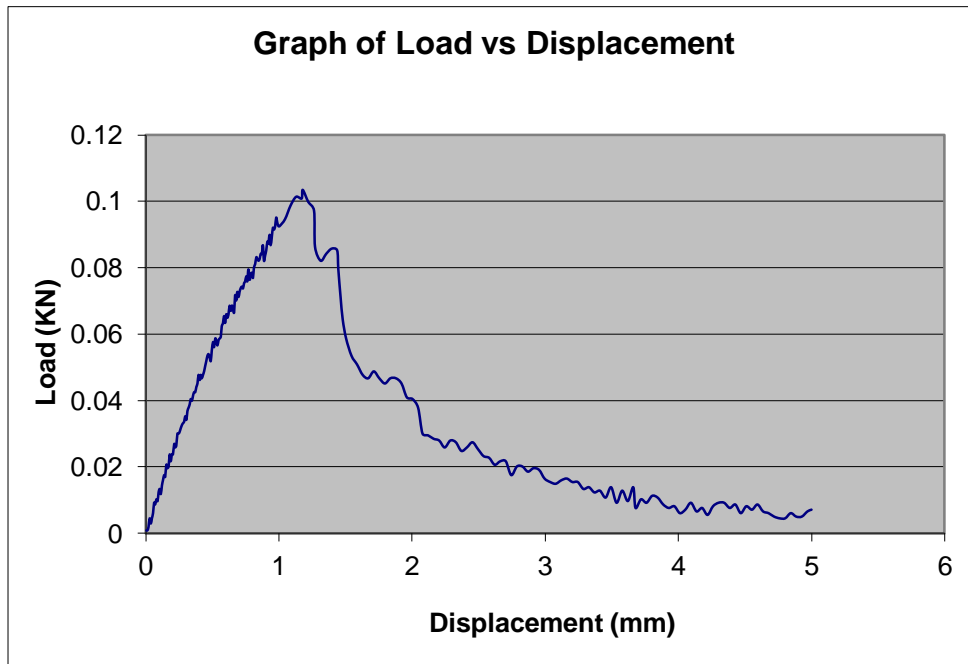
Fig: 4.21. The maximum load was attained at yield point which was also the point where failure occurred. See that the displacement or extension continued to increase even with a drop in load.

In the graph above in fig: 4.21 the yield point of the material was the highest point on the graph and the highest extension did not occur at that point. This shows that once the load reached its maximum which was also where yielding began to occur, when failure occurred part of the material was still intact and carried on with the extension even with dropping load. It is imaginable that as the load continued to drop the extension continued, this so because the strength of the sample in the lateral direction was already weakened by the failure so less loads would still provide further extension.

4.3.4. More tensile tests

In the tensile tests carried out before now, the point of failure of the adhesive always marked the peak of the test this was so because the adhesive holds the mild steel plugs in place. So once the adhesive bond broke the loads could not go beyond a certain level. In the tests described below the approach was to use longer plugs that covered more length of the tubular sample and applying more adhesive making sure sufficient amounts are pushed into the tubular sample as well to ensure greater holding strength. It must be noted that the adhesive is an epoxy one.

Fig: 4.22. The tubular sample with longer plugs and more adhesive covering more length in and out of the tube.

In the first of such tests the sample above (see figs: 4.22 and 4.23) was placed in another set of holding setup much unlike the kind used in the previous tensile and compressive tests. In this case the inner section of the holding setup had V grooves so that they can better grip the tubular sample better.

Fig: 4.23. The V grips- the fixture that secured the tubular test sample in place. The inner sections have V grooves that ensure better gripping of the sample. See attached also the extensometer.

The sample which includes the epoxy adhesive could sustain greater loads as the maximum attained load in this test was 5KN and maximum displacement of 0.43663 mm, see the graph in fig: 4.24. This maximum extension-a significant one- did not occur at the maximum load. As a matter of fact the maximum extension was attained at a load of 0.6405 KN this amount of load at the initial stages of the test would not produce an extension of that magnitude but because the material had already undergone a large amount of load its easier for the extension to continue even with far less load-note this is also the case above in the flexural test.

Graph of Load vs Displacement
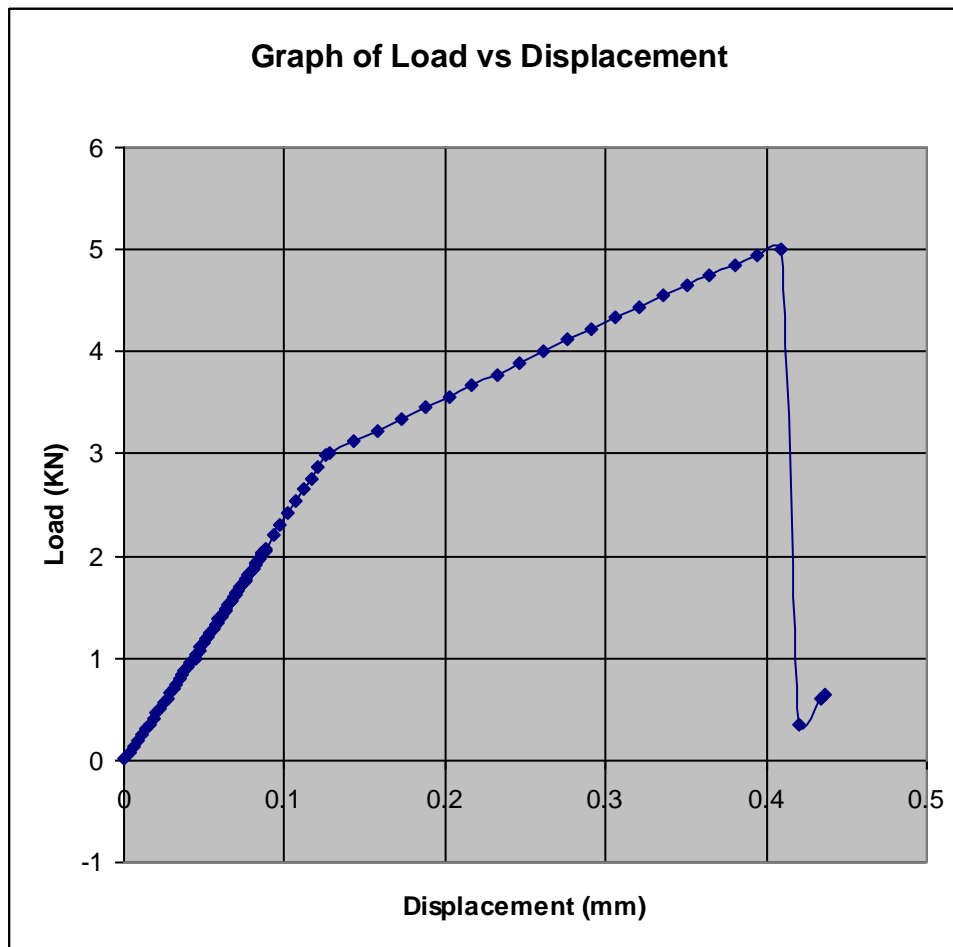
Fig: 4.24. The maximum load from this graph and the test as well was 5KN and the yield point load was 3KN. The displacement value at yield point was 0.1281mm.

Unlike the flexural case described above in earlier sections this case had a yield point separate from the break or failure point. It also has to be noted again that the failure occurred when the adhesive failed not essentially the tubular sample. In the next test that followed, a notch of 1mm depth and 0.5 mm in width was cut into a sample and some tensile load was applied, see fig: 4.25.
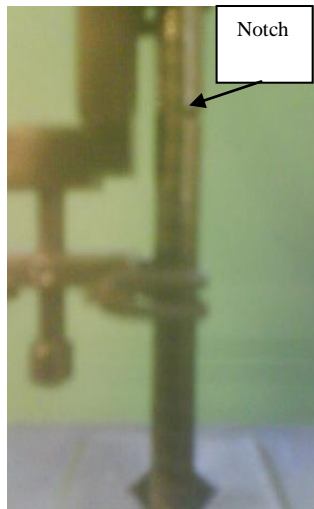
Fig. 4.25. See the notch on the test sample.
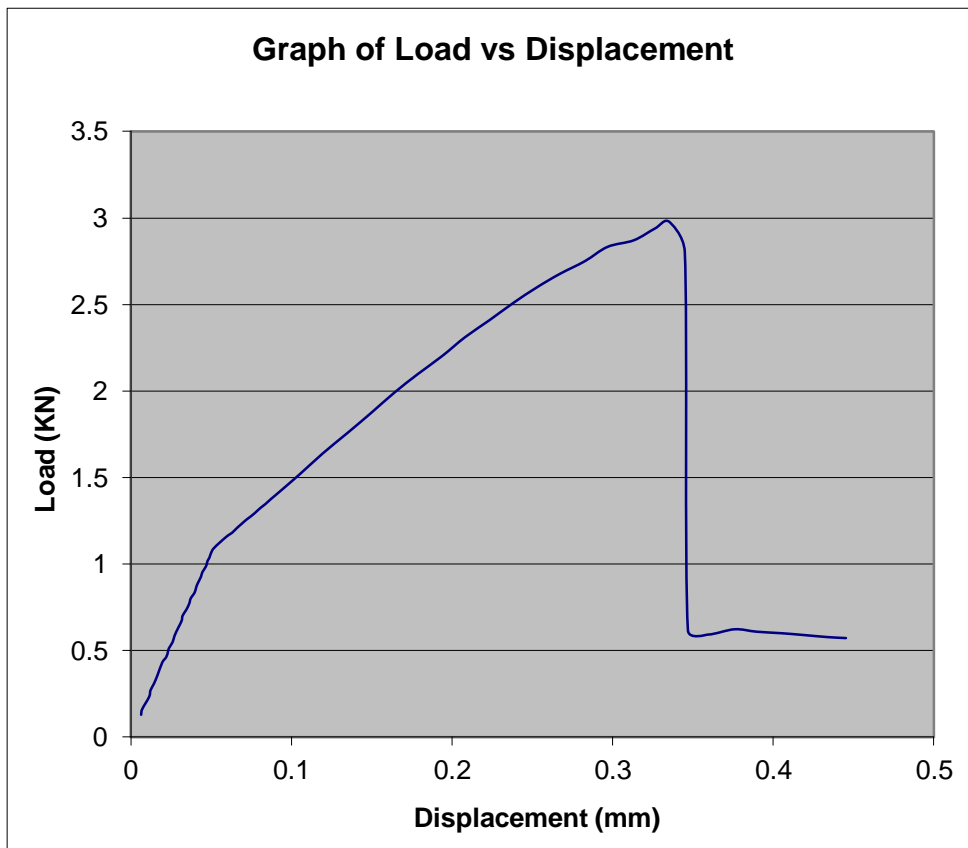
Fig: 4.26. The yield point occurred at 1.0893 KN at a displacement of 0.0512 mm and the break point occurred at 2.8051 KN at a displacement of 0.3448 mm. Note that this sample had a notch on it so damage was expected at less load.

The test whose graph is above in fig: 4.26 also produced a yield point and a failure point as well. The notch increased in width from 0.5mm to a greater dimension significantly and damage followed as the sample split up from the two top corners in the load direction. Once this splitting damage reached the adhesive which was also where the grip was, the failure point which can be seen in the graph failure occurred at that point, see the damaged sample in fig: 4.27.

Fig. 4.27. See split or damaged sample.

When the load reached its maximum which was 2.9794 KN it weakened to 2.8051 KN which was the failure point load possibly because the sample was about to fail completely as failure had already occurred and progressing. See from the graph the sharp drop in load from 2.8051 KN to 0.6173 KN indicating failure. Notice also the progressing deformation common to some of the tests above even with a significant drop in load. The extensometer was removed when the load was at 1.1273 KN this verifies that the yield point which can be seen from the graph was that of the sample and not that of the epoxy adhesive as the yield point load from the graph was 1.0893 KN which of course was recorded before the device was removed.

In the next test case the sample was equally subjected to tensile loading this time around there was no notch involved and it produced a maximum load of 3.9905 KN.

Graph of Load vs Displacement
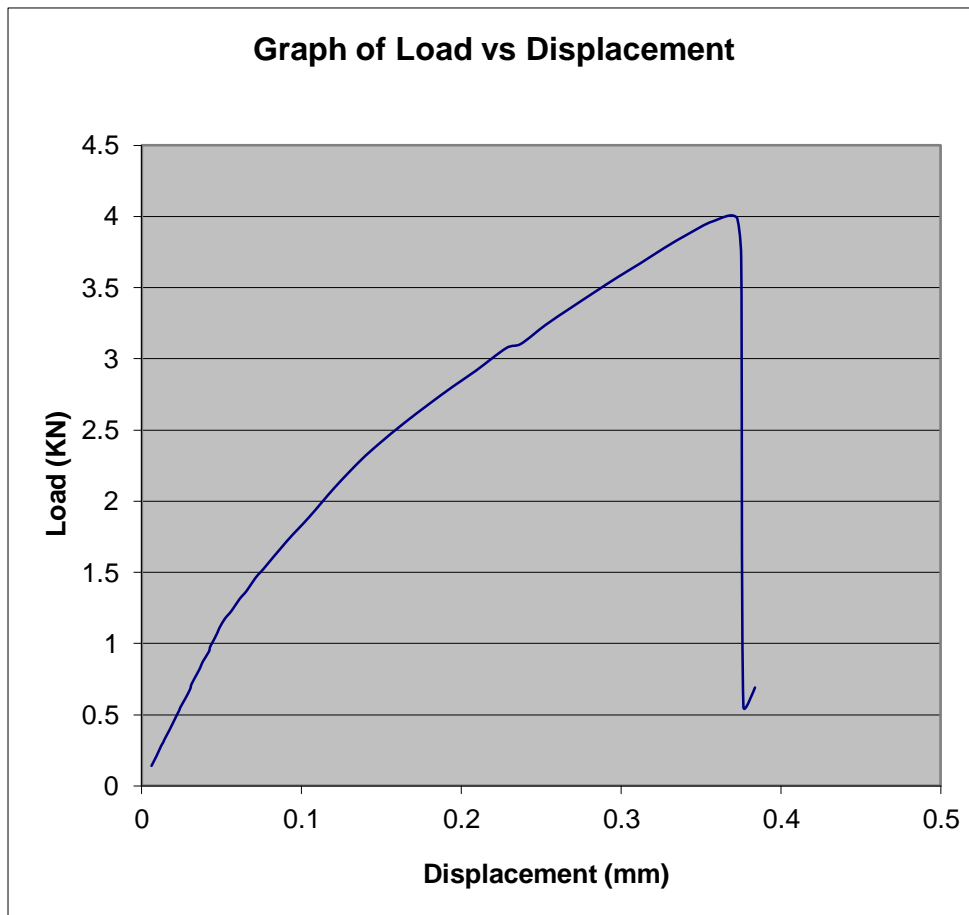
Fig: 4.28. The graph above does not have a clearly marked out yield point, but a closer look one can see a slight kink where it occurred.

The graph above in fig: 4.28 as can be seen has no clear or distinct yield point, but its maximum load and yield point values were about the same with that of the case with the notch in the earlier case. In the next test case a notch of 2.5mm depth was introduced to another sample which could only sustain a maximum load of 0.8025 KN and a maximum extension 0.0405 mm. The sample failed before its yield point could be reached see graph below.

Graph of Load vs Displacement
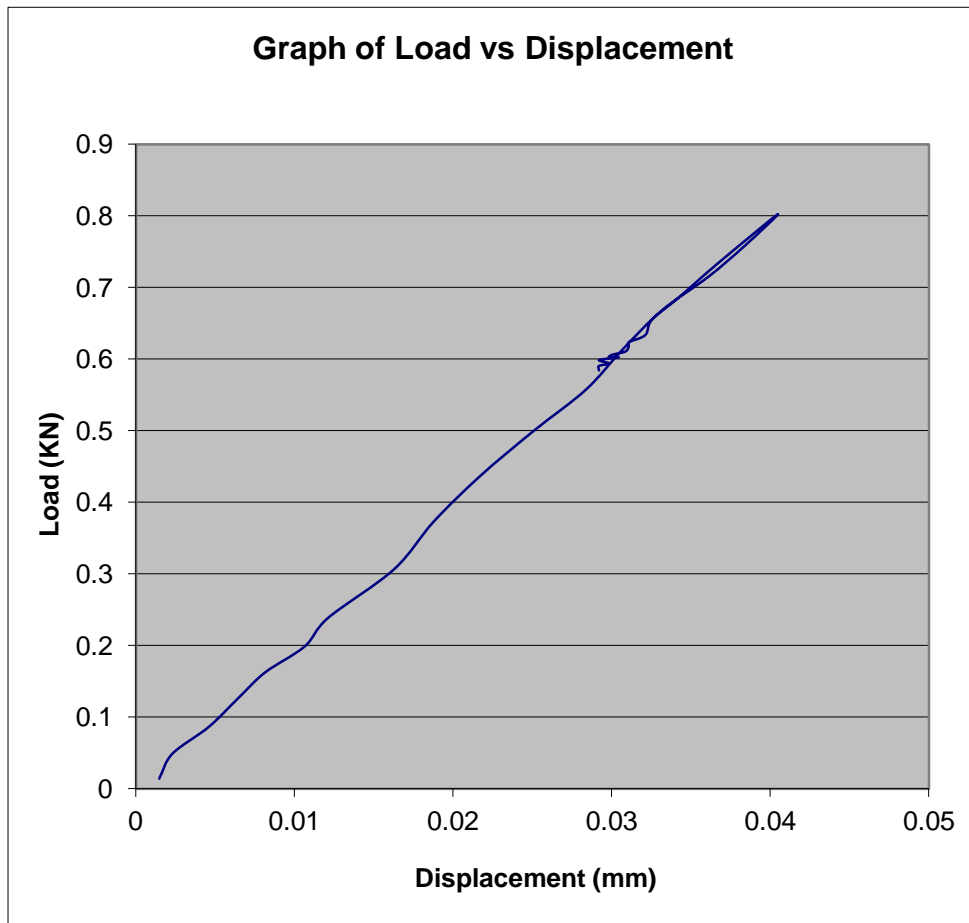
Fig: 4.29. The graph above has a maximum load of 0.8025 KN and a maximum displacement of 0.0405 mm.

In Fig: 4.29 it can be seen that the load reached its peak and dropped but this drop based on how the graph was plotted, it is quite an odd one as one would expect the drop to look like the usual cases as can be seen in earlier graphs above. It happened that as the load dropped the displacement equally dropped this is unlike the previous cases where the displacement continued to increase even with a drop in load. There is no doubt that this is down to the fact that the material has not reached its yield point hence still in its elastic state hence the drop in displacement. At the same time this also explains why the displacements continued to increase after the yield point even with continued drop in load as in previous cases; this is also down to the fact that in those cases the yield points of the material had been exceeded. As a result small loads still continued to result in greater displacement or elongation.

In the next test case a longer sample was used as well as longer brass grips and a sufficient amount of adhesive to hold the grips and held by the V-grips of the test rig the sample was subjected to tensile loading and produced a very high maximum load value-7.6380 KN and a

maximum displacement of 0.9599 mm as well as a yield point load value of 1.1385 KN at a displacement of 0.0488 mm.
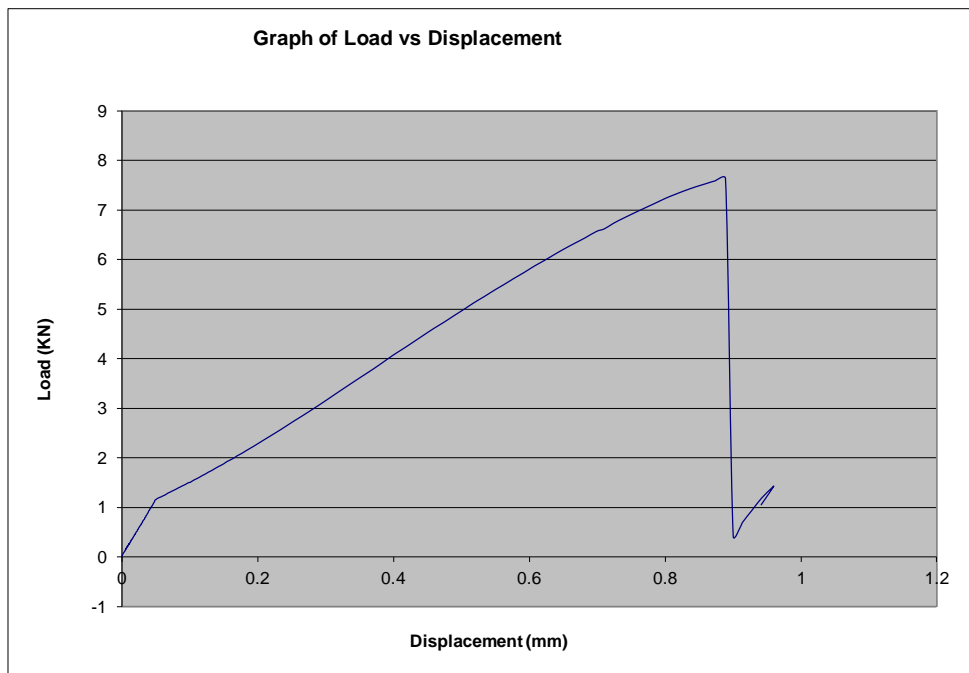
Fig: 4.30. The graph above had a maximum load of 7.6380 KN and a maximum displacement of 0.9599 mm.

The sample in the test whose graph can be found above in fig: 4.30 endured a load up to 7.6380 KN and failed when the adhesive failed meaning that the material was still intact. Just as one can imagine the adhesive-an epoxy one-had some influence on the test in this case, because it was in sufficient quantity the sample could endure the amount of load indicated above. What we can equally see was that because the sample material's yield point was exceeded the displacement continued to increase regardless of the loads magnitude, recall that this had been the case where the yield point was exceeded.

In the next set of tests the sample was filled at the two ends with short brass cylindrical lengths, so unlike the previous cases there were no grips attached to the sample and no adhesives as well. The reason for using these brass inserts was to ensure that the sample would not collapse as it is hollow and has poor shear strength.
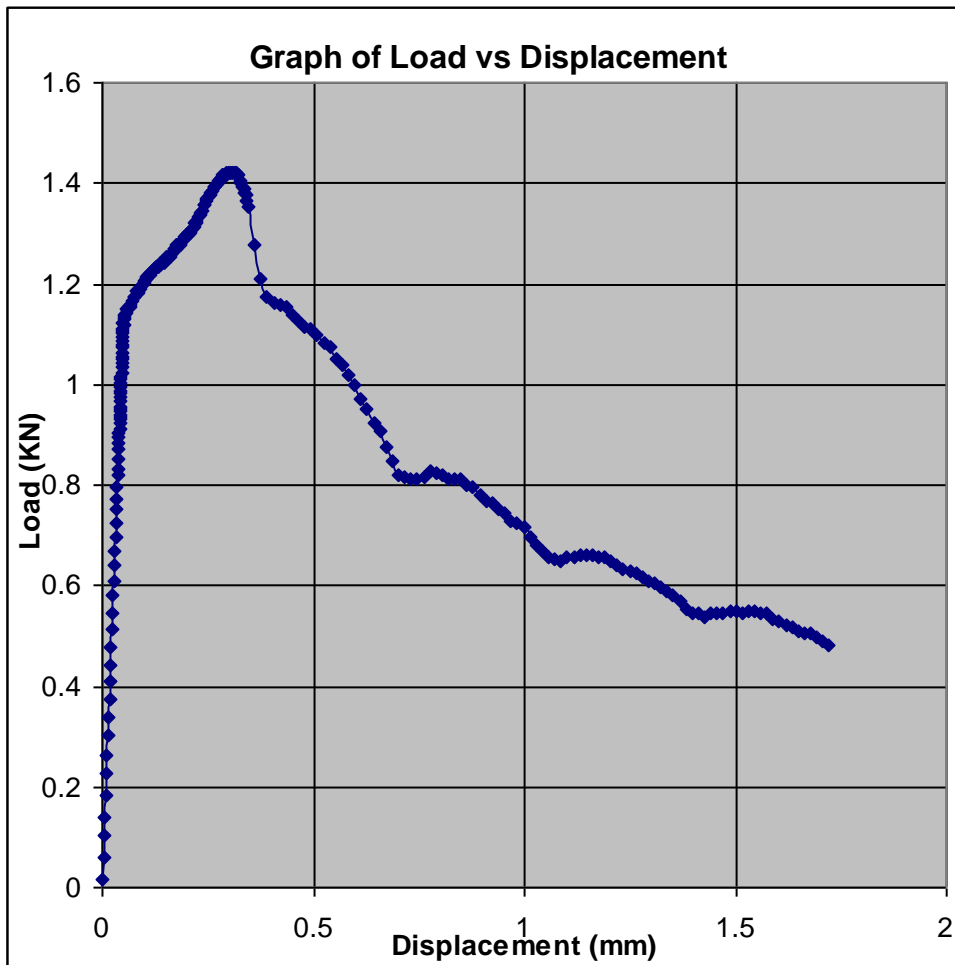
Fig: 4.31. The test whose graph is above produced a maximum load of 1.4225 KN and a maximum displacement of 1.7201 mm.

The test was ended when it was observed that the sample was gradually slipping from the grip this was down to the fact that the sample could not be gripped easily. And of course at this time the load was dropping because of the slip at the lower end of the sample, see fig: 4.31.

In the next test that followed the sample was reversed so that this lower end was fixed to the upper grips, the reason for doing so was because the slipping normally occurs at the lower end and since the part of the sample that went into the lower end was still intact this would provide another chance to test the material again. It must also be noted the material had not failed yet apart from the scrapping of one of the ends at the same time we can also see that the yield point of the material was exceeded based on the graph just right above. This goes to say that the yield point of the sample whose graph we have below in fig: 4.32 had once been attained and exceeded.

Graph of Load vs Displacement
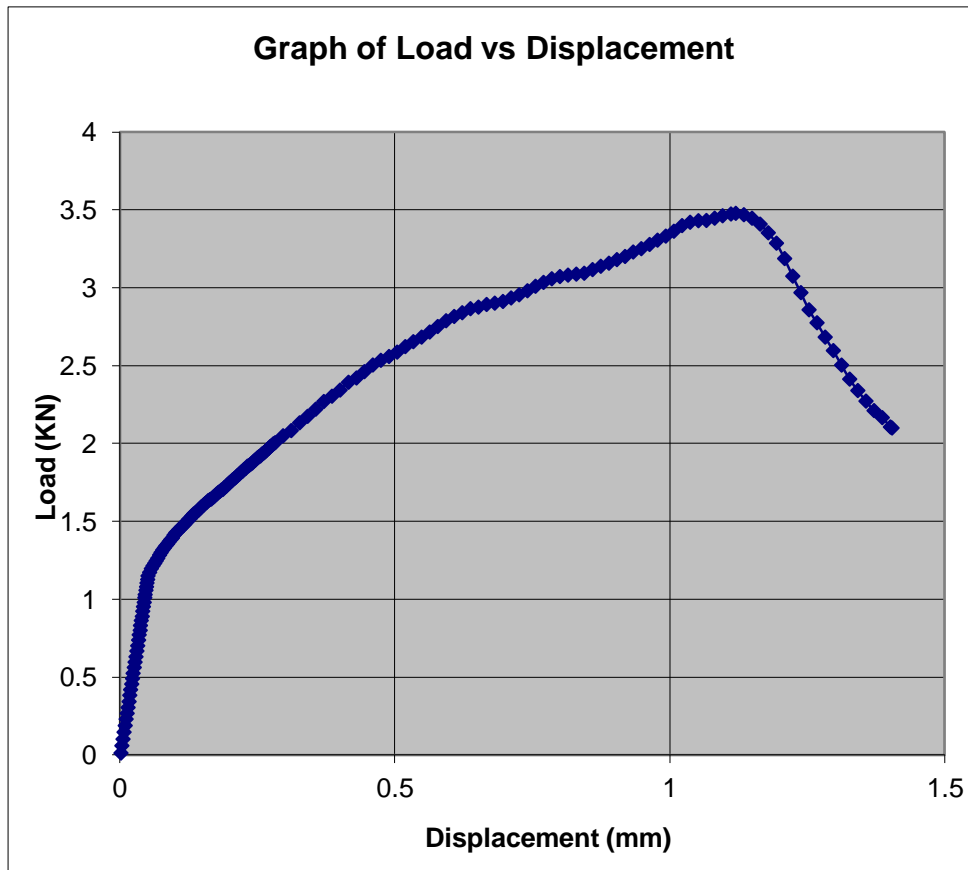
Fig: 4.32. In the graph above the already tested material could hold out longer and endured a maximum load of 3.4797 KN with a displacement of 1.4035 mm.

In the last test a better gripping was achieved hence the higher maximum load attained relative to the former, see fig: 4.33. The sample still did not fail as such, but the test was stopped because of the reoccurrence of the slipping action of the sample from its grips and dropping load. As it was indicated above the material did not fail and was still very much intact so in the light of all these the ramp rate of the load was increased tenfold from 0.5 mm/min to 50 mm/min. The ramp rate is more like the speed at which the sample is been stretched or compressed or speed at which load is applied.

Graph of Load vs Displacement
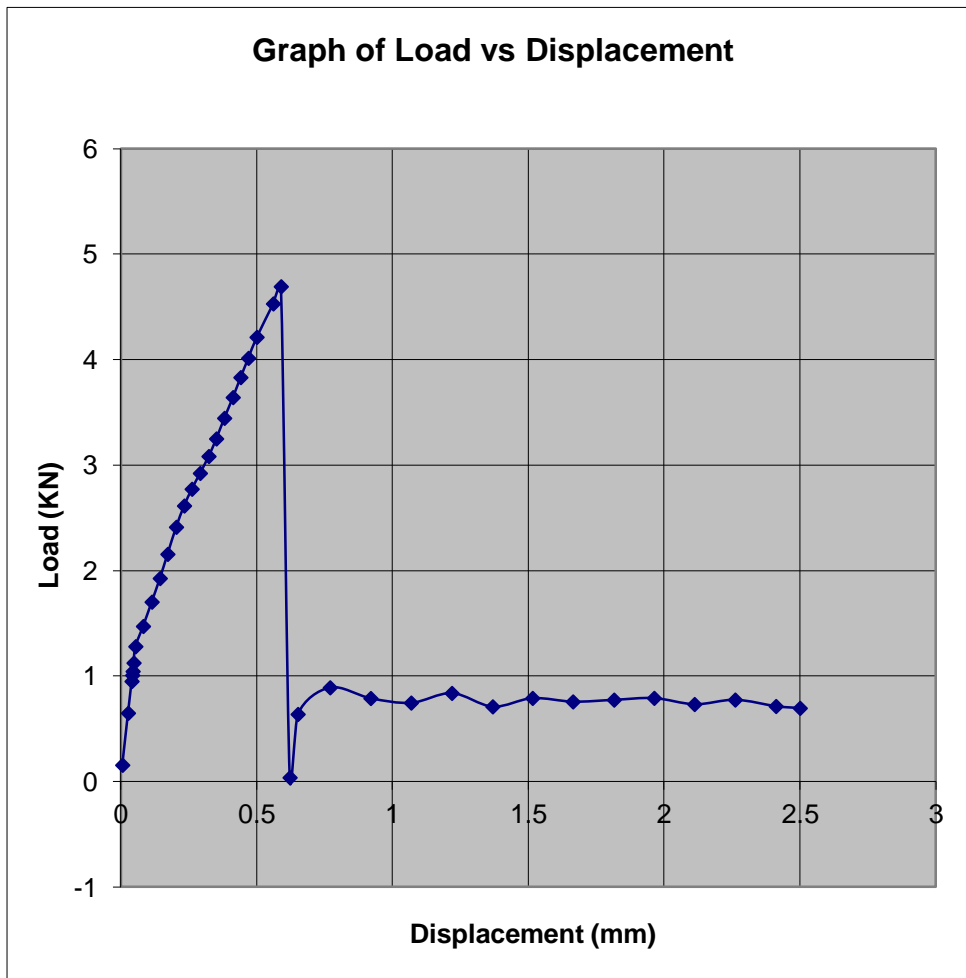
Fig: 4.33. The test whose graph was above carried out under a ramp rate of 50 mm/min as against 0.5 mm/min produced a maximum load of 4.6935 KN and a maximum displacement of 2.5 mm.

The test started and ended in a very short time due to the very high ramp rate, the material endured a 4.6935 KN load and the lower end of the sample-the end that was fitted to the lower V-grip-was badly shattered and destroyed, see (fig 4.34) below. Note again the continued deformation or displacement even with the continued drop in load because the material reached and exceeded its yield point.

Fig: 4.34. Badly shattered sample. The shinny part is the brass insert now visible.

	Displacement at Max. Load (mm)	Load at Max. Load (KN)	Stress at Max. Load (MPa)	Strain at Max. Load (mm/mm)	Young Modulus (MPa)-derived during test.
Test 1 (Tensile)	0.0131	0.9114	128.9	0.0011	122200
Test 1i (Tensile)	0.0079	0.3507	49.61	0.0006	97200
Test 2 (Tensile)	0.0189	0.9014	127.5	0.0015	93230
Test 3 (Tensile)	0.0203	1.133	160.3	0.0016	108000
Test 4 (Compressive)	0.0264	1.156	163.5	0.0021	96690
Test 5 (Compressive)	0.0593	2.142	303.1	0.0047	71450
Test 6 (Compressive)	0.0391	1.262	178.5	0.0031	101100
Test 9 (Tensile)	0.4063	5.002	707.6	0.0163	86120
Test 10 (Tensile-1 mm crack)	0.3355	2.979	421.5	0.0134	75080

Test 11 (Tensile)	0.3726	3.991	564.6	0.0149	78510
Test 12 (Tensile-2.5 mm crack)	0.0363	0.8025	113.5	0.0015	81690
Test 13 (Tensile)	0.8905	7.638	1081	0.0356	73600
Test 14 (Tensile)	0.2977	1.423	201.2	0.0119	82970
Test 15 (Tensile)	1.118	3.480	492.3	0.0447	83150
Test 16 (Tensile)	0.5904	4.693	664	0.0236	83090
	Displacement at yield (mm)	Load at yield (KN)	Stress at yield (MPa)	Strain at yield (mm/mm)	
Test 8 (Flexural)	1.179	0.1035	168.6	0.0055	

Table: 4.4. Array of empirical data from the tests done on the tubular carbon fibre composite.

4.3.5. Constitutive Model for the tubular composite

This begins with the determination of the Poisson's ratio denoted by ν and defined as the ratio of the lateral strain to the axial strain:

$$\nu = \frac{\varepsilon_{yy}}{\varepsilon_{xx}} \qquad (29)$$

In other to determine the value of the Poisson's ratio reference was made to the test data where the lateral strain values were already available, but the axial strain had to be obtained by finding the average of the maximum strains obtained from certain tensile tests. These tests are the cases where the maximum loads were no more than 2.142 KN, and the obtained value was 2.6190. The average of the maximum strains was 0.0021 mm/mm while the lateral strain was 0.0055mm/mm so

$$v_{12} = \frac{0.0055mm/mm}{0.0021mm/mm} = 2.6190 \tag{30}$$

It must also be noted that the y-direction must be the direction of the applied stress, and also the lateral and axial strains were for one particular specimen and not for two specimens as was the case in this work. With the latter above noted, the current approach of using axial strain from one specimen and lateral strain from another would go ahead for comparison purposes.

These set of results stated above in table; 4.4 were selected because their maximum strain values would lead to realistic Poisson's ratio values when divided by the lateral strain value.

During the tests the elastic moduli of the samples were produced and written to file, so reference was made to the moduli of the same set of results mentioned above-those whose maximum load values were no more than 2.142 KN and strain value not more than 0.0047. There were some exceptions like test cases where cracks were introduced to the sample, their results were not included. Referring to the elastic moduli, the averages of the moduli for the tensile and compressive tests were found so we have single values for them, which are 105157.5 MPa and 89746.6667 MPa respectively.

The average of their maximum stress values were also found and were divided by the elastic moduli above respectively, the average of these maximum stress values are 116.5775 MPa and 215. 0333 MPa, so we have axial strains below:

$$\frac{116.5775MPa}{105157.5MPa} = 0.0011 \tag{31}$$

$$\frac{215.0333MPa}{89746.6667MPa} = 0.0024 \tag{32}$$

Then the values above were used to divide the lateral strain values

$$\frac{0.0055}{0.0011} = 5 \tag{33}$$

$$\frac{0.0055}{0.0024} = 2.2916$$

$$(34)$$

These derived Poisson's ratios-2.6190, 5 and 2.2916 on the face of it are not exactly in line with what have been described in many texts books. R. Jones [38] cited Dickerson and DiMartino in his book saying they "measured Poisson's ratios as high as 1.97" using the same expression used above to determine Poisson's ratio- lateral strain over axial strain.

To validate the values above for consistency with mathematical elasticity mode the Poisson's ratios must meet the restriction below

$$|v_{12}| < \sqrt{\frac{E_1}{E_2}} \qquad (35)$$

And

$$\sqrt{\frac{E_1}{E_2}} = 1.9966 \quad (36)$$

With the determined value above it can be seen that the determined Poisson's ratios are not smaller than 1.9966 so they don't satisfy the restriction. Also they did not satisfy the reciprocal relation of the compliance symmetry condition which is

$$\frac{v_{12}}{E_1} = \frac{v_{21}}{E_2} \qquad (37)$$

As a result these Poisson's ratio values cannot be used as engineering constants for any constitutive model. So we look again at the entire results from the tests as they may contain Poisson's ratios that may meet the restriction and condition stated above. The Poisson's ratio was determined for each test case and checked to see if they meet the restriction and condition mentioned above.

Condition of Sample	Displacement at Max. Load (mm)	Load at Max. Load (KN)	Stress at Max. Load (MPa)	Strain at Max. Load (mm/mm)	Modulus (Young) $E_1 or E_x$ (MPa)	Poisson's Ratio	$E_2 or E_y$ (MPa)	$\dfrac{E_1}{E_2}$ (MPa)	$\sqrt{\dfrac{E_1}{E_2}}$ (MPa)	Restriction/ Condition $\lvert v_{12} \rvert < \sqrt{\dfrac{E_1}{E_2}}$
	0.0131	0.9114	128.9	0.0011	122200	1.04282389	30654.546	3.986358238	1.9965866	MEETS RESTRICTION
	0.0079	0.3507	49.61	0.0006	97200	1.17556944	30654.55	3.170818035	1.7806791	MEETS RESTRICTION
	0.0189	0.9014	127.5	0.0015	93230	1.09682353	30654.55	3.041310344	1.7439353	MEETS RESTRICTION
	0.0203	1.133	160.3	0.0016	108000	1.07797879	30654.55	3.5231315	1.8770006	MEETS RESTRICTION
	0.0264	1.156	163.5	0.0021	96690	1.24188991	30654.55	3.154181027	1.7760014	MEETS RESTRICTION
	0.0593	2.142	303.1	0.0047	71450	1.10793468	30654.55	2.330812229	1.5266998	MEETS RESTRICTION
	0.0391	1.262	178.5	0.0031	101100	1.75579832	30654.55	3.298042216	1.8160513	MEETS RESTRICTION
	0.4063	5.002	707.6	0.0163	86120	1.98382702	30654.55	2.809370876	1.6761178	DOES NOT MEET RESTRICTION
CRACK	0.3355	2.979	421.5	0.0134	75080	2.38688493	30654.55	2.449228581	1.5650011	DOES NOT MEET RESTRICTION
	0.3726	3.991	564.6	0.0149	78510	2.07190755	30654.55	2.561120617	1.6003502	DOES NOT MEET RESTRICTION
CRACK-2.5	0.0363	0.8025	113.5	0.0015	81680	1.07947137	30654.55	2.664453104	1.6323391	MEETS RESTRICTION
	0.8905	7.638	1081	0.0356	73600	2.42382979	30654.55	2.400948636	1.5494995	DOES NOT MEET RESTRICTION
*	0.2977	1.423	201.2	0.0119	82970	4.90727137	30654.55	2.706612885	1.6451787	DOES NOT MEET RESTRICTION

1.118	3.48	492.3	0.0447	83150	7.5498 7812	30654.55	2.71 2484 77	1.6469 623	DOES NOT MEET RESTRICTION
0.5904	4.693	664	0.0236	83090	2.9531 988	30654.55	2.71 0527 475	1.6463 68	DOES NOT MEET RESTRICTION

Table: 4.5. An analysis of the Poisson's ratios to see if they meet the restriction.

Looking at table: 4.5 above it can be seen that the test cases where the Load was higher than 2.142 KN did not meet the restriction-though not the rule- with the exception of the test case marked with "*", the test was not concluded because the sample was slipping from its grips. This is also the case for cases where the strains were greater than 0.0047-not the rule as well. So the analysis serves as an empirical verification of the choices made previously, which is choosing to use test values whose maximum loads are no more than 2.142KN and strain no more than 0.0047.

It can be seen also that higher loads can affect the quality of results obtained as it is likely the strain value would be quite significant if not high hence a Poisson's ratio that does not meet the restriction. Another factor which is stress can also affect the results but it cannot do so independently for instance if it were possible to increase the maximum stress for a test case that did not meet the restriction is increased significantly the case would meet the restriction but of course that would not be possible as the strain would also increase tremendously and pushing the Poisson's ratio further away from the restriction condition. The average of all the Poisson's ratios that met the restriction came up to 1.1973.

Looking at table: 4.5 above one will observe that the $E_2 or E_y$ values were constant all the way; these values were taken from a flexural test case as the loading was in the lateral direction. This goes to say that the E_1 and E_2 in the table above for the test cases were not from the same samples as a result of these the condition below was not satisfied in all cases.

$$\frac{v_{12}}{E_1} = \frac{v_{21}}{E_2}$$
(37)

So we go back again to the obtained data and using the equation above the E_2 was determined for all test cases, but before that v_{21} was determined using

$$v_{21} = \frac{\varepsilon_{xx}}{\varepsilon_{yy}} \quad (38)$$

And before that ε_{yy} was determined using

$$v_{12}(\varepsilon_{xx}) = \varepsilon_{yy} \quad (39)$$

So a more realistic set of E_2 values were used in the tables: 4.6 and 4.7 below, as a result of these adjustments all the test cases met the restriction and condition. This is against what was written above especially that the attained load had an influence on the quality or suitability of the Poisson's ratio as regards employing it in a constitutive model.

Condition of Sample	Displacement at Max. Load (mm)	Load at Max. Load (KN)	Stress at Max. Load (MPa)	Strain (ε) at Max. Load (mm/mm)	Modulus (Young) $E_1 or E_x$ (MPa)	Poisson's Ratio	$E_2 or E_y$ (MPa)	$\dfrac{E_1}{E_2}$	$\sqrt{\dfrac{E_1}{E_2}}$	Restriction/ Condition $\lvert v_{12}\rvert < \sqrt{\dfrac{E_1}{E_2}}$
	0.0131	0.9114	128.9	0.0011	122200	1.04282389	112369.71	1.0875	1.0428	MEETS RESTRICTION
	0.0079	0.3507	49.61	0.0006	97200	1.17556944	70334.708	1.3820	1.1756	MEETS RESTRICTION
	0.0189	0.9014	127.5	0.0015	93230	1.09682353	77496.514	1.2030	1.0968	MEETS RESTRICTION
	0.0203	1.133	160.3	0.0016	108000	1.07797879	92940.14	1.1620	1.0780	MEETS RESTRICTION
	0.0264	1.156	163.5	0.0021	96690	1.24188991	62692.468	1.5423	1.2419	MEETS RESTRICTION
	0.0593	2.142	303.1	0.0047	71450	1.10793468	58206.827	1.2275	1.1079	MEETS RESTRICTION
	0.0391	1.262	178.5	0.0031	101100	1.75579832	32794.567	3.0828	1.7558	MEETS RESTRICTION
	0.4063	5.002	707.6	0.0163	86120	1.98382702	21882.474	3.9356	1.9838	MEETS RESTRICTION
CRACK	0.3355	2.979	421.5	0.0134	75080	2.38688493	13178.358	5.6972	2.3869	MEETS RESTRICTION

	0.3726	3.991	564.6	0.0149	78510	2.0719 0755	18288.759	4.29 28	2.0719	MEETS RESTRICTION
CRA CK-2.5	0.0363	0.8025	113.5	0.0015	81680	1.0794 7137	70096.039	1.16 53	1.0795	MEETS RESTRICTION
	0.8905	7.638	1081	0.0356	73600	2.4238 2979	12527.764	5.87 50	2.4238	MEETS RESTRICTION
	0.2977	1.423	201.2	0.0119	82970	4.9072 7137	3445.4102	24.0 813	4.9073	MEETS RESTRICTION
	1.118	3.48	492.3	0.0447	83150	7.5498 7812	1458.755	57.0 007	7.5499	MEETS RESTRICTION
	0.5904	4.693	664	0.0236	83090	2.9531 988	9527.1586	8.72 14	2.9532	MEETS RESTRICTION

Table: 4.6. An analysis of the Poisson's ratios to see if they meet restrictions.

Strain ($\mathcal{E}$) At Max.Load (mm/mm)-YY	v_{21}	v_{12}/E_1	v_{21}/E_2	CONDITION $$\frac{v_{12}}{E_1} = \frac{v_{21}}{E_2}$$
0.001147106	0.9589347	8.53375E-06	8.53375E-06	MEETS CONDITION
0.000705342	0.8506516	1.20943E-05	1.20943E-05	MEETS CONDITION
0.001645235	0.9117237	1.17647E-05	1.17647E-05	MEETS CONDITION
0.001724766	0.927662	9.98129E-06	9.98129E-06	MEETS CONDITION
0.002607969	0.8052244	1.2844E-05	1.2844E-05	MEETS CONDITION
0.005207293	0.9025803	1.55064E-05	1.55064E-05	MEETS CONDITION

0.005442975	0.5695415	1.73669E-05	1.73669E-05	MEETS CONDITION
0.03233638	0.5040762	2.30356E-05	2.30356E-05	MEETS CONDITION
0.031984258	0.4189561	3.17912E-05	3.17912E-05	MEETS CONDITION
0.030871422	0.482647	2.63904E-05	2.63904E-05	MEETS CONDITION
0.001619207	0.9263794	1.32159E-05	1.32159E-05	MEETS CONDITION
0.08628834	0.4125702	3.29325E-05	3.29325E-05	MEETS CONDITION
0.058396529	0.2037792	5.91451E-05	5.91451E-05	MEETS CONDITION
0.337479552	0.1324525	9.07983E-05	9.07983E-05	MEETS CONDITION
0.069695492	0.3386159	3.55422E-05	3.55422E-05	MEETS CONDITION

Table: 4.7. An analysis of the Poisson's ratios to see if they meet restrictions

The samples in these tests were continuous unidirectional prepregs wound round a carbon tube or mandrel as such they were orthotropic composites and should have nine independent material constants as well as at least two orthogonal planes of symmetry whose material properties are independent of direction as far as the plane is concerned [35]. The constitutive compliance matrix can be expressed as such

$$[S] = \begin{bmatrix} \dfrac{1}{E_x} & -\dfrac{\nu_{yx}}{E_y} & -\dfrac{\nu_{zx}}{E_z} & 0 & 0 & 0 \\[2ex] -\dfrac{\nu_{xy}}{E_x} & \dfrac{1}{E_y} & -\dfrac{\nu_{zy}}{E_z} & 0 & 0 & 0 \\[2ex] -\dfrac{\nu_{xz}}{E_x} & -\dfrac{\nu_{yz}}{E_y} & \dfrac{1}{E_z} & 0 & 0 & 0 \\[2ex] 0 & 0 & 0 & \dfrac{1}{2G_{yz}} & 0 & 0 \\[2ex] 0 & 0 & 0 & 0 & \dfrac{1}{2G_{zx}} & 0 \\[2ex] 0 & 0 & 0 & 0 & 0 & \dfrac{1}{2G_{xy}} \end{bmatrix} \tag{40}$$

Where: $\dfrac{\nu_{yz}}{E_y} = \dfrac{\nu_{zy}}{E_z}, \dfrac{\nu_{zx}}{E_z} = \dfrac{\nu_{xz}}{E_x}, \dfrac{\nu_{xy}}{E_x} = \dfrac{\nu_{yx}}{E_y}$

But what would be considered at the moment is the plain stress compliance expression or matrix which goes thus:

$$\begin{bmatrix} \varepsilon_x \\ \varepsilon_y \\ \gamma_{xy} \end{bmatrix} = \begin{bmatrix} \dfrac{1}{E_x} & -\dfrac{\nu_{xy}}{E_x} & 0 \\[2ex] -\dfrac{\nu_{yx}}{E_y} & \dfrac{1}{E_y} & 0 \\[2ex] 0 & 0 & \dfrac{1}{2G_{xy}} \end{bmatrix} \begin{bmatrix} \sigma_x \\ \sigma_y \\ \sigma_{xy} \end{bmatrix} \tag{41}$$

With what is available above the value of the stiffness matrix [C] in the principal directions would be

69

$$[C] = \begin{bmatrix} \dfrac{E_1}{1-v_{12}v_{21}} & \dfrac{v_{12}E_2}{1-v_{12}v_{21}} & 0 \\ \dfrac{v_{21}E_1}{1-v_{12}v_{21}} & \dfrac{E_2}{1-v_{12}v_{21}} & 0 \\ 0 & 0 & G_{12} \end{bmatrix}$$

(42)

$$= \begin{bmatrix} -5.891e10 & -6.550e10 & 0 \\ -6.550e10 & -2.902e10 & 0 \\ 0 & 0 & 1.365e10 \end{bmatrix}$$

The stiffness matrix above has negative values where they do because of the high v_{12} and v_{21} values, see table: 4.8 below the latter is 0.623. The negative values indicate that energy was produced in the work done in moving the developed stress through the strain.

Wang and Lake [39] have it that negative stiffness is possible when systems are preloaded and in this experiment or tests the samples were preloaded without knowing it. This was so because the samples were constrained at both ends before the loads were applied and this was in a bid to have a good grip of the samples by the gripping components of the test rig. So in essence the samples could not be loaded without preloading them with the epoxy adhesive and the plugs. At the same time it was not very clear if these contributed to any preloading. Again the extensometer that was placed on the sample to read the displacement or extension could also have contributed some force. The supposed deformations brought about by the pre-loadings were not far reaching and the samples normally returned to their normal lengths hence the deformations were unstable and this instability could be pointing to negative stiffness as Wang and Lake put it [39]. In their own illustration they talked about the material returning to a new shape not to the normal length as were the case here. Above all these may not be the reasons for the negative stiffness elements we have in the matrix above.

Jaglinski and Lakes [40] described negative stiffness as the result of the change in direction from the norm of the resulting deformations caused by the prevailing or imposed forces and can possibly be sustained by physical constraints [40].

Material Properties	Values
E_X	0.8894e14 (GPa)
E_Y	0.4382e14 (GPa)
E_Z	0.3066e14 (GPa)
v_{12}	2.257
v_{23}	1
v_{13}	2.257
G_{XY}	0.1365e14 (GPa)
G_{YZ}	0.7664e13 (GPa)
G_{XZ}	0.1365e14 (GPa)

Table: 4.8. The determined engineering constants for the tubular composite

Table: 4.8 above contains the engineering constants-Young's Moduli, Poisson's ratios and Bulk moduli. These values were determined by taking the averages of the respective moduli and ratios based on what was obtainable in the previous tables above.

Young's Modulus values E_2 and E_3 were measured in the same way across the fibre hence they are equal [39]. With the foregoing this implies that $v_{13} = v_{12}$ so equally $v_{31} = v_{21}$.

Also the samples were assumed to have identical deformations irrespective of whether shear stresses are applied or not due to the fact that the same orientation exists for the samples onto which these shear stresses τ_{12} and τ_{13} were applied; as a result $G_{12} = G_{13}$ [38].

Maximum Load Value from Experiment (KN)	Maximum Stress Value from Experiment (MPa)	Stress Intensity Element Solution (KPa)
1.262	178.5	15.433
2.142	303.1	26.318
3.991	564.6	48.991
4.693	664	57.640

7.638	1081	93.762

Table: 4.9. Comparing experimental values with numerical values.

To determine E_x we have to refer back again to the test data to the cases where the maximum loads were no more than 2.142 KN, see table: 4.4 and table: 4.9 above, we also refer to the second Poisson's ratio that was adopted above and its associated parameters-maximum stresses and elastic modulus. So the average of σ_x was determined as well as that of ε_x from the sample described or noted above for the first case, in the second case only the data or values from the compressive tests are used.

Then:

$$E_x = \frac{\sigma_x}{\varepsilon_x} \quad (43)$$

1st case:
$$E_x = \frac{158.7729 MPa}{0.0021} = 75606.1429 MPa \quad (44)$$

2nd case:
$$= \frac{215.0333 MPa}{0.0024} = 89597.2083 MPa \quad (45)$$

Also

$$E_y = \frac{\sigma_y}{\varepsilon_y} \quad (46)$$

Here reference was made to the results data where there was only one test result for transverse loading as a result the value below is also the same for the second case. See table: 4.4.

$$E_y = \frac{168.6}{0.0055} = 30654.5455 MPa \quad (47)$$

To determine G or the shear or rigidity modulus we have to use the expression below:

$$G = \frac{E}{2(1+v)} \quad (48)$$

In order to determine G the value of E_x was used.

1st case: $$G = \frac{75606.1429 GPa}{2(1+0.381818)} = 27357.4895 MPa \tag{49}$$

2nd case: $$= \frac{89597.2083}{2(1+0.4363)} = 31190.2835 MPa \tag{50}$$

4.4. Carbon fibre Phenolic composite fabric

4.4.1. Testing Carbon fibre Phenolic composite fabric

The fabric was manufactured by SGL group and is of the Twill 2/2 type and contains a Phenolic resin. It normally comes uncured meaning it has minimal stiffness and the resin not sufficiently bound to the fibres, in other to give it some stiffness the fabric or prepreg had to be cured. In curing it care was taken to ensure that the prepreg turned out in the desired form or shape. In other to achieve this in this case some pressure was applied to the prepreg while the curing was taking place. This pressure was applied by means of dead weights and the oven was heated to 350°c before the prepregs were introduced and were left there to cure for 20 minutes. The prepreg was actually cut to 300mm X 50mm strips and stacked up to four layers before they were cured, and later machined to produce the dumbbell test strips. It must be noted that the first strip that was tested did not meet the standards set by the machined lot. In this strip that did not meet the standards aluminium tabs were placed at both ends of the strip and held in place with the aid of an epoxy adhesive and was left to set for one week.

Fig: 4.34a. Picture of the poorly made dumbbell strip with aluminium tabs

The purpose of the using the aluminium tabs was to safeguard the test strip from being damaged by the grips of the test rig. When the standardized test strips were produced they seemed sturdy enough to withstand the pressure from the grips, so no tabs were placed on them as such the strip that was tested had no tabs.

At the initial stage two tensile tests were carried out on the poorly made test strips (see fig: 4.34a) and the third on the standardized strip. The graph below is the graph of load against displacement for the better of the initial two tests as the other was not adequate.

Graph of Load vs Displacement
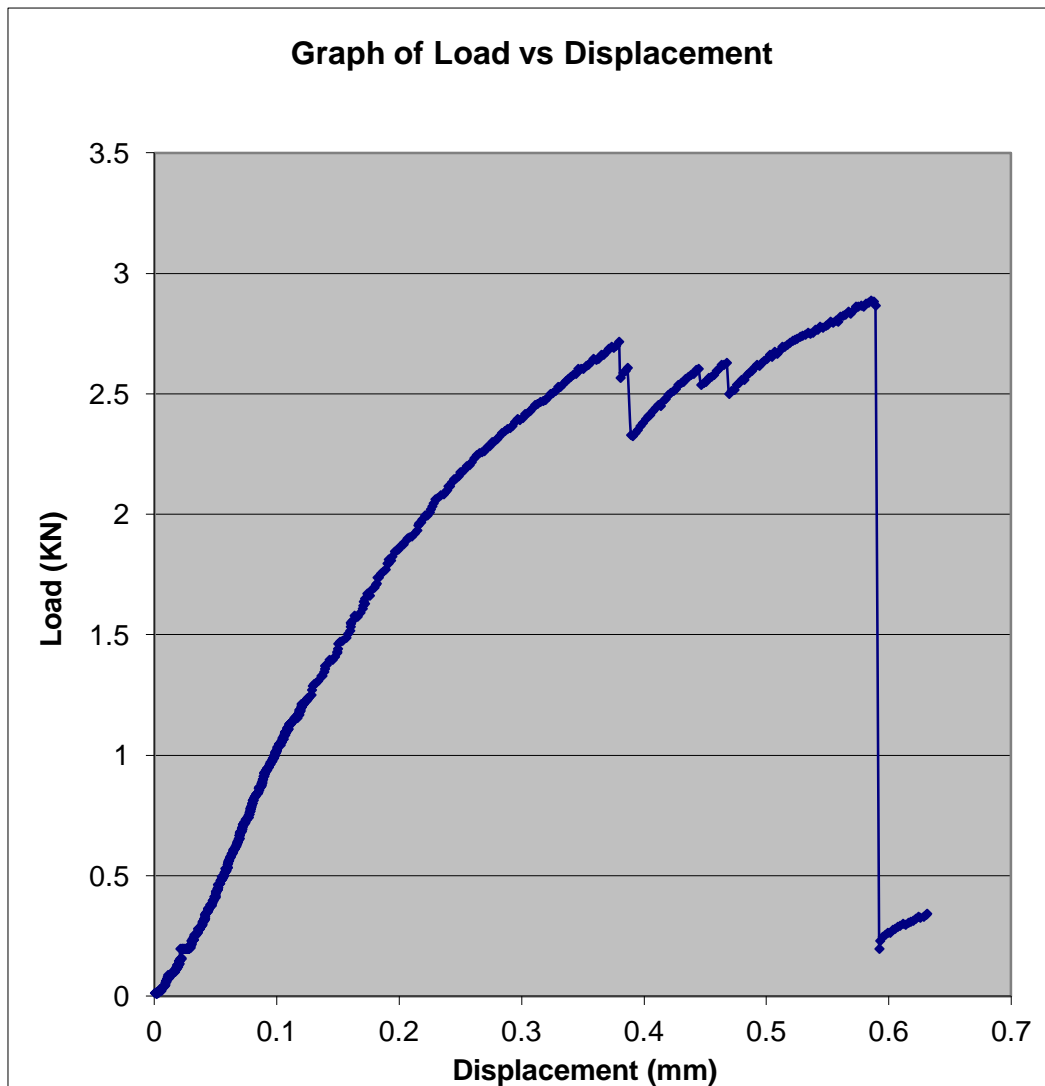
Fig. 4.35. The test whose graph is above produced a maximum load of 2.888 KN and a maximum displacement of 0.63111 mm.

In fig: 4.35 above a graph of 745 data points were used which was also what was saved from the test, hence the thickness of the curve. The load when initiated rose from zero and reached 2.7172 KN at a displacement of 0.3794 mm as can be seen then dropped to 2.3257 KN while the displacement increased to 0.3906 mm. This drop in load was brought about by some slight delamination of one or more of the laminates. The test strip could still sustain more load after this delamination as such the load rose yet again to 2.888 KN with an increased displacement of 0.63111 mm albeit with further load decrease; see fig 4.40 for the damaged

strip. At this maximum load the strip failed in a major way due to more significant delamination, but the load did not drop off sharply as can be seen above indicating this delamination or damage was a gradual one at those points. This drop in load was also a significant one as it fell to 0.1971 KN though it still began to rise again; the test was ended at that point.
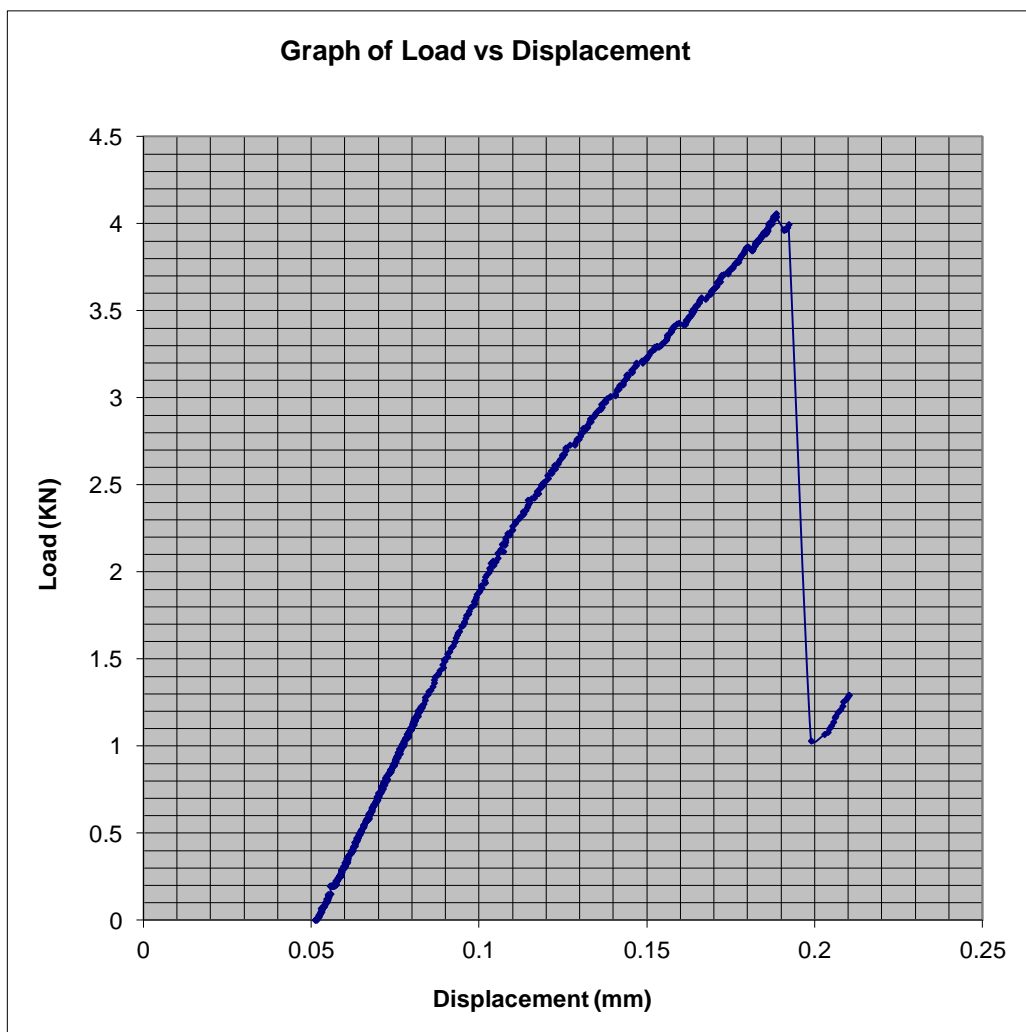

Fig: 4.36. The test whose graph is above produced a maximum load of 4.0585 KN and a maximum displacement of 0.2102 mm.

The graph above in fig: 4.36 is a graph of load against displacement as can be seen, for the data acquired from the tensile loading test of the standardised strip. The load for some reason was flat while some displacement of up to 0.05 mm occurred as can be seen. In this case no failure occurred; the test was ended because what was need was a significant curve that would produce the Young's modulus. The load climbed steeply to 2.2882 KN at a displacement of 0.1108 mm and over a displacement range of only 0.0608 mm- 0.1108 mm before some yielding began to occur in the strip, and then went further to reach 4.0585 KN

75

over a displacement of 0.1602 mm but at 0.2102 mm displacement value; see fig 4.41 for the strip used in this case.
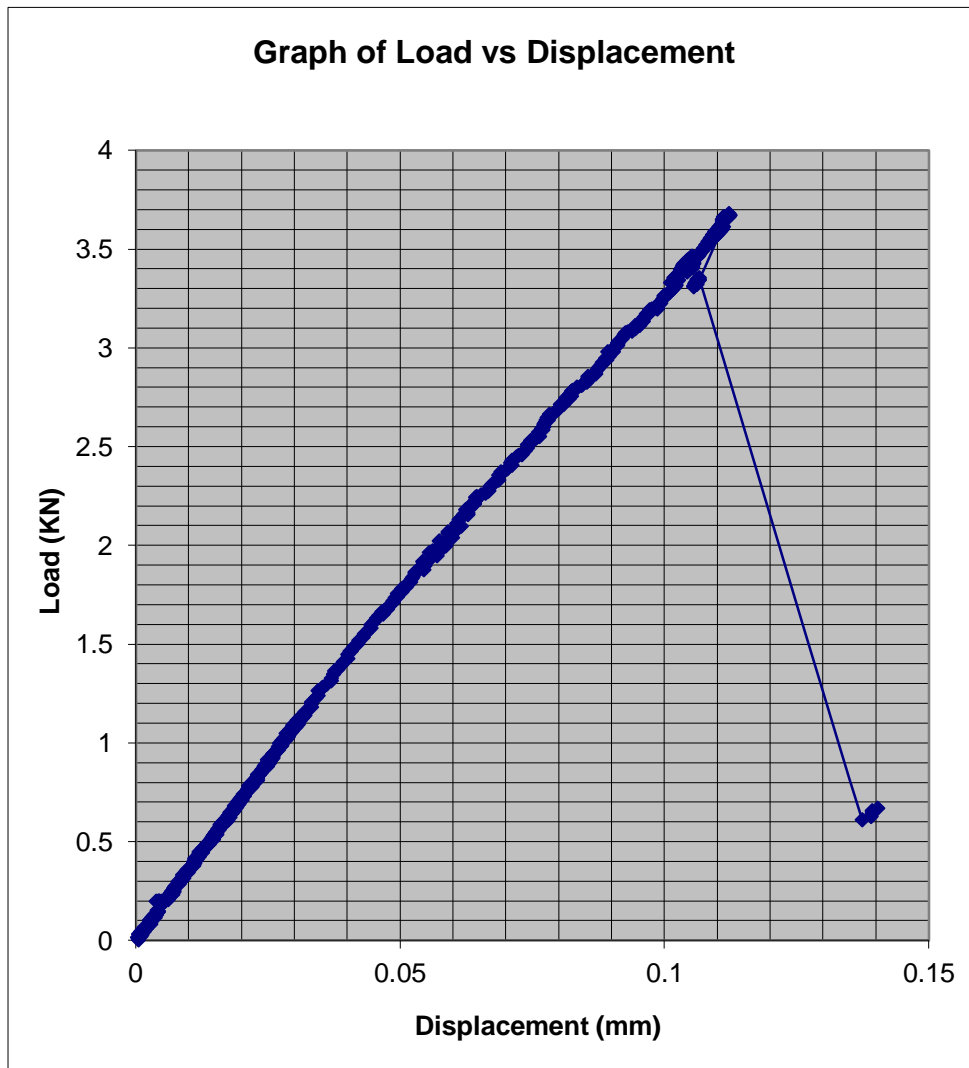

Fig. 4.37. The test whose graph is above produced a maximum load of 3.682 KN and a maximum displacement of 0.1123 mm.

In the case in fig: 4.37, the load climbed steadily up to the maximum 3.682 KN over a displacement of 0.1123 mm but the strip failed at the lower gripped end with one or two yarns splitting from the fabric weave.

In the next test case whose graph is below in fig: 4.38 the extensometer switch value is 1.0% - meaning that the extensometer is expected to be disconnected or removed from the test process after an extension of 1.0%. It is also at this point that the computer calculates the Young's modulus; as a result this extensometer value can influence the value of the Young's modulus, it has to be set by the user so the 1.0% we have was actually set. The samples were

all from the same stock but they never had the same Young's modulus though they failed at about the same load range, so one can see that a particular sample may have a high Young's modulus if it succeeds in sustaining a lot more load and again if the extensometer switch value was set high; this is not always the case but it was in this test case whose graph is below in fig: 4.38. In this case the load continued and the switch for the extensometer did not come into play, so the material failed and the test ended the computer then calculated the Young's modulus using possibly the entire length of the curve hence the high modulus value of 53180 MPa. In the test the load was initiated at 0.0018 KN and it made a steady and continuous rise to the maximum 4.1789 KN though changing path due to a levelling- 3.4966 KN that occurred twice at different displacement values of 0.1245 mm and 0.1251 mm respectively. At 4.1789 KN it dropped to 4.0083 KN after which it picks up again to reach 4.1082 KN, this load drop equally occurred twice. The first drop in load occurred after 3.9250 KN to 3.8002 KN from where it then rose to the peak load mentioned above. At this first load drop point the sample developed some amount of fibre damage which came with a slight cracking noise; on getting to the maximum load this noise seemed to remain and with the sample now weak at the bottom of the stem which is also the area where such damage always occurred in this kind of test the load began to dither at the same time dropping until it dropped to 2.6354 KN at which point a very significant cracking noise was heard and the load collapsed to 0.2972 KN. At this point the sample could not sustain any relatively significant load so the test was stopped.
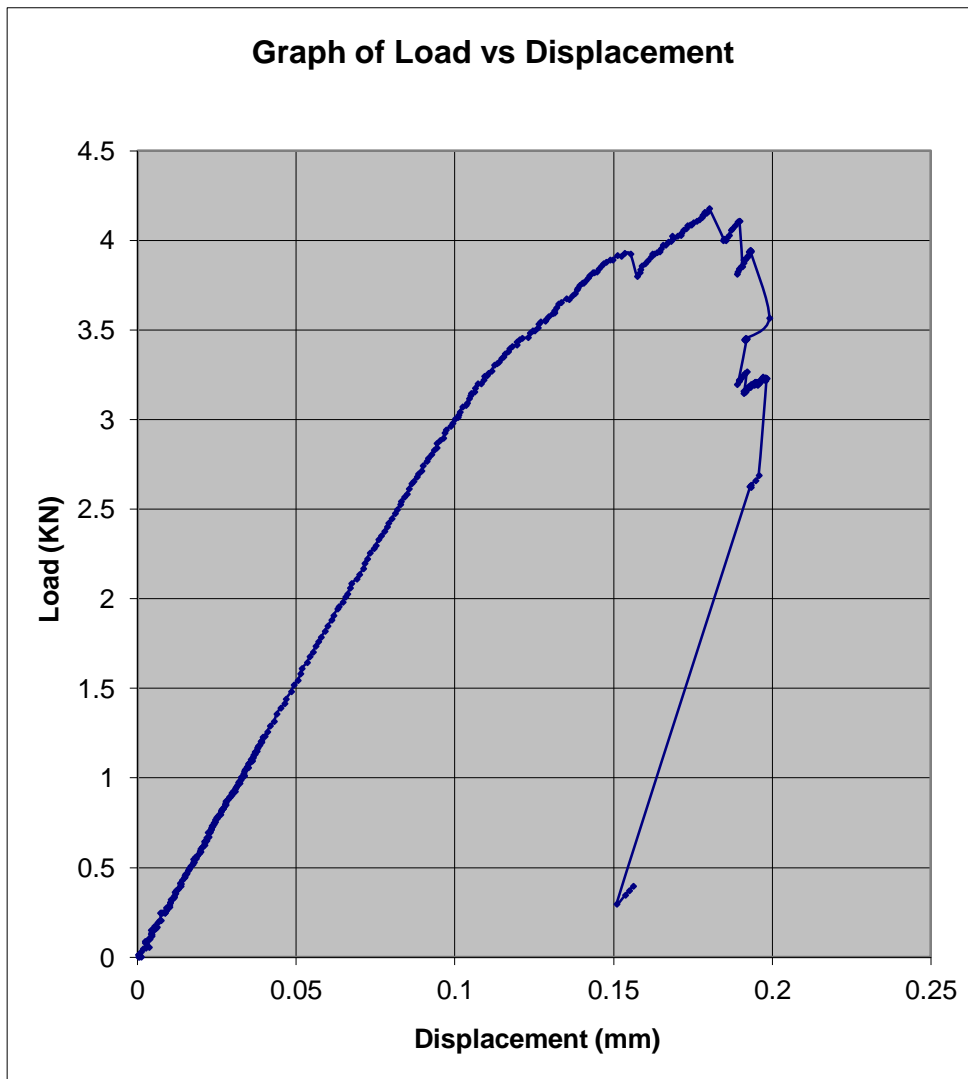
Fig: 4.38. Graph of load against displacement whose maximum load and extension are 4.1789 KN and 0.1991 mm respectively.

In the next tensile test case whose graph is below in fig: 4.39 some dithering in load can also be observed. The same kind of observation we just read about was also recorded for this test case as regards failure. The maximum load reached 4.3661 KN at a displacement of 0.1917 mm from a steady and consistent load increase though there seemed to be a slight dent in the curve right after 3.0972 KN load point. After that load point the following displacement and load values were recorded respectively see table: 4.9a below:

Displacement (mm)	Load (KN)
0.123615	3.109653
0.12424	3.122134
0.125283	3.142936
0.125323	3.142936

Table: 4.9a. Recorded Load and Displacement Values

So as can be seen from table: 4.9a these load values were roughly the same up to 1 decimal place, up to 2 decimal places there was progression but for the last two load values which are absolutely the same. In the case of the displacements this is also the case; up to 3 decimal places the first two values were the same then there was a progression to the last two which are nearly equal. This case above explains the slight dent observed in the curve below.
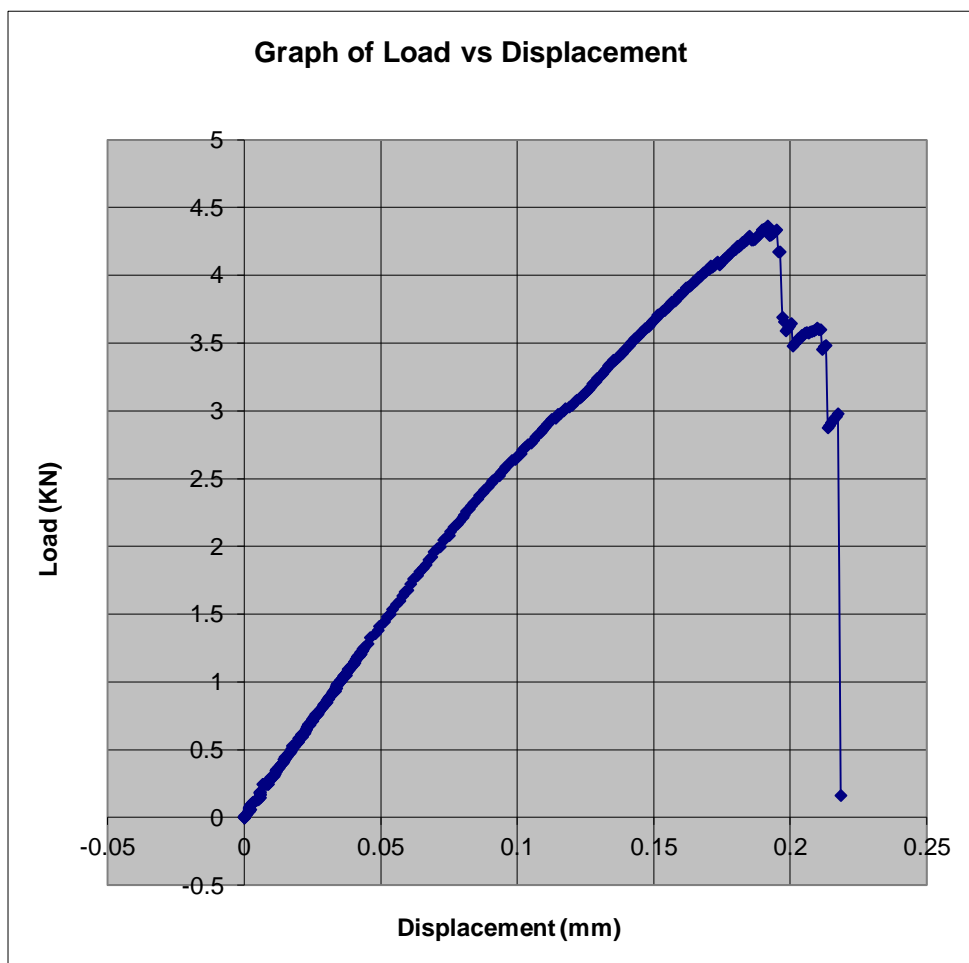

Fig.4.39. Graph of load against displacement whose maximum load an extension are 4.3661 KN and 0.2185 mm respectively.

Three more tensile tests were carried out so as to substantiate the quality of the derived conclusions regarding the properties of the structure or material.

Fig: 4.40. Damaged sample from the first of the three tests mentioned above.

Fig: 4.41. Damaged sample from the second of the three tests mentioned above.
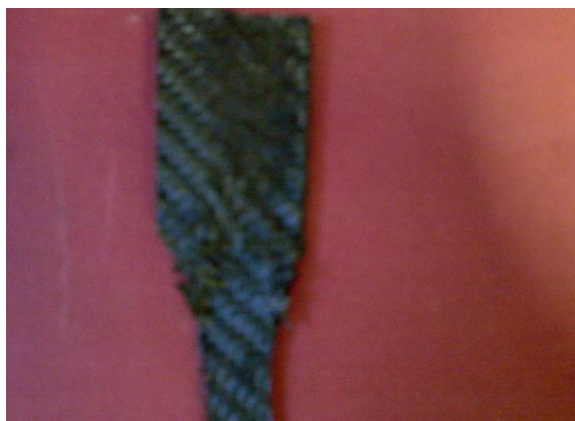
Fig: 4.42. Damaged sample from the last of the three tests mentioned above.

The sample in the last test whose picture is equally that of Fig: 4.42 above as one can see was mistakenly left to cure for 2 hours instead of 20 minutes. This left the sample damaged to

some extent; note that the curing temperature was 350°C. This damage may have affected the strength of the sample as it produced a lower Young's modulus value. The other two samples were equally cured longer than normal-10 minutes longer, the normal is 20 minutes.
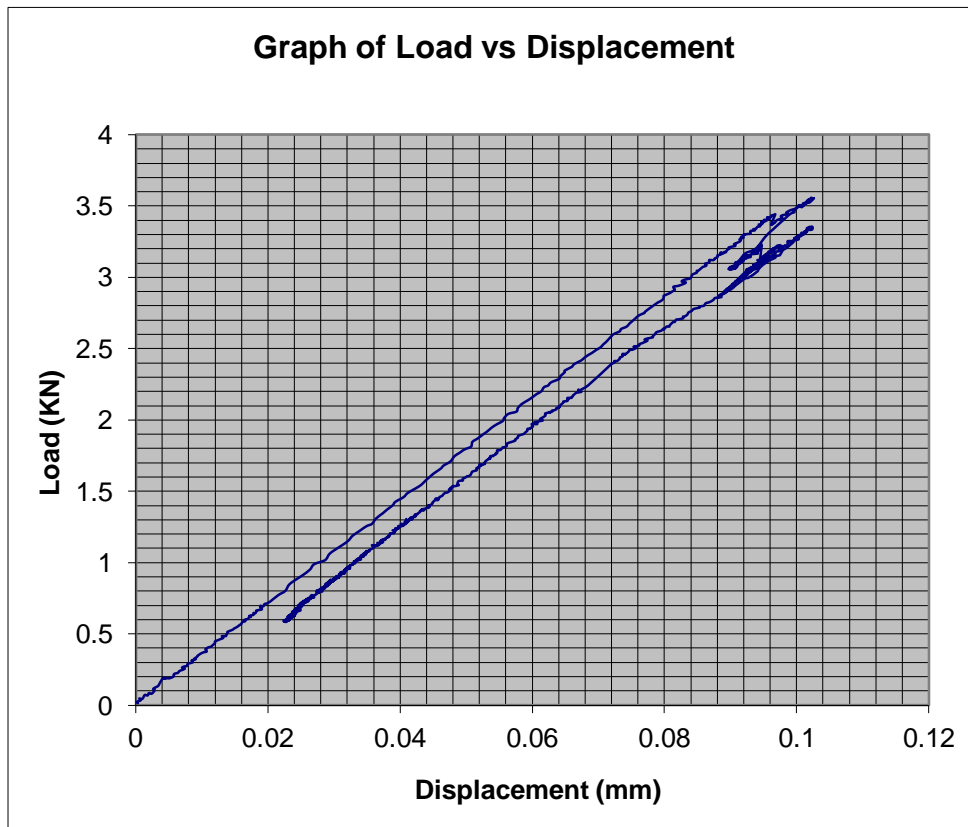

Fig: 4.43. Graph of load against displacement whose maximum load and extension are 3.5596 KN and 0.0226 mm respectively.

From the graph in fig: 4.43 above we can see that the load went steadily from 0 to 3.4430 KN and dropped to 3.3722 KN and finally reached the 3.5596 KN peak after which it drops to 3.0598 KN and made an attempt to reach another peak. The loading and its drop was a gradual one which is why the curve of the graph is in the form of two parallel lines joined at undulating ends. The drop in load from 3.4430 KN to 3.3722 KN and the attempt to peak is known as negative stiffness. Bear in mind that the sample in this test got damaged and there was a sudden drop in load as can be seen from the nature of the curve. Note also the relatively small maximum displacement.
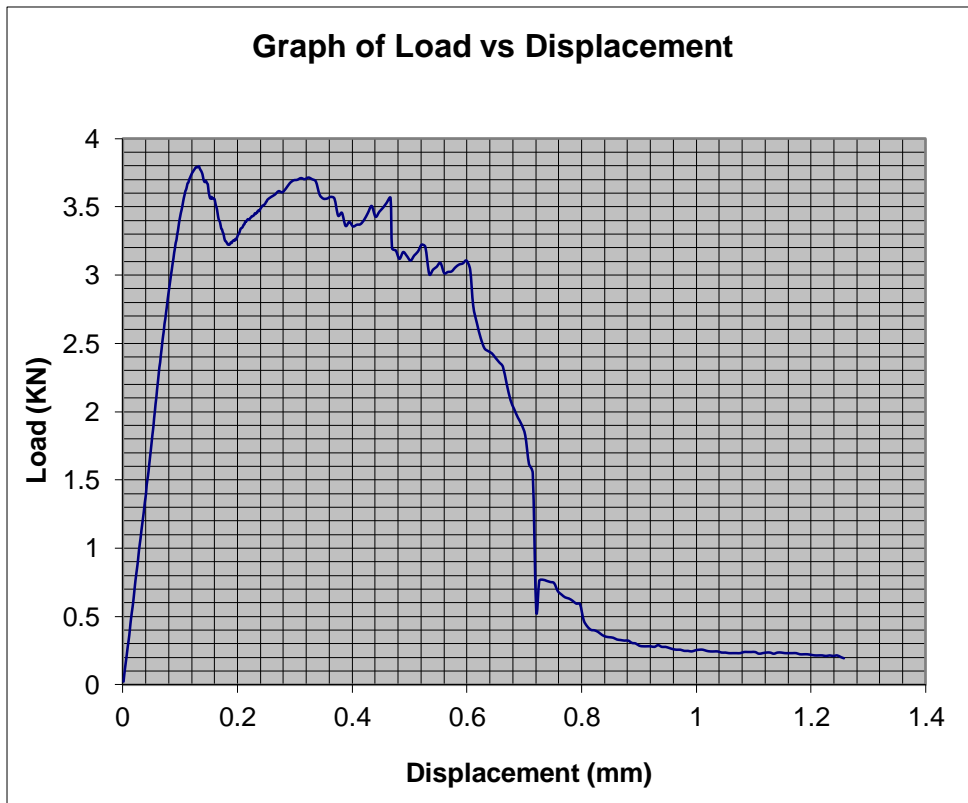
Fig: 4.44. Graph of load against displacement whose maximum load and extension are 3.7969 KN and 1.2579 mm respectively.

One can see that the graph in fig: 4.44 above is significantly different from the previous one also notice the high displacement of 1.2579 mm relative to that of the previous case. The loading and its drop were equally gradual up until there was a significant damage at 1.5481 KN from where the load dropped to 0.5445 KN and continued to drop.
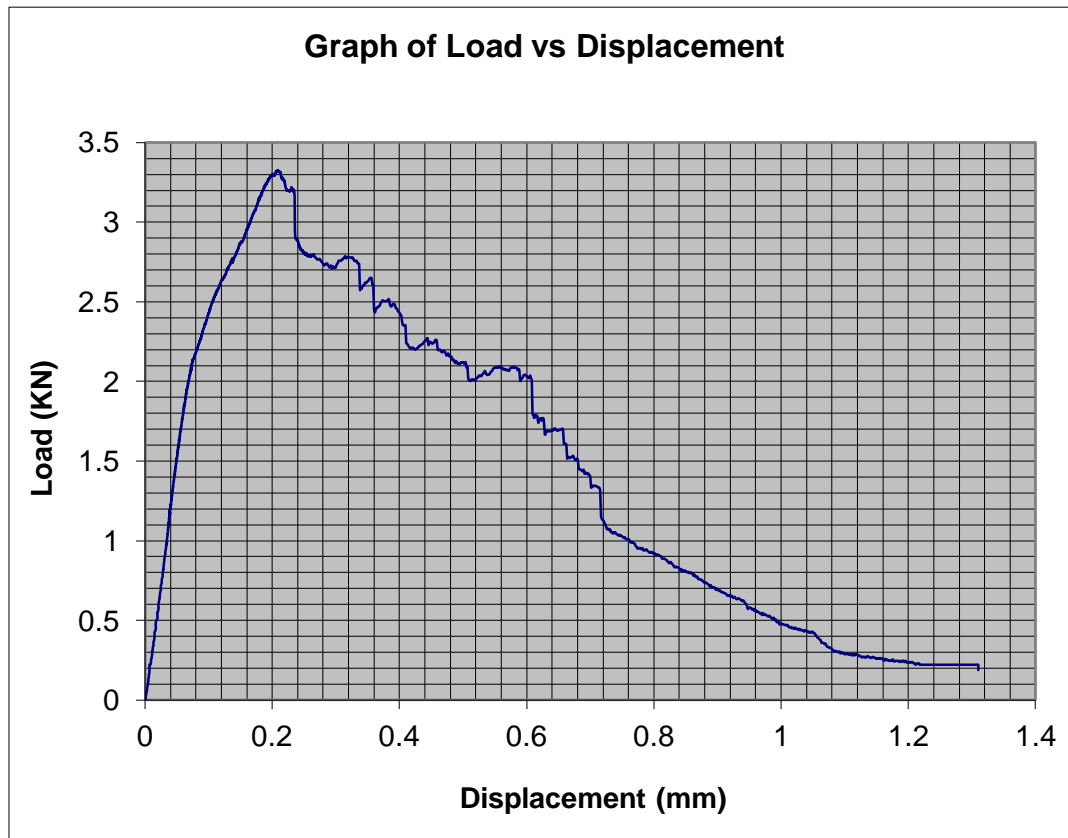
Fig. 4.45. Graph of load against displacement whose maximum load and extension are 3.3255 KN and 1.3103 mm respectively.

In the graph of fig: 4.45 above one can see that once the load reached its peak of 3.3255 KN there was no other substantial bid for the peak again; it began to decay while undulating as well until it dropped to a major low where the test was stopped. Note also that this graph is that of the material that was over cured: it seems that this very long curing time did not affect the strength of the material as it withstood as much load as other samples in the previous tests. Over curing leads to yet more Carbonization and damage; which can affect the elastic strength of materials, so it was suspected that this over cured sample may show such a tendency. The over curing of this sample was not the intended outcome it was expected to cure for as long as the other samples did. See tables: 4.12 and 4.13 below and see what the material properties derived from this sample looks like.

4.4.2. Constitutive Model of the Carbon fibre prepreg or fabric

The software for controlling the test determines the Young's modulus value and in the first case the value was 39790 MPa. Since the load was applied in what was known to be the

longitudinal direction though it has a fibre direction whose inclination was 0° or 90° or perpendicular hence that value was regarded as E_1 or E_x.

In order to determine the other properties they have to be obtained using some know formulae.

$$v_{12} = \frac{\varepsilon_x E_x}{\sigma} \quad (51)$$

$$v_{21} = \frac{\varepsilon_x}{\varepsilon_y} \quad (52)$$

$$\varepsilon_y = \varepsilon_x v_{12} \quad (53)$$

$$E_y = \frac{v_{21} E_x}{v_{12}} \quad (54)$$

$$\gamma_{12} = 2\varepsilon_{12} \quad (55)$$

$$\tau_{12} = -\sigma_x \sin\theta\cos\theta \quad (56)$$

$$G_{12} = \frac{\tau_{12}}{\gamma_{12}} = \frac{E_x}{2(1+v_{12})} \quad (57)$$

The stress that was applied to the material described above was a plane stress in the 1-2 directions. Hence the strain-stress and stress-strain relation can be written thus:

$$\begin{bmatrix} \varepsilon_1 \\ \varepsilon_2 \\ \gamma_{12} \end{bmatrix} = \begin{bmatrix} S_{11} & S_{12} & 0 \\ S_{12} & S_{22} & 0 \\ 0 & 0 & S_{66} \end{bmatrix} \begin{bmatrix} \sigma_1 \\ \sigma_2 \\ \tau_{12} \end{bmatrix} \quad (58)$$

Where

$$S_{11} = \frac{1}{E_1} = 2.5132e - 5MPa \quad (59)$$

$$S_{22} = \frac{1}{E_2} = 4.6185e - 5MPa \quad (60)$$

$$S_{12} = -\frac{v_{12}}{E_1} = -\frac{v_{21}}{E_2} = -3.4069e - 5MPa \tag{61}$$

$$S_{66} = \frac{1}{G_{12}} = 1.1840e - 4MPa \tag{62}$$

$$\varepsilon_1 = \frac{l}{L} = 0.0054 \tag{63}$$

$$\varepsilon_2 = \varepsilon_x v_{12} = 0.0073 \tag{64}$$

$$\sigma_1 = 158.5MPa(Given)$$

$$\sigma_2 = E_y \times \varepsilon_y = 158.0592MPa \tag{65}$$

$$\tau_{12} = -\sigma_x \sin\theta \cos\theta = 0 \tag{66}$$

$$\gamma_{12} = \frac{\tau_{12}}{G_{12}} = 0$$

So we have

$$\begin{bmatrix} 0.0054 \\ 0.0073 \\ 0 \end{bmatrix} = \begin{bmatrix} 2.5123e - 5 & -3.4069e - 5 & 0 \\ -3.4069e - 5 & 4.6185e - 5 & 0 \\ 0 & 0 & 1.1840e - 4 \end{bmatrix} \begin{bmatrix} 158.5 \\ 158.0592 \\ 0 \end{bmatrix} MPa \tag{67}$$

And

$$\begin{bmatrix} \sigma_1 \\ \sigma_2 \\ \tau_{12} \end{bmatrix} = \begin{bmatrix} Q_{11} & Q_{12} & 0 \\ Q_{12} & Q_{22} & 0 \\ 0 & 0 & Q_{66} \end{bmatrix} \begin{bmatrix} \varepsilon_1 \\ \varepsilon_2 \\ \gamma_{12} \end{bmatrix} \tag{68}$$

Where

$$Q_{11} = \frac{E_1}{1 - v_{12}v_{21}} = -1523.4MPa \tag{69}$$

$$Q_{22} = \frac{E_2}{1 - \nu_{12}\nu_{21}} = -828.94 MPa \tag{70}$$

$$Q_{12} = \frac{\nu_{12}E_2}{1 - \nu_{12}\nu_{21}} = \frac{\nu_{21}E_1}{1 - \nu_{12}\nu_{21}} = -1123.7 MPa \tag{71}$$

$$Q_{66} = G_{12} = 8445.8312 MPa \tag{72}$$

Hence we have below

$$\begin{bmatrix} 158.5 \\ 158.0592 \\ 0 \end{bmatrix} = \begin{bmatrix} -1523.4 & -1123.7 & 0 \\ -1123.7 & -828.94 & 0 \\ 0 & 0 & -8445.8312 \end{bmatrix} \begin{bmatrix} 0.0054 \\ 0.0073 \\ 0 \end{bmatrix} MPa \tag{73}$$

The expressions above are for the first test case, so for the second case we have:

$$S_{11} = \frac{1}{E_1} = 2.8313e - 5 MPa \tag{74}$$

$$S_{22} = \frac{1}{E_2} = 3.4588e - 5 MPa \tag{75}$$

$$S_{12} = -\frac{\nu_{12}}{E_1} = -\frac{\nu_{21}}{E_2} = -3.1293e - 5 MPa \tag{76}$$

$$S_{66} = \frac{1}{G_{12}} = 1.1921e - 4 MPa \tag{77}$$

$$\varepsilon_1 = \frac{l}{L} = 0.0045 \tag{78}$$

$$\varepsilon_2 = \varepsilon_x \nu_{12} = 0.005 \tag{79}$$

$$\sigma_1 = 143.8 MPa (Given) \tag{80}$$

$$\sigma_2 = E_y \times \varepsilon_y = 144.5580 MPa \tag{81}$$

$$\tau_{12} = -\sigma_x \sin\theta \cos\theta = 0 \tag{82}$$

$$\gamma_{12} = \frac{\tau_{12}}{G_{12}} = 0 \tag{83}$$

So we have

$$\begin{bmatrix} 0.0045 \\ 0.005 \\ 0 \end{bmatrix} = \begin{bmatrix} 2.8313e-5 & -3.1293e-5 & 0 \\ -3.1293e-5 & 3.4588e-5 & 0 \\ 0 & 0 & 1.1921e-4 \end{bmatrix} \begin{bmatrix} 143.8 \\ 144.5580 \\ 0 \end{bmatrix} MPa \tag{84}$$

And

$$\begin{bmatrix} \sigma_1 \\ \sigma_2 \\ \tau_{12} \end{bmatrix} = \begin{bmatrix} Q_{11} & Q_{12} & 0 \\ Q_{12} & Q_{22} & 0 \\ 0 & 0 & Q_{66} \end{bmatrix} \begin{bmatrix} \varepsilon_1 \\ \varepsilon_2 \\ \gamma_{12} \end{bmatrix} \tag{68}$$

Where

$$Q_{11} = \frac{E_1}{1 - v_{12} v_{21}} = 1006.5546 MPa \tag{85}$$

$$Q_{22} = \frac{E_2}{1 - v_{12} v_{21}} = 823.9269 MPa \tag{86}$$

$$Q_{12} = \frac{v_{12} E_2}{1 - v_{12} v_{21}} = \frac{v_{21} E_1}{1 - v_{12} v_{21}} = 910.6864 MPa \tag{87}$$

$$Q_{66} = G_{12} = 8388.3532 MPa \tag{88}$$

Hence we have below

$$\begin{bmatrix} 143.8 \\ 144.5580 \\ 0 \end{bmatrix} = \begin{bmatrix} 1006.5546 & 910.6864 & 0 \\ 910.6864 & 823.9269 & 0 \\ 0 & 0 & 8388.3532 \end{bmatrix} \begin{bmatrix} 0.0045 \\ 0.005 \\ 0 \end{bmatrix} MPa \tag{89}$$

It must be noted that the modulus, stress and strain values used in the strain-stress relations and vice versa were the ones determined by the processing module of the test equipment. The test equipment has an extensometer gauge length which is 25mm; this is the length at the

middle of the test specimen it gauges for strain, stress and possibly loads, this is also the length from which the maximum stress and strain as well as the displacement at maximum load values are taken from. This does not seem to be the case for the elastic modulus even though the obtained values have been adopted. Working with these values from the test one would find out that the modulus is much lower that the displayed value, in other words a different methodology was used by the equipments processor to determine these elastic modulus values. This was the case with all the tests carried out using this test equipment.

Furthermore the test cases above were simulated using ANSYS and the first test case turned out to be the most satisfactory. In doing so a rectangular model of 25mm by 16mm by 1.6mm was created and meshed (see fig: 4.39 below), and then a load of 4.058 KN was applied in the X-direction.
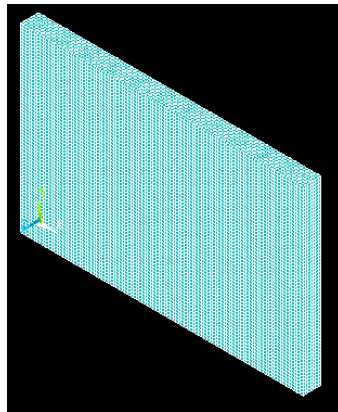

Fig: 4.39. Meshed rectangular model.

Element Type

The Element type adopted in this analysis was Solid and the type was Solid-45

Meshing

Hexahedra and wedge elements were used consisting of:

1 Volume

52520 Nodes

44800 Elements

Element Edge Length: 0.25e-3 m

Displacement

UX = 0.0001360 mm

UY = 0

UZ = 0

Load

FX = 4.058e3 N   (Force of 4.058e3 N was applied in the X-direction)

The displacement and the load values were from the test results meaning the maximum displacement was 0.136e-3 m while the maximum load was 4.058e3 N. The maximum stress value from the test was 158.5 MPa while that of the simulation was 158.267 MPa. So all the results were almost the same apart from the strain values that were significantly divergent which was due to the fact the simulation might exaggerate the strain as other physical conditions could not be sufficiently accounted for; and on the other hand the fact that the structure was likely to have defects or imperfections that can affect the strain values.

With the foregoing the first test case was adopted as a standard for the time being, that means the E_x value of 39790 MPa is the value that is currently been worked with. Therefore E_y can be determined using the expression below:

$$E_y = \frac{v_{21}E_x}{v_{12}}$$

Using the above expression E_y is 21651.9529 MPa, but v_{12} is greater than 0.5 which of course occurs in composites. Employing this value as the Young's modulus and using the same ANSYS routine used in the case described above and applying the load in the Y-direction a maximum stress value for the Y-direction that was half of that of the X-direction was obtained. In other to ascertain the number of planes of symmetry in this structure the same ANSYS routine was employed again to determine E_z and also to validate E_y. The validation turns out to be inaccurate i.e. E_y value from the simulation was not the same with that derived using the test values.

Interestingly the E_x value obtained from the test and the derived E_y value together with the Poisson's ratios meets the engineering restrictions which goes thus:

$$v_{12} \leq \sqrt{\frac{E_1}{E_2}}$$

This goes to say that those values can be used in engineering applications, so can the values derived using the routine described above in ANSYS simulations to determine the material properties of the structure; they equally meet the above restriction. All these give credence to the $E_x = 39790$ MPa value that has been adopted as the value that most represents the Young's modulus of this structure in the X-direction based on the conditions of the test. This is so because the v_{12} value above was employed in the simulation as the materials Poisson's ratio. It must be noted that based on the values that were obtained from these simulations that E_y was less than E_z. See below the values

$$E_x = 44834.8442 MPa$$
$$E_y = 40252.4725 MPa$$
$$E_z = 42593.7873 MPa$$

There is a departure from the norm-though not unusual- which is that E_y is normally greater than or equal to E_z. The reason for this not hard to see; to obtain E_z using the same kind of sample the sample would have to be folded possibly at the mid-section and a tensile load applied. With that it is even expected that one would obtain an E_z value equal to E_x. In one of the many simulations that was run using ANSYS an attempt was made to run a simulation with only E_x and E_y values knowing quite well that it may not work; ANSYS suggested nine orthotropic material values where E_y was less than E_z and equal to E_x. This goes to show that it is possible to have a constitutive model where the case described above exists. Interesting enough in the same ANSYS suggestion the three shear moduli were all equal, this was also the case for the set of elastic moduli values we have stated above, the shear moduli that are associated with them are equal to each other though not absolutely, see the values below.

$$G_{xy} = 1329.2 MPa$$
$$G_{xz} = 1322.6 MPa$$
$$G_{yz} = 1330 MPa$$
$$v_{xy} = 1$$
$$v_{xz} = 1$$
$$v_{yz} = 1.0031$$

These set of values above were obtained from the simulations carried out using ANSYS and the Poisson's ratios were determined with the general expression below:

$$v = \frac{\varepsilon E}{\sigma}$$

It must be noted that in ANSYS simulations the Poisson's ratio values used were 0.4999 this is because ANSYS would not be able to work with values higher than 0.5. The reason why a very high Poisson's ratio was obtained was because of errors in its computation; there was in consistency in the units of the values used hence the high value. After correcting the errors the Poisson's ratio turned out to be:

$$v_{12} = 0.0014$$

This value falls into place going by the values of the related displacement and strain respectively. Stated below are the Poisson's ratio values from the other tests.

$$v_{12} = 0.0011$$
$$v_{12} = 0.0013$$
$$v_{12} = 0.0013$$

So the strain-stress and stress-strain relations for the test cases can be rewritten as:

$$\begin{bmatrix} \varepsilon_1 \\ \varepsilon_2 \\ \gamma_{12} \end{bmatrix} = \begin{bmatrix} S_{11} & S_{12} & 0 \\ S_{12} & S_{22} & 0 \\ 0 & 0 & S_{66} \end{bmatrix} \begin{bmatrix} \sigma_1 \\ \sigma_2 \\ \tau_{12} \end{bmatrix} \quad (58)$$

$$S_{11} = \frac{1}{E_1} = 2.5100e - 11 MPa \quad (90)$$

$$S_{22} = \frac{1}{E_2} = 2.5130e - 11 MPa \quad (91)$$

$$S_{12} = -\frac{v_{12}}{E_1} = -\frac{v_{21}}{E_2} = 3.50e - 14 MPa \quad (92)$$

$$S_{66} = \frac{1}{G_{12}} = 5.0267e - 11 MPa \tag{93}$$

$$\varepsilon_1 = 0.315e - 13 \tag{94}$$

$$\varepsilon_2 = 0.291e - 13 \tag{95}$$

$$\sigma_1 = 1.255e - 9 MPa \tag{96}$$

$$\sigma_2 = 1.158e - 9 MPa \tag{97}$$

$$\tau_{12} = -\sigma_x \sin\theta\cos\theta = 0 \tag{98}$$

$$\gamma_{12} = \frac{\tau_{12}}{G_{12}} = 0 \tag{99}$$

So we have

$$\begin{bmatrix} 0.315e - 13 \\ 0.294e - 13 \\ 0 \end{bmatrix} = \begin{bmatrix} 2.5160e - 11 & 3.410e - 14 & 0 \\ 3.410e - 14 & 2.5214e - 11 & 0 \\ 0 & 0 & 5.0388e - 11 \end{bmatrix} \begin{bmatrix} 1.252e - 9 \\ 1.166e - 9 \\ 0 \end{bmatrix} MPa \tag{100}$$

$$\begin{bmatrix} \sigma_1 \\ \sigma_2 \\ \tau_{12} \end{bmatrix} = \begin{bmatrix} Q_{11} & Q_{12} & 0 \\ Q_{12} & Q_{22} & 0 \\ 0 & 0 & Q_{66} \end{bmatrix} \begin{bmatrix} \varepsilon_1 \\ \varepsilon_2 \\ \gamma_{12} \end{bmatrix}$$

Where

$$Q_{11} = \frac{E_1}{1 - \nu_{12}\nu_{21}} = 39841.2698 MPa \tag{101}$$

$$Q_{22} = \frac{E_2}{1 - \nu_{12}\nu_{21}} = 39793.8144 MPa \tag{102}$$

$$Q_{12} = \frac{\nu_{12}E_2}{1 - \nu_{12}\nu_{21}} = \frac{\nu_{21}E_1}{1 - \nu_{12}\nu_{21}} = 54 MPa \tag{103}$$

$$Q_{66} = G_{12} = 19893.6671 MPa \tag{104}$$

Hence we have below

$$
\begin{bmatrix} 1.255e-9 \\ 1.158e-9 \\ 0 \end{bmatrix} = \begin{bmatrix} 39841.2698 & 54 & 0 \\ 54 & 39793.8144 & 0 \\ 0 & 0 & 19893.6671 \end{bmatrix} \begin{bmatrix} 0.315e-13 \\ 0.291e-13 \\ 0 \end{bmatrix} MPa
$$

(105)

The expressions for the second case follow below:

$$
S_{11} = \frac{1}{E_1} = 2.8322e-11 MPa
$$

(106)

$$
S_{22} = \frac{1}{E_2} = 2.8304e-11 MPa
$$

(107)

$$
S_{12} = -\frac{v_{12}}{E_1} = -\frac{v_{21}}{E_2} = 3.13e-14 MPa
$$

(108)

$$
S_{66} = \frac{1}{G_{12}} = 5.6707e-11 MPa
$$

(109)

$$
\varepsilon_1 = 0.260e-13
$$

(110)

$$
\varepsilon_2 = 0.242e-13
$$

(111)

$$
\sigma_1 = 0.918e-3 MPa
$$

(112)

$$
\sigma_2 = 0.855e-3 MPa
$$

(113)

$$
\tau_{12} = -\sigma_x \sin\theta \cos\theta = 0
$$

(114)

$$
\gamma_{12} = \frac{\tau_{12}}{G_{12}} = 0
$$

(115)

So we have

$$
\begin{bmatrix} 0.260e-13 \\ 0.242e-13 \\ 0 \end{bmatrix} = \begin{bmatrix} 2.8322e-11 & 3.13e-14 & 0 \\ 3.13e-14 & 2.8304e-11 & 0 \\ 0 & 0 & 5.6707e-11 \end{bmatrix} \begin{bmatrix} 0.918e-3 \\ 0.855e-3 \\ 0 \end{bmatrix} MPa
$$

(116)

And

$$
\begin{bmatrix} \sigma_1 \\ \sigma_2 \\ \tau_{12} \end{bmatrix} = \begin{bmatrix} Q_{11} & Q_{12} & 0 \\ Q_{12} & Q_{22} & 0 \\ 0 & 0 & Q_{66} \end{bmatrix} \begin{bmatrix} \varepsilon_1 \\ \varepsilon_2 \\ \gamma_{12} \end{bmatrix}
$$

Where

$$
Q_{11} = \frac{E_1}{1 - \nu_{12}\nu_{21}} = 35307.6923 MPa
$$

(117)

$$
Q_{22} = \frac{E_2}{1 - \nu_{12}\nu_{21}} = 35330.5785 MPa
$$

(118)

$$
Q_{12} = \frac{\nu_{12}E_2}{1 - \nu_{12}\nu_{21}} = \frac{\nu_{21}E_1}{1 - \nu_{12}\nu_{21}} = 39 MPa
$$

(119)

$$
Q_{66} = G_{12} = 17634.3552 MPa
$$

(120)

Hence we have below

$$
\begin{bmatrix} 0.918e-3 \\ 0.855e-3 \\ 0 \end{bmatrix} = \begin{bmatrix} 35307.6923 & 39 & 0 \\ 39 & 35330.5785 & 0 \\ 0 & 0 & 17634.3552 \end{bmatrix} \begin{bmatrix} 0.260e-13 \\ 0.242e-13 \\ 0 \end{bmatrix} MPa
$$

(121)

The expressions for the third case follow below:

$$
S_{11} = \frac{1}{E_1} = 1.8745e-11 MPa
$$

(122)

$$
S_{22} = \frac{1}{E_2} = 1.8758e-11 MPa
$$

(123)

$$
S_{12} = -\frac{\nu_{12}}{E_1} = -\frac{\nu_{21}}{E_2} = 2.4811e-14 MPa
$$

(124)

$$S_{66} = \frac{1}{G_{12}} = 3.7658e - 11MPa$$

$$\tag{125}$$

$$\varepsilon_1 = 0.257e - 13$$

$$\tag{126}$$

$$\varepsilon_2 = 0.278e - 13$$

$$\tag{128}$$

$$\sigma_1 = 0.001371MPa$$

$$\tag{129}$$

$$\sigma_2 = 0.001482MPa$$

$$\tag{130}$$

$$\tau_{12} = -\sigma_x \sin\theta \cos\theta = 0$$

$$\tag{131}$$

$$\gamma_{12} = \frac{\tau_{12}}{G_{12}} = 0$$

$$\tag{132}$$

So we have

$$\begin{bmatrix} 0.257e - 13 \\ 0.278e - 13 \\ 0 \end{bmatrix} = \begin{bmatrix} 1.8745e - 11 & 2.4811e - 14 & 0 \\ 2.4811e - 14 & 1.8758 - 11 & 0 \\ 0 & 0 & 3.7658e - 11 \end{bmatrix} \begin{bmatrix} 0.001371 \\ 0.001482 \\ 0 \end{bmatrix} MPa$$

$$\tag{133}$$

And

$$\begin{bmatrix} \sigma_1 \\ \sigma_2 \\ \tau_{12} \end{bmatrix} = \begin{bmatrix} Q_{11} & Q_{12} & 0 \\ Q_{12} & Q_{22} & 0 \\ 0 & 0 & Q_{66} \end{bmatrix} \begin{bmatrix} \varepsilon_1 \\ \varepsilon_2 \\ \gamma_{12} \end{bmatrix}$$

Where

$$Q_{11} = \frac{E_1}{1 - v_{12}v_{21}} = 53346.3035MPa$$

$$\tag{134}$$

$$Q_{22} = \frac{E_2}{1 - v_{12}v_{21}} = 53309.3525MPa$$

$$\tag{135}$$

$$Q_{12} = \frac{v_{12}E_2}{1 - v_{12}v_{21}} = \frac{v_{21}E_1}{1 - v_{12}v_{21}} = 70.3375MPa$$

$$\tag{136}$$

95

$$Q_{66} = G_{12} = 26554.9628 MPa \qquad (137)$$

Hence we have below

$$\begin{bmatrix} 0.001371 \\ 0.001482 \\ 0 \end{bmatrix} = \begin{bmatrix} 53346.6304 & 70.3375 & 0 \\ 70.3375 & 53309.3525 & 0 \\ 0 & 0 & 26554.9628 \end{bmatrix} \begin{bmatrix} 0.257e-13 \\ 0.278e-13 \\ 0 \end{bmatrix} MPa \qquad (138)$$

The expressions for the fourth case follow below:

$$S_{11} = \frac{1}{E_1} = 2.0293e-11 MPa \qquad (139)$$

$$S_{22} = \frac{1}{E_2} = 2.0277e-11 MPa \qquad (140)$$

$$S_{12} = -\frac{v_{12}}{E_1} = -\frac{v_{21}}{E_2} = 2.5396e-14 MPa \qquad (141)$$

$$S_{66} = \frac{1}{G_{12}} = 4.0643e-11 MPa \qquad (142)$$

$$\varepsilon_1 = 0.277e-13 \qquad (143)$$

$$\varepsilon_2 = 0.293e-13 \qquad (144)$$

$$\sigma_1 = 0.001365 MPa \qquad (145)$$

$$\sigma_2 = 0.001445 MPa \qquad (146)$$

$$\tau_{12} = -\sigma_x \sin\theta\cos\theta = 0 \qquad (147)$$

$$\gamma_{12} = \frac{\tau_{12}}{G_{12}} = 0 \qquad (148)$$

So we have

$$\begin{bmatrix} 0.277e-13 \\ 0.293e-13 \\ 0 \end{bmatrix} = \begin{bmatrix} 2.0293e-11 & 2.5396e-14 & 0 \\ 2.5396e-14 & 2.0277-11 & 0 \\ 0 & 0 & 4.0643e-11 \end{bmatrix} \begin{bmatrix} 0.001365 \\ 0.001445 \\ 0 \end{bmatrix} MPa \quad (149)$$

And

$$\begin{bmatrix} \sigma_1 \\ \sigma_2 \\ \tau_{12} \end{bmatrix} = \begin{bmatrix} Q_{11} & Q_{12} & 0 \\ Q_{12} & Q_{22} & 0 \\ 0 & 0 & Q_{66} \end{bmatrix} \begin{bmatrix} \varepsilon_1 \\ \varepsilon_2 \\ \gamma_{12} \end{bmatrix}$$

Where

$$Q_{11} = \frac{E_1}{1-v_{12}v_{21}} = 49277978339.3502 MPa \quad (150)$$

$$Q_{22} = \frac{E_2}{1-v_{12}v_{21}} = 49317406143.3447 MPa \quad (151)$$

$$Q_{12} = \frac{v_{12}E_2}{1-v_{12}v_{21}} = \frac{v_{21}E_1}{1-v_{12}v_{21}} = 61.7084 MPa \quad (152)$$

$$Q_{66} = G_{12} = 24604.2140 MPa \quad (153)$$

Hence we have below

$$\begin{bmatrix} 0.001365 \\ 0.001445 \\ 0 \end{bmatrix} = \begin{bmatrix} 49277.9783 & 61.7084 & 0 \\ 61.7084 & 49317.4061 & 0 \\ 0 & 0 & 24604.2140 \end{bmatrix} \begin{bmatrix} 0.277e-13 \\ 0.293e-13 \\ 0 \end{bmatrix} MPa \quad (154)$$

Having established the strain-stress relations one can see that the case of negative stiffness and compliance matrix components has been eliminated.

It was mentioned that the last two test cases provided doubtful Young's modulus values but from what can be seen from the relations above the third case actually has more consistent values than the first two.

Experimental and Numerical Stress values respectively (MPa)	Experimental and Numerical Strain values respectively	Experimental and Numerical Young's modulus values respectively (MPa)

158.5	1.255e-9	0.0054	3.15e-11	39790	39841.2698
143.8	0.918e-9	0.0045	2.60e-11	35320	35307.6923
290.2	1.371e-9	0.0072	2.57e-11	53180	53346.3035
303.2	1.365e-9	0.0077	2.77e-11	49270	49277.9783

Table: 4.10. Experimental and Numerical Stress, Strain and Young's modulus values

Table: 4.10 above states the experimental and numerical values of stress, strain and Young's modulus and provides an easy comparison of the values. The stress and strain values differ greatly but the Young's modulus values do not, see how much these values differ as the case may be. Earlier it was noted that the Young's modulus must have been determined by the test rig's computer using a different methodology other than stress/strain. It also turned out that the latter was what was used to determine the values of the numerical Young's modulus values and they really compare well with those from the experiment. The variance between the experimental and numerical and vice versa as the case may be was not exactly consistent as can be seen. This inconsistency is also the case with the other derived values see table below.

	1st Test case	2nd Test case	3rd Test case	4th Test case	Mean Values
E_x (MPa)	39841.2698	35307.6923	53346.3035	49277.9783	44443.31
E_y (MPa)	39793.8144	35330.5785	53309.3525	49317.4061	44437.79
$-\dfrac{\nu_{yx}}{E_y}$ (MPa)	3.5181e-14	3.1304e-14	2.4811e-14	2.5396e-14	2.92e-14
$-\dfrac{\nu_{xy}}{E_x}$ (MPa)	3.5139e-14	3.1293e-14	2.4811e-14	2.5396e-14	2.92e-14
G_{xy} (MPa)	19893.6671	17634.3552	26554.9628	24604.2140	22171.80
$\dfrac{\nu_{xy}E_y}{1-\nu_{xy}\nu_{yx}}$ (MPa)	53.9453	39.0504	70.3375	61.7084	56.2604
$\dfrac{\nu_{yx}E_x}{1-\nu_{xy}\nu_{yx}}$ (MPa)	53.8330	39.0367	70.3375	61.7084	56.2289

Table: 4.11. Engineering Constants of the first four test case in this section

Looking at table: 4.11 above one can see the inconsistencies that were talked about in that some of the values that are supposed to be equal to the other are not. In the first test case $-\dfrac{V_{yx}}{E_y}$ was supposed to be equal to $-\dfrac{V_{xy}}{E_x}$ but that was not the case, but they can be said to be approximately equal as they are different by very tiny fractions. This was also the case with $\dfrac{V_{xy}E_y}{1-V_{xy}V_{yx}}$ and $\dfrac{V_{yx}E_x}{1-V_{xy}V_{yx}}$, and in this case their difference was significant. The third case happened to be the only test case whose compliance condition was met completely if not absolutely, see the values for that test case in table: 4.11 above. It must be noted that in some of the strain-stress relations and vice-versa stated above some of the values on either side of the compliance conditions were approximated so that they can achieve equality. In the fourth case the Young's modulus value derived from the numerical analysis compares relatively better with that from the experimental but at the same time its derived E_y was greater, see table: 4.10. In this case as well these values were approximated to achieve equality. One can equally observe that the difference between the E_x and E_y values was not significant (47.4554MPa, 22.8862MPa, 36.951MPa, 39.4278MPa and 5.52MPa respectively) this was also the case in the Carbon fibre Phenolic composite Lee and Lee [14] used in their work. At the same time they are not equal the difference leaves some room to suspect that the fabric/structure was not isotropic. In trying to determine this, the numerical method described above was employed again; below is a table of the determined values as well as that of the already determined; this is for easy comparison.

	1st Test case	2nd Test case	3rd Test case	4th Test case	Mean Values
E_x (MPa)	39841.2698	35307.6923	53346.3035	49277.9783	44443.31
E_y (MPa)	39793.8144	35330.5785	53309.3525	49317.4061	44437.79
E_z (MPa)	39887.0056	35403.7267	53040	49389.3130	44430.01
$-\dfrac{V_{yx}}{E_y}$ (MPa)	3.5181e-14	3.1304e-14	2.4811e-14	2.5396e-14	2.92e-14

$-\dfrac{\nu_{xy}}{E_x}$ (MPa)	3.5139e-14	3.1293e-14	2.4811e-14	2.5396e-14	2.92e-14
$-\dfrac{\nu_{zx}}{E_z}$ (MPa)	3.4069e-14	3.1294e-14	2.4936e-14	2.5396e-14	2.89e-14
$-\dfrac{\nu_{xz}}{E_x}$ (MPa)	3.4069e-14	3.1294e-14	2.4936e-14	2.5396e-14	2.89e-14
$-\dfrac{\nu_{yz}}{E_y}$ (MPa)	3.3987e-14	3.122e-14	2.4876e-14	2.5334e-14	2.89e-14
$-\dfrac{\nu_{zy}}{E_z}$ (MPa)	3.3987e-14	3.122e-14	2.4876e-14	2.5334e-14	2.89e-14
G_{xy} (MPa)	19893.6671	17634.3552	26554.9628	24604.2140	22171.80
$\dfrac{\nu_{xy}E_y}{1-\nu_{xy}\nu_{yx}}$ (MPa)	53.9453	39.0504	70.3375	61.7084	56.2604
$\dfrac{\nu_{yx}E_x}{1-\nu_{xy}\nu_{yx}}$ (MPa)	53.8330	39.0367	70.3375	61.7084	56.2289
ν_{12}	-0.0014	-0.0011	-0.0013	-0.0013	-0.0013
ν_{21}	-0.0014	-0.0011	-0.0013	-0.0013	-0.0013
ν_{23}	-0.0013	-0.0011	-0.0013	-0.0012	-0.0012
ν_{32}	-0.0014	-0.0011	-0.0013	-0.0013	-0.0013
ν_{13}	-0.0014	-0.0011	-0.001	-0.0013	-0.0012
ν_{31}	-0.0014	-0.0011	-0.0013	-0.0013	-0.0013

Table: 4.12. Table: 4.11. Engineering Constants of the first four test case in this section

Looking at table: 4.12 above one can observe that the value of the material properties in all the three directions do not differ so much. In some cases based on the tests and the numerical analyses the samples were showing greater strength in the transverse directions E_2 and E_3:

this was the case with the second test case. The latter-E_3 was greater than the others- this was not exactly what was expected. The fourth test case also exhibited this in the same way. In the first test it was not exactly the case, the E_1 value was greater than that of the E_2 but the E_3 was the greatest. It is only the third test case and the mean values that exhibited what was expected: the material properties descended from E_1 to E_3. Jones [39] in his book has it that if a lamina (in this case a laminate) is compacted in the 3- or Z-direction during the curing process the values of the material property in the 2- and 3- directions may differ slightly. This was the case with these test structures; they were compacted in the 3 or Z-direction, in some of the cases as we already know the E_3 values were greater. He went on to conclude that the structure would be orthotropic in the three dimensional sense [39]. Now looking at the third test case and the means values we can see that the properties differ in all the three directions and as a result we can treat the material as orthotropic. One may wonder why the fore mentioned set of readings were used to make this conclusion: this was because they were the only ones that followed the order and most of all the mean values are the best of the series.

In the light of all these three more tests were carried out and the obtained values from the tests were used for validation as well as to derive the other material properties just as in the cases just discussed above. Hence we now have a more encompassing table: see table: 4.13 below.

	1st Test case	2nd Test case	3rd Test case	4th Test case	5th Test case	6th Test case	7th Test case	Mean Values
E_x (MPa)	39841.2698	35307.6923	53346.3035	49277.9783	63129.2517	67027.027	58970.0997	52414.23
E_y (MPa)	39793.8144	35330.5785	53309.3525	49317.4061	63121.0191	67106.599	58953.4884	52418.89
E_z (MPa)	39887.0056	35403.7267	53040	49389.3130	63105.4131	67084.2825	58921.5686	52404.47
$-\dfrac{\nu_{yx}}{E_y}$ (MPa)	3.5181e-14	3.1304e-14	2.4811e-14	2.5396e-14	1.6667e-14	1.9719e-14	3.4025e-14	2.67e-14
$-\dfrac{\nu_{xy}}{E_x}$ (MPa)	3.5139e-14	3.1293e-14	2.4811e-14	2.5396e-14	1.6667e-14	1.9719e-14	3.4025e-14	2.67e-14

a)								
$-\dfrac{\nu_{zx}}{E_z}$ (MPa)	3.4069e-14	3.1294e-14	2.4936e-14	2.5396e-14	1.6667e-14	1.9719e-14	3.4025e-14	2.66e-14
$-\dfrac{\nu_{xz}}{E_x}$ (MPa)	3.4069e-14	3.1294e-14	2.4936e-14	2.5396e-14	1.6667e-14	1.9719e-14	3.4025e-14	2.66e-14
$-\dfrac{\nu_{yz}}{E_y}$ (MPa)	3.3987e-14	3.122e-14	2.4876e-14	2.5334e-14	1.6657e-14	1.9718e-14	3.4024e-14	2.65e-14
$-\dfrac{\nu_{zy}}{E_z}$ (MPa)	3.3987e-14	3.122e-14	2.4876e-14	2.5334e-14	1.6657e-14	1.9718e-14	3.4024e-14	2.65e-14
G_{xy} (MPa)	19893.6671	17634.3552	26554.9628	24604.2140	31500.3496	33495.6927	29401.0583	26154.9
$\dfrac{\nu_{xy}E_y}{1-\nu_{xy}\nu_{yx}}$ (MPa)	53.9453	39.0504	70.3375	61.7084	66.3507	88.767	118.1868	71.1923
$\dfrac{\nu_{yx}E_x}{1-\nu_{xy}\nu_{yx}}$ (MPa)	53.8330	39.0367	70.3375	61.7084	66.3507	88.767	118.1868	71.1743
ν_{12}	-0.0014	-0.0011	-0.0013	-0.0013	-0.0011	-0.0013	-0.002	-0.0014
ν_{21}	-0.0014	-0.0011	-0.0013	-0.0013	-0.0011	-0.0013	-0.002	-0.0014
ν_{23}	-0.0013	-0.0011	-0.0013	-0.0012	-0.0011	-0.0013	-0.002	-0.0013
ν_{32}	-0.0014	-0.0011	-0.0013	-0.0013	-0.0011	-0.0013	-0.002	-0.0014
ν_{13}	-0.0014	-0.0011	-0.001	-0.0013	-0.0011	-0.0013	-0.002	-0.0013
ν_{31}	-0.0014	-0.0011	-0.0013	-0.0013	-0.0011	-0.0013	-0.002	-0.0014

Table: 4.13. A more encompassing table of material properties

One can see from the table above that there was a spike in the reduced stiffness $\dfrac{\nu_{xy}E_y}{1-\nu_{xy}\nu_{yx}}$

values for the seventh test case. The major reason for that as we can equally see is the relatively reduced Poisson's ratio of -0.002: that could be down to the fact that the sample was over cured as well as other factors. The other factors are that the sample had a relatively high strain of 0.008 mm/mm-some other samples had 50% less than that, the other being that this strain value when divided by the Young's modulus forms a ratio that was multiplied by the resulting stress value to obtain this Poisson's ratio value. This sounds quite methodological but it holds some substance.

The sixth test case produced an E_2 value that was higher than the E_1 value as a result of this it affected the E_2 mean value making it greater than the E_1 mean value. This of course tarnishes the potency of these mean values, as a result individual test cases were considered as well as the initial mean values in determining the properties that most describe the material properties of this material. So we look at the set of values who's E_1, E_2 and E_3 values turned out in the expected order: that is in descending order of magnitude as well as their average.

	3rd Test case	5th Test case	7th Test case	Initial Mean Values	Current Mean Values
E_x (MPa)	53346.3035	63129.2517	58970.0997	44443.31	54972.24
E_y (MPa)	53309.3525	63121.0191	58953.4884	44437.79	54955.41
E_z (MPa)	53040	63105.4131	58921.5686	44430.01	54874.25
$-\dfrac{\nu_{yx}}{E_y}$ (MPa)	2.4811e-14	1.6667e-14	3.4025e-14	2.92e-14	2.62e-14
$-\dfrac{\nu_{xy}}{E_x}$ (MPa)	2.4811e-14	1.6667e-14	3.4025e-14	2.92e-14	2.62e-14
$-\dfrac{\nu_{zx}}{E_z}$ (MPa)	2.4936e-14	1.6667e-14	3.4025e-14	2.89e-14	2.61e-14
$-\dfrac{\nu_{xz}}{E_x}$ (MPa)	2.4936e-14	1.6667e-14	3.4025e-14	2.89e-14	2.61e-14

$-\dfrac{\nu_{yz}}{E_y}$ (MPa)	2.4876e-14	1.6657e-14	3.4024e-14	2.89e-14	2.61e-14
$-\dfrac{\nu_{zy}}{E_z}$ (MPa)	2.4876e-14	1.6657e-14	3.4024e-14	2.89e-14	2.61e-14
G_{xy} (MPa)	26554.9628	31500.3496	29401.0583	22171.80	27407.04
$\dfrac{\nu_{xy}E_y}{1-\nu_{xy}\nu_{yx}}$ (MPa)	70.3375	66.3507	118.1868	56.2604	77.7839
$\dfrac{\nu_{yx}E_x}{1-\nu_{xy}\nu_{yx}}$ (MPa)	70.3375	66.3507	118.1868	56.2289	77.7760
ν_{12}	-0.0013	-0.0011	-0.002	-0.0013	-0.00143
ν_{21}	-0.0013	-0.0011	-0.002	-0.0013	-0.00143
ν_{23}	-0.0013	-0.0011	-0.002	-0.0012	-0.0014
ν_{32}	-0.0013	-0.0011	-0.002	-0.0013	-0.00143
ν_{13}	-0.001	-0.0011	-0.002	-0.0012	-0.0013
ν_{31}	-0.0013	-0.0011	-0.002	-0.0013	-0.0014

Table: 4.14. Engineering constants for the third, fifth, seventh and the initial mean values respectively

The decision to involve the initial mean values helps to make the current values a little more conservative; this is so because these values are significantly less than the other values hence the current mean values were marked down somewhat.

Using these set of values stated in table: 4.14 above a piston was modelled using the information derived in the design of the piston. The applied load 4.7e3 N was applied in the Z-direction and this load value was also known as the rupture force. This rupture force happened to be the highest force value derived in the design of the piston; hence its use in this simulation. The aim is to find out the set of material properties above that are suitable for characterising the structure of this piston. In the actual concept the piston is a hybrid one but

in the case below what was modelled was a homogeneous one, which is one material-the composite fabric that has been under discussion. On this occasion the materials were treated as isotropic materials, this was so because the three principal values do not differ in a very significant way. There are five cases that were looked at and for each case the displacements that were obtained in these tests were also used in the simulations. The details of the simulations are stated below:
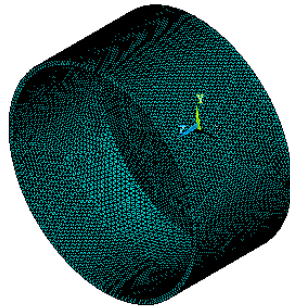
Fig: 4.40. The mesh model of the piston cap.

Element Type

The Element type adopted in this analysis is Solid and the type is Solid-45

Meshing

Hexahedra and wedge elements were used consisting of:

1 Volume

52520 Nodes

44800 Elements

Element Edge Length: 0.0025 mm

Displacement

UX = 0 (X-direction)

UY = 0 (Y-direction)

UZ = 0.0001805, 0.0001024, 0.0002041, 0.0001553, 0.0001606 mm (respectively for the various simulation cases)

The conditions stated above indicate that there was no displacement in the X and Y directions or that the model was fixed in such a way that the displacements in the X and Y directions were restricted but there were displacements in the Z-direction for the respective case whose values are also stated.

Load

FX = 4.7e3 N   (Force of 4.7e3 N was applied in the Z-direction)

A force of 4.7e3 N was applied in the Z-direction, the same direction that was also allowed some displacement.

Material Properties

E_X = 53346.3035, 63129.2517, 58970.0997, 44443.31, 54972.24 MPa (respectively for the various simulation cases)

v_{12} = -0.0013, -0.0011, -0.002, -0.0013, -0.00143 (respectively for the various simulation cases)

Density = 1.55 g/cm

The table below contains some results from the element solution of the simulation:

	$E_X =$ 53346.3035 MPa case	$E_X =$ 63129.2517 MPa case	$E_X =$ 58970.0997 MPa case	$E_X =$ 44443.3100 MPa case	$E_X =$ 54972.2400 MPa case
Z-component of stress	0.0036 MPa	0.189e-4MPa	0.000299MPa	0.00157MPa	0.000645MPa
Z-component of strain	0.680e-13	0.299e-15	0.122e-13	0.353e-13	0.117e-13
Y-component of stress	0.0066 MPa	0.000113MPa	0.001299MPa	0.002867MPa	0.001198MPa
Y-component of strain	0.124e-12	0.179e-14	0.220e-13	0.645e-13	0.218e-13
X-component of stress	0.0015MPa	0.0000248MPa	0.000719MPa	0.000663MPa	0.000222MPa

| X-component of strain | 0.286e-13 | 0.393e-15 | 0.507e-14 | 0.149e-13 | 0.404e-14 |
| Displacement | 0.000372 mm | 0.000102 mm | 0.000212mm | 0.000229mm | 0.000170mm |

Table: 4.15. The table above states the derived values and provides easier comparison.

It is obvious that the best case was that of $E_X = 63129.2517$ MPa-lowest stress, strain and displacement values, but we need to be more critical, meaning we have to consider the amount of the load that was applied during the empirical tests as well as other possible factors.

First of all the test case above had a displacement of 0.0001024mm in the empirical test and this displacement value was applied in validating its constitutive model and was equally used in the simulation whose results are above. As a matter of fact the other test cases yielded displacements higher than the applied case apart from this test case in question. Interestingly the load applied in the analyses above – 4.7KN was higher than the one in its empirical test which was 3.555KN. What is note worthy here is that even with a higher load it still maintained its displacement. The other notable factor was that the sample was mistakenly left to cure for an extra 10 minutes and cooled off gradually on its own. Indeed the numerical model could not exactly inherit the resulting properties that must have come about due to this extended curing assuming the latter improved its quality which of course was possible. It was equally one of three test cases whose compliance and stiffness matrices components were most consistent and met required conditions. See table: 4.16 below.

$-\dfrac{v_{yx}}{E_y}$ (MPa)	1.6667e-14
$-\dfrac{v_{xy}}{E_x}$ (MPa)	1.6667e-14
$-\dfrac{v_{zx}}{E_z}$ (MPa)	1.6667e-14
$-\dfrac{v_{xz}}{E_x}$ (MPa)	1.6667e-14

$-\dfrac{v_{yz}}{E_y}$ (MPa)	1.6657e-14
$-\dfrac{v_{zy}}{E_z}$ (MPa)	1.6657e-14
$\dfrac{v_{xy}E_y}{1-v_{xy}v_{yx}}$ (MPa)	66.3507
$\dfrac{v_{yx}E_x}{1-v_{xy}v_{yx}}$ (MPa)	66.3507

Table: 4.16. Shows some of the Compliance and Stiffness matrices components for $E_X = 63129.2517$ MPa test case.

So far some of the merits of adopting 63129.2517 MPa as the E_x value of this structure have been discussed, but adopting it may not be exactly be the best decision. This is so because it is just one test case, it may seem more like it if an average value is adopted instead of that of a single value. The next best test case was the 7th case- the much talked about case above is the 5th. The former has a lower E_x value of 58970.0997 MPa so finding their average would lead to a value lower than 63129.2517 MPa for the sake of having a slightly conservative value. This 7th test case was the case whose sample was left to cure for 2 hours: this of course may have affected its strength negatively or positively. As we know from the discussions in earlier sections, carbon influences the strength of materials positively in the longitudinal direction and having undergone such an extensive curing the sample was sure to have carbonized to some extent. The last three test cases which include the 5th and 7th uniquely produced graphs whose curves show a gradual drop in load as against the earlier ones. This lends to the case of carbonization at the same time it also points to the possibility of the attainment of a more optimal structure as such the reason the average of these material properties had to be determined. The average value was 61049.6757 MPa; this was the estimated value obtainable if the laminate was cured for more than 30 minutes and possibly longer. Note that the word laminate has come in; this is so because that was what the samples we employed above are. As a result of that they are not materials they are structures. So classical laminate theory was used to analyse the laminate whose E_x value has been stated as 61049.6757 MPa.

4.4.3. Classical laminate theory analysis

The extensional stiffness matrix is denoted by [A], the strain-curvature coupling stiffness matrix by [B] and bending stiffness matrix by [D]. The extensional stiffness matrix ensures that the resultant forces are related to the mid-plane strains of the laminate, the bending stiffness matrix ensures that the resultant moments are related to the laminate curvatures resulting from twisting as well, while the strain-curvature coupling stiffness matrix couples the extension and bending of laminates. So we have:

$$[A] = \sum_{k=1}^{N} \left(\overline{C}_{ij} \right)_k t_k \qquad (155)$$

$$[A] = \begin{vmatrix} 18.314 & 0.0292 & 0 \\ 0.0292 & 18.311 & 0 \\ 0 & 0 & 9.135 \end{vmatrix} GPa - mm \quad (156)$$

$\left(\overline{C}_{ij} \right)_k$ denotes the stiffness of the k_{th} layer and t_k is the thickness of that layer which is 0.3mm. So we have for the E_x value 61049.8320 MPa case; 15262.4580 MPa for each lamina since the are four and

$$A_{11} = A_{22} = \frac{Et}{1 - v^2} \qquad (157)$$

$$1 - v^2 = 0.9999 \qquad (158)$$

So for each lamina we have:

$$15262.4580 X 0.3 = 4578.7374 X 4 = 18314.4496 MPa$$

Also E_y value is 61037.2538 MPa and G_{xy} is 30450.704 MPa

So for each case we have below:

$$15259.3525 X 0.3 = 4577.8058 X 4 = 18311.2232 MPa$$

And

$$7612.6760 X 0.3 = 2283.8028 X 4 = 9135.2112 MPa$$

$$[B] = \sum_{k=1}^{N} \left(\overline{C}_{ij} \right)_k t_k \, \overline{z_k} \qquad (159)$$

$$[B] = \begin{vmatrix} 0 & 0 & 0 \\ 0 & 0 & 0 \\ 0 & 0 & 0 \end{vmatrix} GPa - mm^2 \qquad (160)$$

$\overline{z_k}$ is the distance between the mid-plan and the centroid of the k_{th} layer.

$$[D] = \sum_{k=1}^{N} \left(\overline{C}_{ij} \right)_k \left(t_k \, \overline{z_k}^2 + \frac{t_k^3}{12} \right) \qquad (161)$$

$$[D] = \begin{vmatrix} 0.3984 & 0.0006 & 0 \\ 0.0006 & 0.3983 & 0 \\ 0 & 0 & 0.1987 \end{vmatrix} GPa - mm^3 \qquad (162)$$

In the section before this one, lamina theory was used in the analysis of the laminate; the demerit of doing so is that the laminate was treated as lamina. As such the stiffness and compliance values stated in that section are wrong for a laminate though correct if we were dealing with a lamina. In other to compensate for that, stated below are the Extensional, Coupling and Bending Stiffnesses of the last five set of results. These happened to be the most acceptable of the whole lot hence the reason for analysing them.

The first of them is the 3rd test case whose E_x value is 53346.3035 MPa

$$[A] = \begin{vmatrix} 16.00 & 0.0208 & 0 \\ 0.0208 & 15.99 & 0 \\ 0 & 0 & 7.9665 \end{vmatrix} GPa - mm \qquad (163)$$

$$[B] = \begin{vmatrix} 0 & 0 & 0 \\ 0 & 0 & 0 \\ 0 & 0 & 0 \end{vmatrix} GPa - mm^2$$

$$[D] = \begin{vmatrix} 0.3481 & 0.0005 & 0 \\ 0.0005 & 0.3478 & 0 \\ 0 & 0 & 0.1733 \end{vmatrix} GPa - mm^3$$

(164)

The next test case is the 5th case whose E_x value is 63129.2517 MPa

$$[A] = \begin{bmatrix} 18.9388 & 0.0208 & 0 \\ 0.0208 & 18.9363 & 0 \\ 0 & 0 & 9.4501 \end{bmatrix} GPa - mm$$

(165)

$$[B] = \begin{bmatrix} 0 & 0 & 0 \\ 0 & 0 & 0 \\ 0 & 0 & 0 \end{bmatrix} GPa - mm^2$$

$$[D] = \begin{bmatrix} 0.2060 & 0.0005 & 0 \\ 0.0005 & 0.2059 & 0 \\ 0 & 0 & 0.1028 \end{bmatrix} GPa - mm^3$$

(166)

The next test case is 7th case whose E_x value is 58970.0997 MPa

$$[A] = \begin{bmatrix} 17.6910 & 0.0354 & 0 \\ 0.0354 & 17.6860 & 0 \\ 0 & 0 & 8.8203 \end{bmatrix} GPa - mm$$

(167)

$$[B] = \begin{bmatrix} 0 & 0 & 0 \\ 0 & 0 & 0 \\ 0 & 0 & 0 \end{bmatrix} GPa - mm^2$$

$$[D] = \begin{bmatrix} 0.1924 & 0.0004 & 0 \\ 0.0004 & 0.1923 & 0 \\ 0 & 0 & 0.0959 \end{bmatrix} GPa - mm^3$$

(168)

Having determined the Stiffness values above one can see how the thickness of the structures influences the extensional and bending stiffness especially the latter.

4.5. Fatigue

Fig: 4.41. Picture shows a sample damaged after 27,600 cycles at maximum and minimum loads of 1600 N and 400 N respectively.

In this fatigue analyses the loads applied were tensile loads, so the cases described below were just like the ones in the constituent model section as well as earlier sections.

Figs: 4.41, 4.42 and 4.43 show the sort of damage that occurred at one end of the sample, this was so because it was the fixed end or the end that had zero displacement; as a result the load was felt the most at this part. This was also the case for the picture right below in fig: 4.42. The load was applied such that one end or the lower end was fixed and the other was not as the load tries to pull the samples upwards, this was also the case in the tensile test cases.

Fig: 4.42. Notice the sample is bent; this was to emphasize the extent of the damage.

Fig: 4.43. Delamination also occurred; see the separated Plies.

In the first fatigue loading that was carried out the following values in table: 4.17 were applied:

Preload Value	1.8KN
Maximum Load Value	3.2 KN
Minimum Load Value	0.8 KN
Frequency	10 Hz
Number of Cycles	24

Table: 4.17. Fatigue test values

One can see that 24 cycles was very small, the sample failed and it was an instantaneous one. With relatively high preload and maximum load values and a frequency of 10 Hz that kind of failure should be expected.
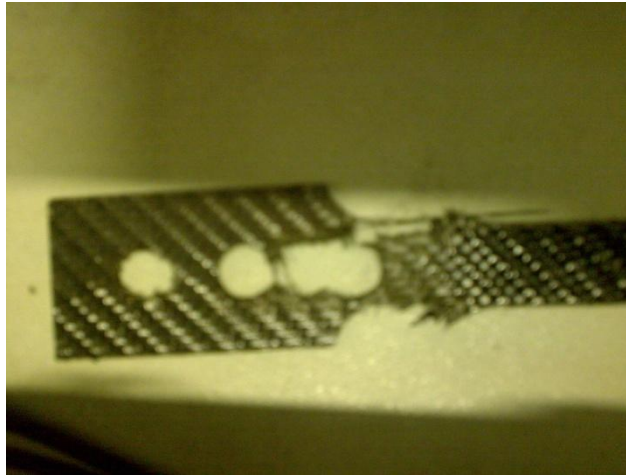
Fig: 4.44. See the damaged sample in the first case.

Notice in the picture above in fig: 4.44 the kind of damage that occurred as a result of the load applied and the frequency; it was largely fibre breakage, no delamination was observed.

This first case was just an attempt to determine what can work in this fatigue loadings using or applying as much load as possible. In the subsequent case a more conservative preload of 500N was used, see details of that case below in table: 4.18.

Preload Value	500N
Maximum Load Value	200N
Minimum Load Value	200N
Frequency	10 Hz
Number of Cycles	1000

Table: 4.18. Fatigue test values

It was concluded that the load values above were not significant enough, so higher values were used hence the third case. In this case the displacements were observed see table below in table: 4.19.

Preload Value	1000N
Maximum Load Value	500N
Minimum Load Value	500N
Frequency	10 Hz

Number of Cycles	10000
Initial Position (@ preload)	0.45mm
Final Position	0.4766

Table: 4.19. Fatigue test values

Notice that after 10000 cycles at 10 Hz and all other factors in place there was a displacement or elongation of 0.0266 mm, see table: 4.19 above. This kind of displacement was somewhat expected as the sample had gone through 10000 cycles; simple loadings as can be seen from earlier sections produced about 0.0045 mm in displacement so a displacement of 0.0266 mm after 10000 cycles was roughly 10 times that of a simple and single loading which is remarkable. In the next case the following values in table: 4.20 were adopted to carry out the exercise

Preload Value	1000N
Maximum Load Value	1600N
Minimum Load Value	400N
Amplitude	600N
Position at 1600 N (maximum)	0.303 mm
Position amplitude	0.112 mm
Frequency	10 Hz
Number of Cycles	27600

Table: 4.20. Fatigue test values

The test case in table: 4.20 above ended after 27600 cycles. The first three pictures in this section above are the sample pictures from this fatigue test. The damage that occurred as can be seen from the first and second pictures of this fatigue section happened at the lower end of the sample which was also where the load or tension was felt the most. The load was so significant that one can actually feel the yarns go through an up and down reciprocatory motion; using a micro-telescope it could equally be seen.

The next test took place over a five day period and the following below was recorded.

Preload Value	1000N
Maximum Load Value	1600N
Minimum Load Value	400N
Amplitude	600N
Position at 1600 N (maximum)	0.325 mm
Position amplitude	0.114 mm
Frequency	10 Hz
Number of Cycles	818181

Table: 4.21. Fatigue test values

However the readings above were taken after 818181 cycles, the material did not exactly fail. Using the data from the entire tensile tests that were carried out the following fatigue parameters in table: 4.22 were determined for each test case:

	1st case	2nd case	3rd case	4th case	5th	6th	7th	8th	9th
N_f , Life	$1.7*10^5$	$1.2*10^5$	$1.2*10^5$	$6.5*10^4$	$1.2*10^5$	$6.2*10^4$	$7.7*10^4$	$7.2*10^4$	$7.9*10^4$
E (MPa)	33580	16240	39790	53180	35320	49270	63070	67080	58920
S_u (MPa)	84.86	152	158.5	290.2	143.8	303.2	246.9	263.7	241
S_F'(MPa)	135.776	243.2	253.6	464.32	230.08	485.12	395.04	421.92	385.6
B	-0.085	-0.085	-0.085	-0.085	-0.085	-0.085	-0.085	-0.085	-0.085
S_{FL}(MPa)	42.3213	75.9641	79.25	145.0416	71.8206	152.489	123.3534	131.0183	120.1141
K_f (mm)	78.5274	27.5022	25.5055	8.5868	30.3893	7.9355	11.4855	10.2021	11.9965
S_{max} (MPa)	84.86	152	158.5	290.2	143.8	303.2	246.9	263.7	241
S_{min} (MPa)	0.2216	0.0732	0.0553	0.1272	0.1627	0.1280	0.2198	1.6659	0.7697
N_{FL} Cycles	$9.0*10^5$	$8.8*10^5$	$8.8*10^5$	$8.8*10^5$	$8.9*10^5$	$8.2*10^5$	$8.8*10^5$	$9.4*10^5$	$9.1*10^5$
K_t	1	1	1	1	1	1	1	1	1
k_L	1	1	1	1	1	1	1	1	1
k_{size}	1	1	1	1	1	1	1	1	1

k_{SF}	1	1	1	1	1	1	1	1	1
S_a (MPa)	42	76	79	150	72	150	120	130	120
S_m (MPa)	43	76	79	150	72	150	120	130	120
$S_{m,}$ calculated (MPa)	-41.5	-71.5	-74.3	-118	-68	-121	-106	-110	-104
S_{eq}	1.1	5.4	6.1	32	4.7	36	21	25	19
Slope	-0.4	-0.32	-0.32	-0.24	-0.33	-0.23	-0.26	-0.25	-0.26

Table: 4.22. Fatigue parameters for all the structures that were used in the tensile tests.

Using the internet based tool www.fatiguecalculator.com/constamp/stresslife.htm [47] some of these parameters in the tables above and below were determined. Table: 4.22 above contains the values for all the tensile test cases for carbon fibre Phenolic composite structures. In doing so the equation below was used.

$$\frac{S_a}{S_{fl}} + \frac{S_{mean}}{S_u} = 1 \qquad (169)$$

S_a, S_{fl}, S_{mean} and S_u are amplitude stress or load, endurance limit, mean stress, and ultimate stress. Below are some of the formulae for some the parameters in the tables above and below.

$$S_f' = 1.6 S_u \qquad (170)$$

$$S_{max} = S_u \qquad (171)$$

S_{max} and S_{min} which are maximum and minimum stresses were from the test results. The stress concentration factor equation is given below:

$$N_f = \left(\frac{S_{eq}}{S_f}\right)^{\frac{1}{slope}} \qquad (172)$$

$$S_{eq} = S_a\left(1 + \frac{S_m}{S_u}\right) \qquad (173)$$

Where S_m is mean stress.

$$Slope = b - \frac{\log_{10}\left(\frac{K_f}{K_{sf}K_l K_{size}}\right)}{6}$$ (174)
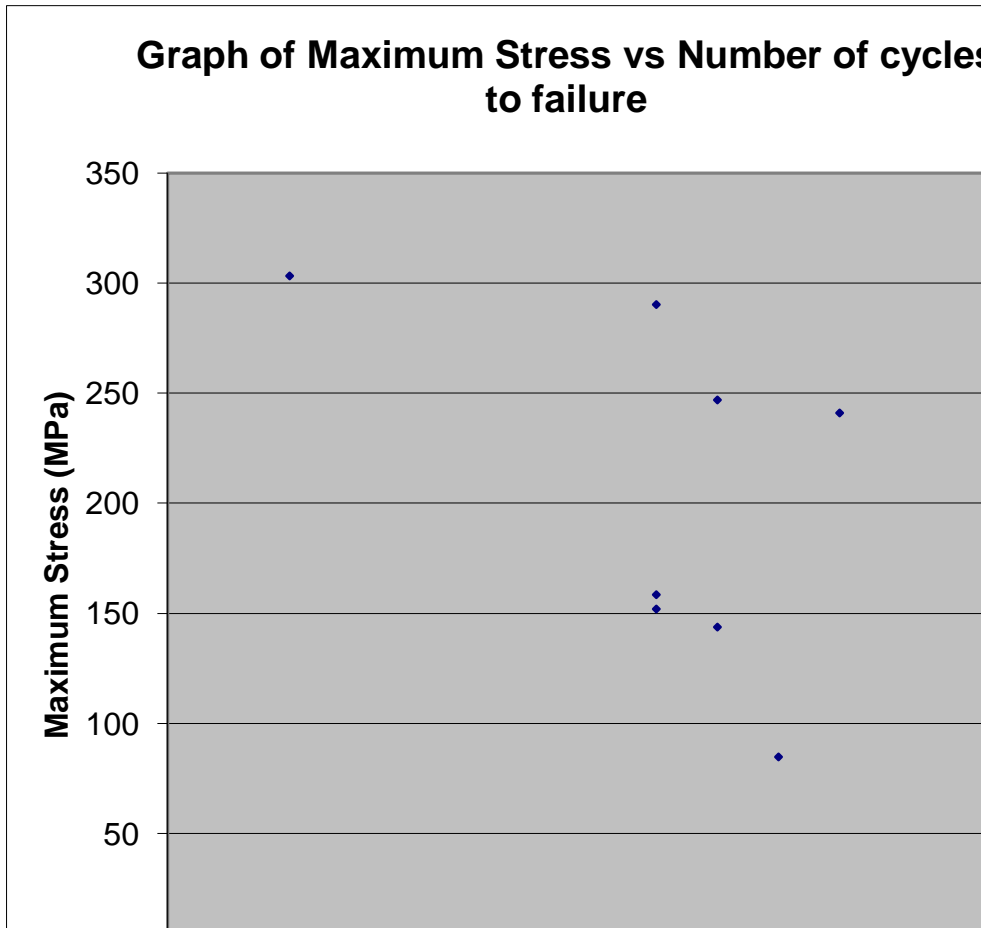
Fig: 4.45. Graph of Maximum Stress against Number of cycles to failure.

From fig: 4.45 based on the data in table: 4.22 all above, one can see that there is a relatively diverse scatter, this was largely down to the fact that the data were from different samples of the composite structure. At the same time they had varying curing treatments but tested by the same person on different days as well. These are likely to have affected the nature of the results, and it was not exactly expected that they will form a nice curve. This was also the case with the tests documented in G.D. Sims' [42] work. In that work tests were carried out on GFRP and CFRP and in one of the graphs the maximum stress was plotted against cycles; though he had a relatively low scatter in that particular graph. And in another of such graphs he explained that the wider scatter band was the actual dispersion of the *S-N* for a mat material with chopped strands [42] of different samples or plates.
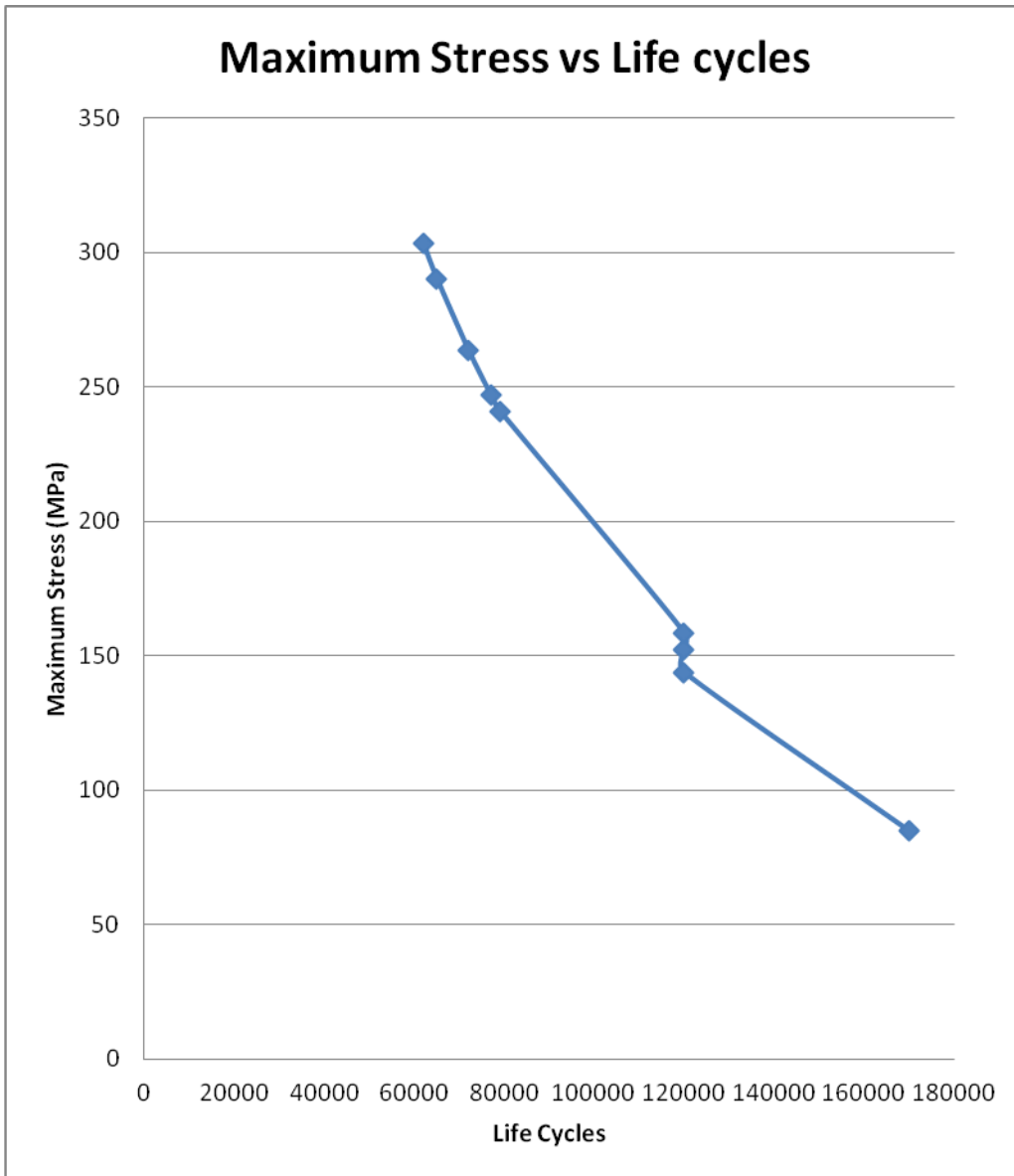
Fig: 4.46. Graph of Maximum Stress against Life Cycles for various samples.

In the Fig: 4.46 based on the data in table: 4.22 above, it can clearly be seen that stress was a factor of life; this was pointing to the fact that if a material or structure endures more stress it is less likely to stay around for a very long time.
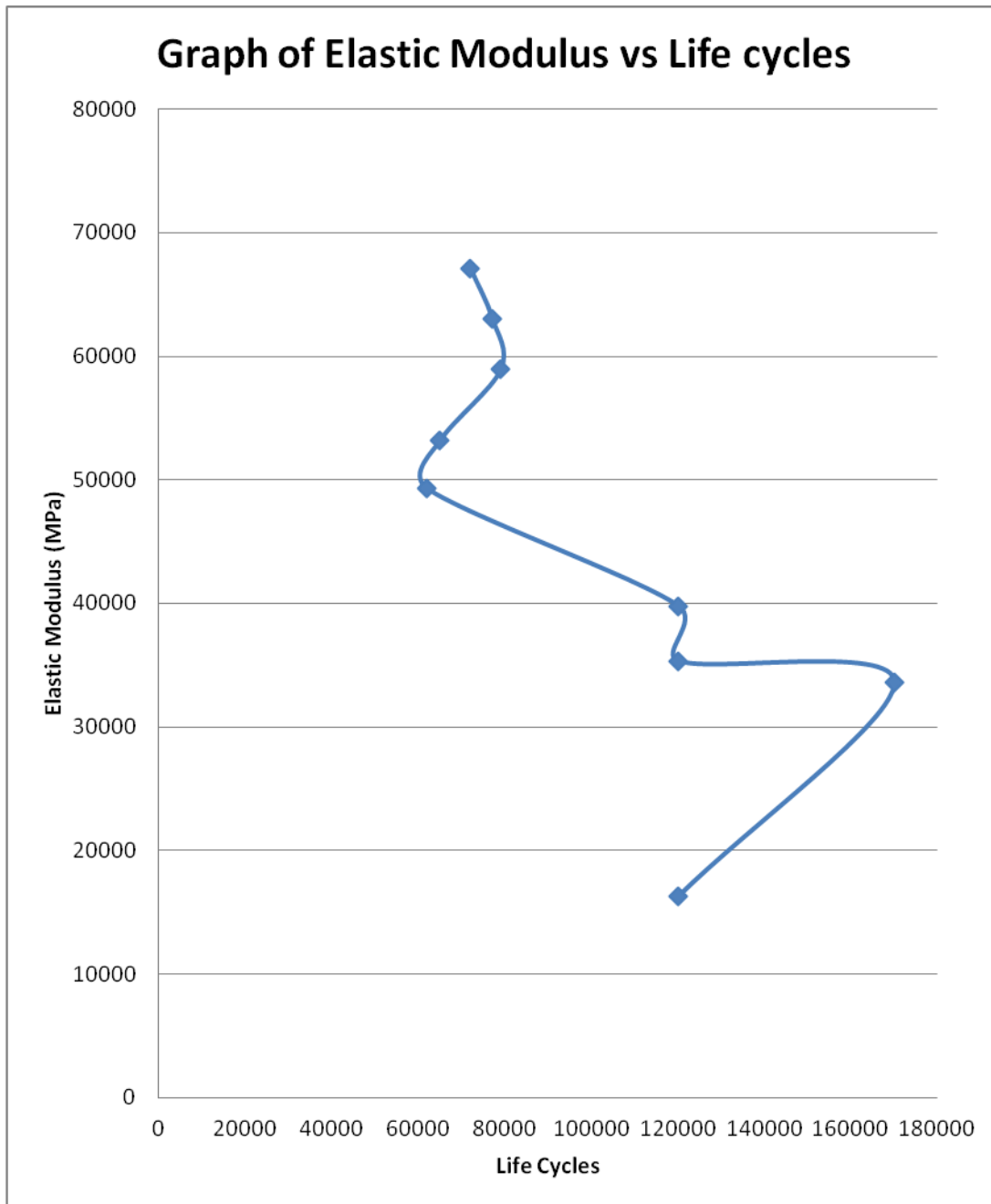
Fig: 4.47. Graph of Elastic Modulus against Life Cycles.

As can be seen from Fig: 4.47; based on the methodology for determining these parameters, Elastic Modulus may not be a factor of life as against the foregoing above where we can see that the sustained stress was a factor of life. In fig: 4.47, the graph right above there was equally this much talked about scatter. This was down to the variety of structures employed though not all were from the same material stock.
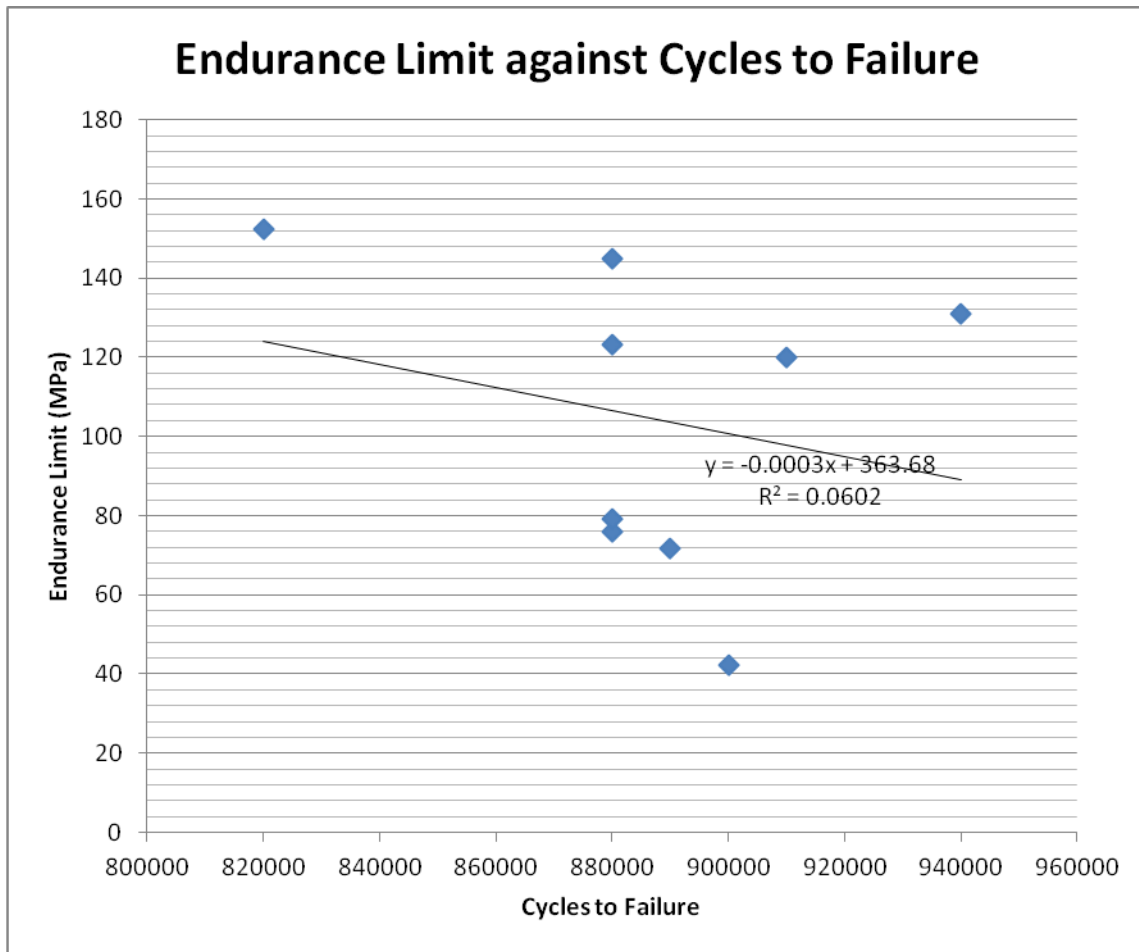
Fig: 4.48. Graph of Endurance Limit against Cycles to Failure for tensile test cases.

Observe the scatter yet again though not surprising, but observe the straight line marking what looks like the general trend. This sort of trend can equally be seen in the next Endurance-Cycle to Failure graph in fig: 4.50 below.

	1st case	2nd case	3rd case	4th case	5th	6th	7th
N_f, Life	$3.8*10^4$	$3.8*10^4$	$3.8*10^4$	$3.8*10^4$	$3.8*10^4$	$3.8*10^4$	$3.8*10^4$
Log N_f	4.5798	4.5798	4.5798	4.5798	4.5798	4.5798	4.5798
E (MPa)	61050	61050	61050	61050	61050	61050	61050
S_u (MPa)	88.0669	88.0669	88.0669	88.0669	88.0669	88.0669	88.0669
S_F'(MPa)	140.9070	140.9070	140.9070	140.9070	140.9070	140.9070	140.9070
B	-0.085	-0.085	-0.085	-0.085	-0.085	-0.085	-0.085
S_{FL}(MPa)	53.8590	54.3310	48.5204	52.0640	48.8270	59.0820	44.2935
K_f (mm)	1	1	1	1	1	1	1
S_{max} (MPa)	88.0669	88.0669	88.0669	88.0669	88.0669	88.0669	88.0669
S_{min} (MPa)	22.0167	22.0167	22.0167	22.0167	22.0167	22.0167	22.0167
N_{FL} Cycles	82,000	74,000	280,000	122,181	260,000	27,600	818181
K_t	1	1	1	1	1	1	1
k_L	1	1	1	1	1	1	1
k_{size}	1	1	1	1	1	1	1
k_{SF}	1	1	1	1	1	1	1
S_a (MPa)	33	33	33	33	33	33	33
S_m (MPa)	55	55	55	55	55	55	55
$S_{m, calculated}$ (MPa)	37.4	37.4	37.4	37.4	37.4	37.4	37.4
S_{eq}	57	57	57	57	57	57	57
Slope	-0.085	-0.085	-0.085	-0.085	-0.085	-0.085	-0.085

Table: 4.23. Fatigue parameters for structures that were used in empirical fatigue tests.

In fig: 4.49 the graph below we have maximum stress against number of cycles to failure we can see that because the maximum stresses were all the same we have what looks like a straight line graph. In the next one where we have endurance limit against number of cycles to failure we can see the effect of prolonged cycling though not very significant. These indeed was expected but note also that the difference between the endurance limit of the lowest number of cycles 27600 and the highest 818181 is 14.7885 MPa. With all these scatter, diversity and variability in the empirical data obtained it was important to consider defining failure criteria as a way of drawing a line to what is considered failure. This is in the

122

light of the fact that once a structure has lost its integrity as a load bearing object it seems pointless to continue applying more load. This happened to be the case with some of the samples in the tensile tests and their results were used in this fatigue analysis.
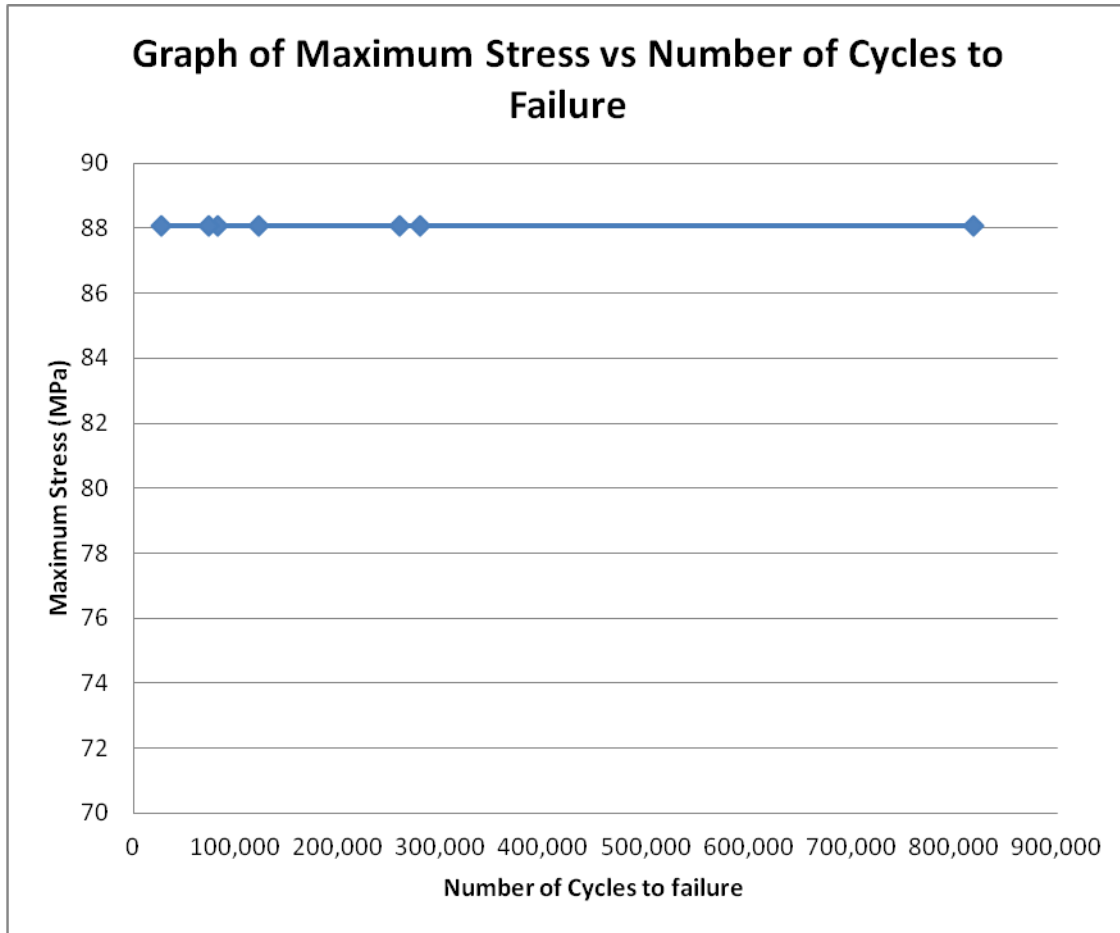
Fig: 4.49. Graph of Maximum stress against number of cycles to failure for the fatigue test cases.

According to B. Harris [42] the kind of graph we have above of fig: 4.49 (see also table: 4.23) indicates a resistance to fatigue but only in the case of $\sigma/\mathrm{Log}N_f$ for the earliest unidirectional Carbon Fibre Reinforced Plastic samples. Below in fig: 4.50 we can see the graphs of Endurance Limit against Number of Cycles to Failure.
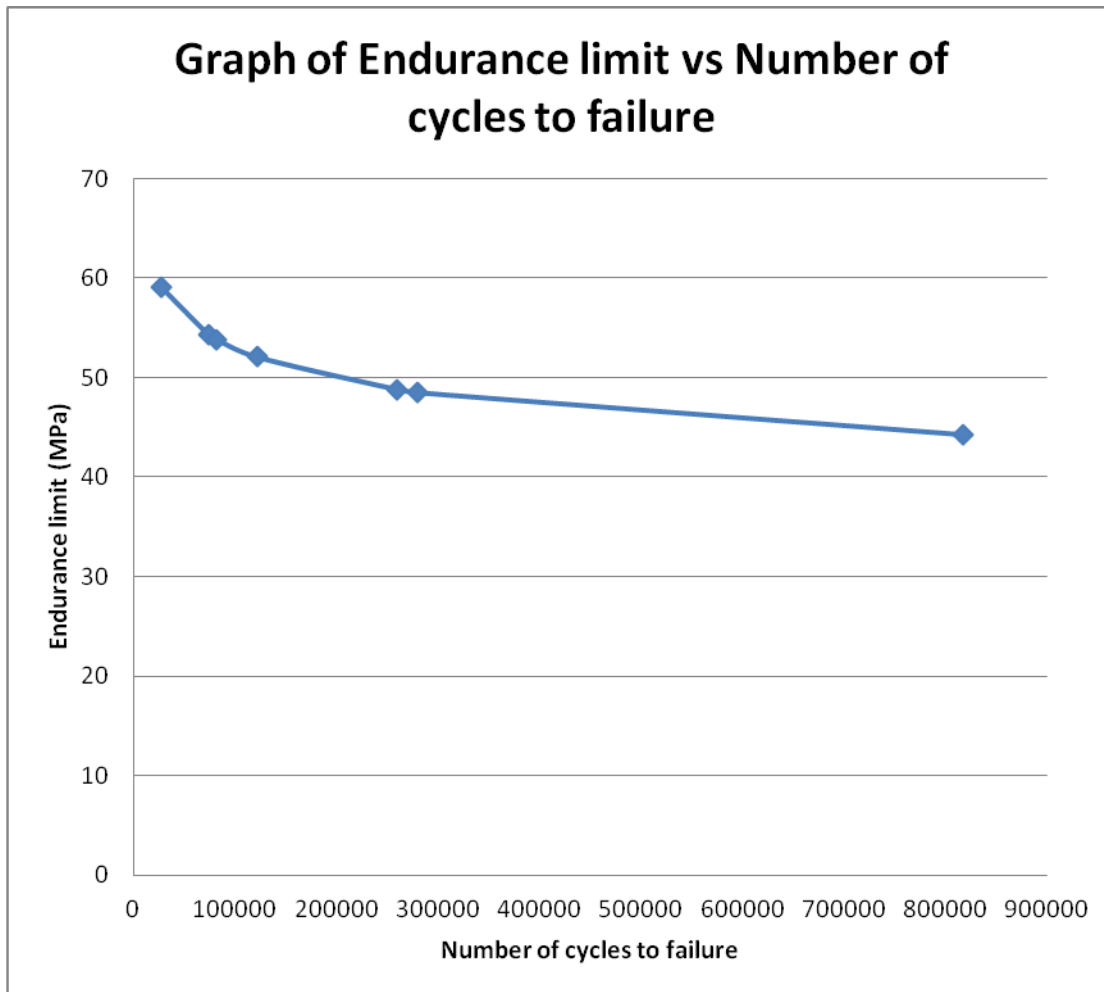
Fig: 4.50. Graph of Endurance limit against number of cycles to failure for the fatigue test cases.

Table: 4.24 below contains more fatigue values from later tests that were carried out; some of the parameters were calculated.

	1st	2nd	3rd
N_f , Life	$3.0*10^4$	$3.0*10^4$	$3.0*10^4$
Log N_f	4.4771	4.4771	4.4771
E (MPa)	61050	61050	61050
S_u (MPa)	137.6046	137.6046	137.6046
S_F'(MPa)	220.1674	220.1674	220.1674
B	-0.085	-0.085	-0.085
S_{FL}(MPa)	55.0424	55.0424	55.0424
S_{FL} calculated(MPa)	113.8307	98.6404	96.6476

K_f (mm)	1	1	1
S_{max} (MPa)	137.6046	137.6046	137.6046
S_{min} (MPa)	27.5209	27.5209	27.5209
$N_{FL\ empirical}$ Cycles	2,347	12,657	16,092
K_t	1	1	1
k_L	1	1	1
k_{size}	1	1	1
k_{SF}	1	1	1
S_a (MPa)	55	55	55
S_m (MPa)	83	83	83
$S_{m,\ calculated}$ (MPa)	55	55	55
$N_{FL\ probalistic}$ Cycles	$1.2*10^7$	$1.2*10^7$	$1.2*10^7$
Safety Factor	1.1	1	1
S_{eq}	92	92	92
slope	-0.085	-0.085	-0.085

Table: 4.24. Fatigue parameters from a test whose maximum load was 2500N (137.6046 MPa), minimum load 500N (27.5209 MPa) and frequency 10Hz.

4.6. Thermo-Mechanical Analysis

The lifetime of a polymer-matrix composite like the one in use in this work Carbon fibre Phenolic composite is not exactly simple. This is so because so many factors go to work on them and influence their long term life under dynamic or static loads. These factors go to work on the constituents of the composites which are fibres and matrices or fillers as the case may be. So these factors can also go to work on the interface between these constituents and once they are compromised one can expect a reduced strength to occur if not complete failure itself, Jones [42]. Above all the environment where these composites are can influence their behaviour as well as affect their life.

According to Jones [42] composites absorb moisture at different rates and degrees depending on some factors. As a result their thermo-mechanical properties may be influenced. Depending on the resin and its network in question chemical degradation or hydrolysis may occur or even plasticization, Jones [42]. The diffusion of moisture equally affects the

transverse properties of the composite and diffusion depends on the environment where the composite is been employed and of course on the latter's relative humidity. As a result of this, the relative humidity determines the amount of moisture the composite holds and just as one can imagine the temperature would influence or determine the rate at which this diffusion would occur.

The Carbon fibre Phenolic composite in this work was more of a prepreg than anything else, meaning it did not have a very significant amount of matrix. As a result we will go on to the factors that were more likely to affect it.

4.7. Prediction of lifetime of fibre bundles under static fatigue

According to Jones [42] Kelly and McCartney combined the statistics of fibre strength with conventional power law for crack growth. In it we have below:

$$N = N_0 \exp\left[-\left(\frac{\sigma}{\sigma_0}\right)^m\right]$$
(175)

N is the number of fibres left undamaged out of N_0. σ is the applied stress, σ_0 is the characteristic ratio and m is the Weibull modulus. The distribution of the force on the undamaged filaments of a fibre bundle is expressed as:

$$F = NA\sigma$$
(176)

Where A is the cross-sectional area of a fibre and F is the force. As can be seen N is a factor of this force as a result if it drops significantly the bundle will fail meaning that the remaining ones may not be able sustain the force. Going further we have that the critical flaw length is:

$$a_c = \left(\frac{K_{1c}}{y\sigma}\right)^2$$
(177)

K_{1c} is the stress intensity factor and it has a role to play as a factor but it is the size of the flaw a that determines how strong fibres would turnout and would fail if the size is greater than a_c, and y is a constant that is a factor of the samples geometry, Jones [42]. Therefore we have a crack growth rate expressed as:

$$\frac{da}{dt} = \alpha K_1^n \quad (178)$$

Hence the power crack growth law can be rewritten as:

$$N = N_0 \exp\left[\left(\frac{a_0}{a}\right)^{m/2}\right] \quad (179)$$

All in all the lifetime can be express in the equation below after incorporating time dependence:

$$t_f \approx \frac{m^{2/m}\left[1 - F/F_m\right]}{\frac{1}{2}\alpha K_{1c}^{n-2} y^2 \sigma_0^2} \quad (180)$$

It can also be said that as F approaches the maximum load that the fibre bundle F_m can sustain the equation above equally holds provided it does not get larger than the latter.

We have the following as:

$$m = 4, n = 15, F/F_m = 0.6 \quad (181)$$

In the same vane we can equally bring all this closer to thermo-mechanical effects by bring in creep and plasticity both of which are extreme effects. And these two parameters combined are known as inelastic strain. So we can go ahead and write the following:

$$t_f \approx \frac{m^{2/m}\left[1 - \varepsilon_{in}/\varepsilon_{total}\right]}{\frac{1}{2}\alpha K_{1c}^{n-2} y^2 \sigma_0^2} \quad (182)$$

Where ε_{in} and ε_{total} are elastic strain and total strain respectively, we will go ahead and analyse the data we have using these failure time equations.
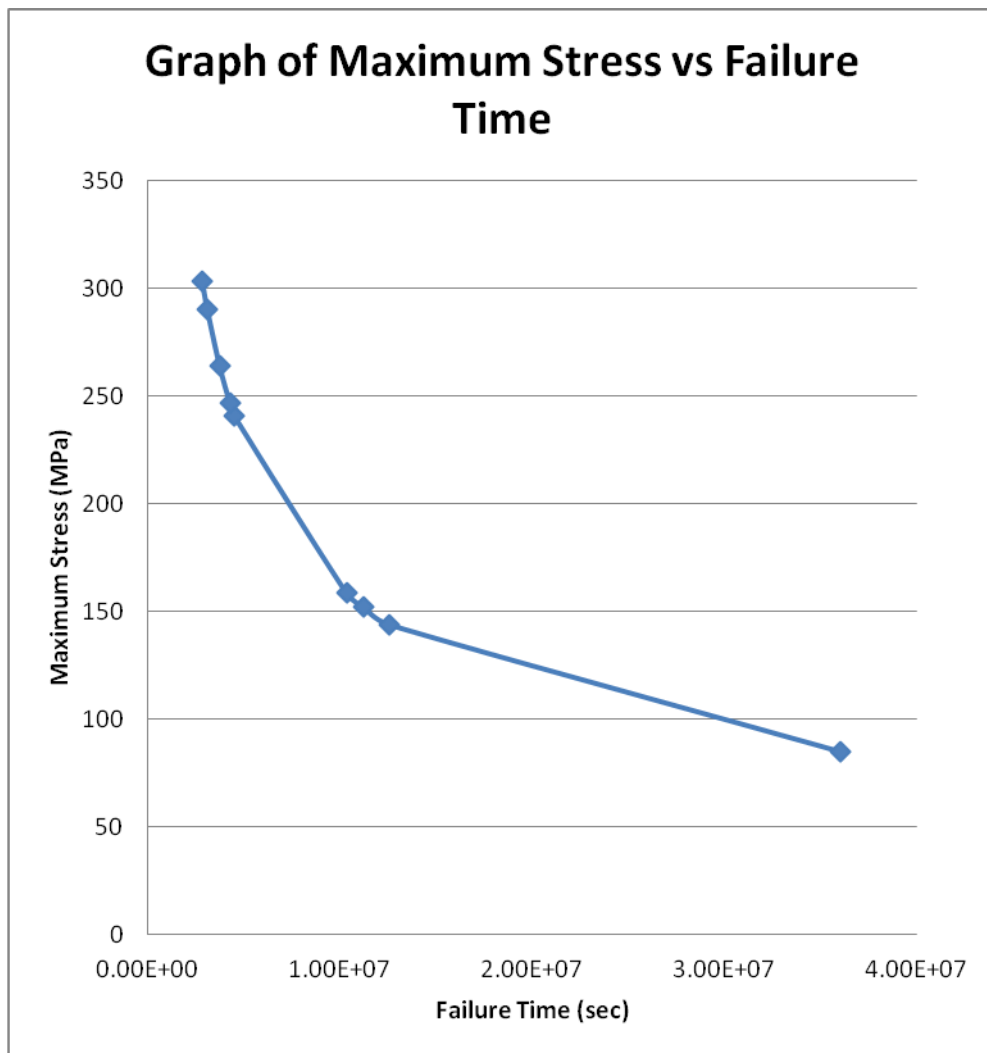
Fig: 4.50. Graph of Maximum Stress against Failure Time using data from the tensile test cases.

In working out some of the parameters in the equations above some of them were not exactly stated or readily available; so some assumptions were made so as to determine one or two of them. So it was assumed that the flaw length was 1.0e-6mm and with that the constant *y* was determined using the critical crack length equation stated above.

Bear in mind that we are working with the data from the tensile tests (see table: 4.4) as they have varying values. So for each test a *y* was determined and the average of these values was then used to determine their failure times in the relevant equation.

The stress intensity factor value employed in this analysis which was 0.49 MN. m^3/2 was influenced by a laboratory environment where the humidity was at 34% on the average as such it was not as high as those that are dried or redried [42]. This of course can have an

influence on the failure time values of these test cases, the more the moisture content the higher the failure time.

Using the elastic and inelastic parameters the same sets of data were analysed and *fig: 4.50* and *fig: 4.51* are graphs of maximum stress against failure time and maximum stress against log of failure time respectively.
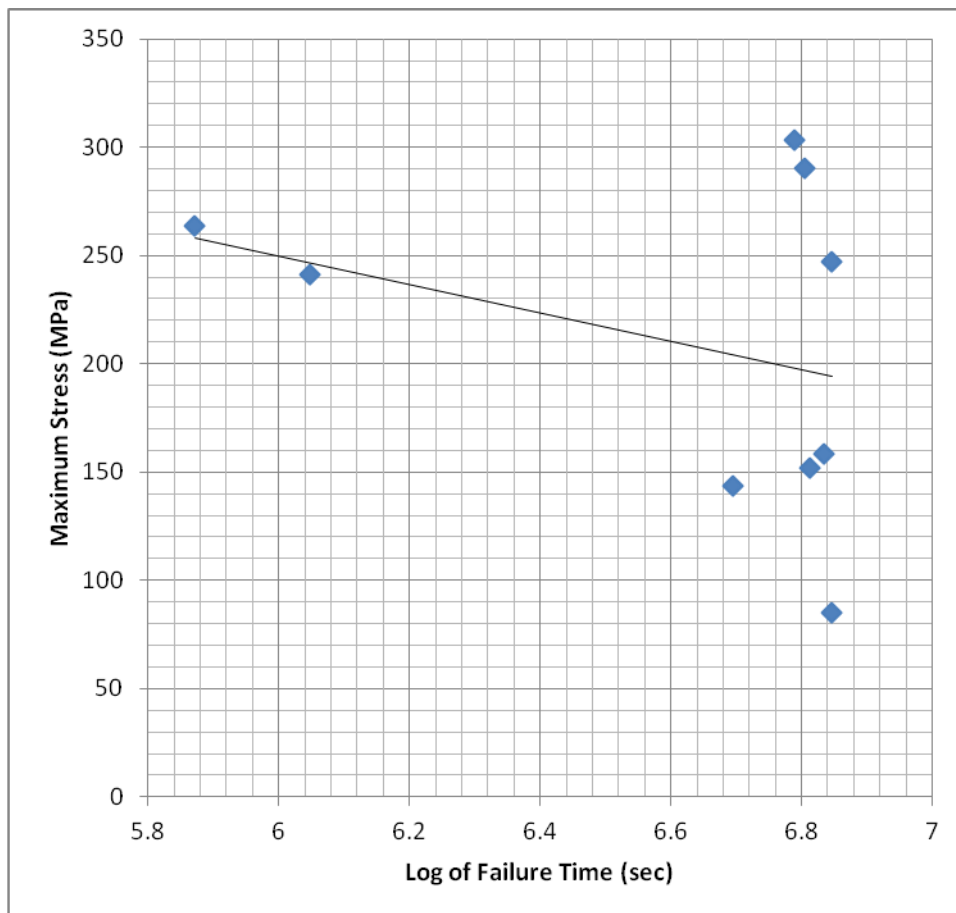
Fig: 4.51. Graph of Maximum Stress against Log of Failure Time.

In doing so the total strain was determined by calculating the ratio of the maximum extension to the extension gauge length and the latter was a constant for all the test cases.

In order to determine the inelastic strain the maximum extension at maximum load was subtracted from maximum extension and then divided by the extension gauge length. The extension gauge length was used because the extension was taking place at this length of the samples hence the name. The reason for subtracting the extension at maximum load from the maximum extension is because that would yield the elastic limit of these samples. They seemed to have suffered some damage once they reached these loads and we all know that

with damage elasticity does not exist anymore with that we are now talking about inelastic limit. Below in table: 4.25 we have a table of the two sets of failure times. We can see that the load based approach has the benefit of a descending order; the more the load the less the failure time. For the strain approach this has not played out that way this is so because of the factors inherent in the samples as we already know from the discussions in the previous sections. One other point was that the strain approach though not orderly provides a more conservative estimate of the failure times. The fact that the strain approach is a form of damage model equally makes the case for it consideration.

Failure Times using the Strain approach (sec)	Failure Times using the Load approach (sec)
7014848.185	3.60E+07
4960424.2	1.25E+07
6497865.619	1.12E+07
6811266.077	1.03E+07
1117462.822	4.47E+06
7020411.746	4.26E+06
743351.3977	3.73E+06
6385498.957	3.08E+06
6162836.095	2.82E+06
7014848.185	3.60E+07

Table: 4.25. Comparing Strain approach and Load approach failure times outcomes
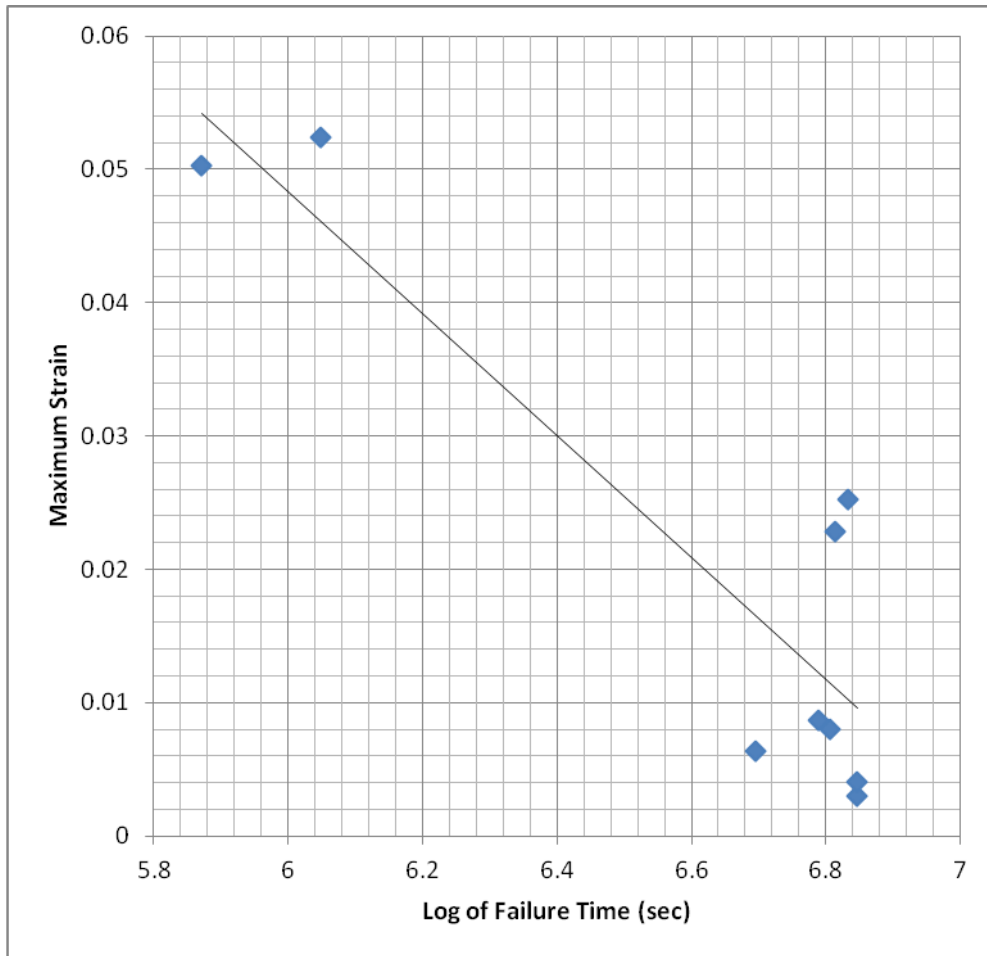
Fig: 4.52. Graph of Maximum Strain against Log of Failure Time (sec)

Fig: 4.52 above is the graph of maximum strain against log of failure time and we can still see the same scatter as in the last graph before it. The standard deviation from the mean of the log of failure time was 0.3777 which is 37.77%. These values can equally be said to be volatile in the excess of 37.77% and that is quite significant.

Having determined the failure time with respect to inelastic strain using the said assumptions a window was opened into what creep and plasticity led fatigue would look like. These two parameters also occur from thermal cycling and loads and they are also extreme states of structural and material damage.

4.8. Life times under load in aqueous environments

Using the data from the tensile test cases the analysis of the life times of samples or coupons were determined using the equation below:

$$t_c = \frac{2}{A\sigma^3 y^3 a_i}\left(1 - \frac{\sigma_a}{\sigma_{max}}\right) \qquad (183)$$

And we have t_c as the life time of the composite, A is a constant and y was established in the section above. In determining A the Reifsnider critical-element model was employed and it is stated below:

$$\frac{\sigma_a}{\sigma_{uc}} = A + B\left(\log t_f\right)^p \qquad (184)$$

σ_a and σ_{uc} are applied stress amplitude and initial strength of the coupon or samples respectively. A, B and p are constants that can be determined from the data set and the $\log t_f$ for the various test cases have already been established in the previous section above. In other to determine A the values of $\log t_f$ and those of the stress ratios were set in Microsoft Excel columns respectively. And using the LINEST function the values of A and B were determined as 0 and 1 respectively. Having A as 0 will almost invalidate the outcomes so it was set as 1. So using the determined values a graph of stress against log of life times was plotted below.
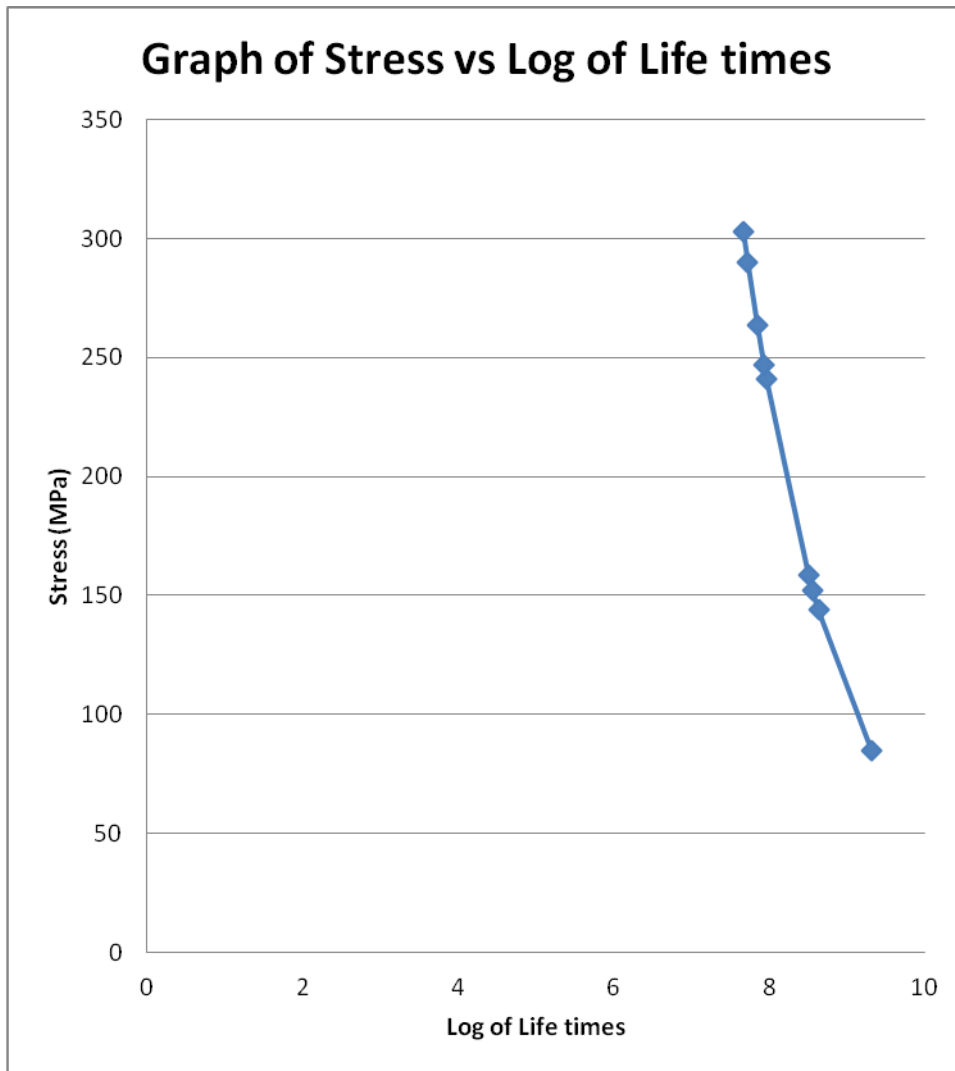
Fig: 4.53. Graph of Stress against Log of Life times

Notice that the graph in fig: 4.53 above produced a more orderly curve as against the curve of other graphs in previous sections. The major reason for such orderliness was down to the varying parameters we have in the Reifsnider equation above. These parameters were stress related as a result the values for the graph mirror themselves or correspond.

4.9. Optimization

In carrying out optimization what usually happens is maximization or minimization of parameters with constraints as factors as the case may be. In doing so, weighing factors have to be assigned. These weighing factors can be α and β or more and they must sum up to 1 that is $\alpha + \beta = 1$. They equally describe an objective function F in this way:

$$F = \alpha + \beta \qquad (185)$$

In order to sufficiently describe an objective function as the case may be the expression goes thus:

$$F = -\alpha S + \beta V \qquad (186)$$

Assuming S and V are stiffness and volume respectively and they depend on some design variables or parameters like fibre angle, radius, and length and so on as the case may be. They can be expressed thus:

$$S = \ (E,\ t,\ l,\ w) \qquad (187)$$

$$V = \ (E,\ t,\ l,\ w) \qquad (188)$$

Therefore F can be written thus:

$$F = -\alpha S\ (E,\ t,\ l,\ w) + \beta V\ (E,\ t,\ l,\ w) \qquad (189)$$

This goes to say that the objective function F is equally dependent on these design variables or parameters or that they are its factors.

In this work Ansys a finite element code was employed in these Design Optimization exercises. Pressure was applied on the models in these optimization cases in the X-direction; the thickness of the sample was the value that was determined in the empirical sections and a function of the number of Plys.

4.9.1. Optimization with Thickness of Plies as Objective Function

The objective function formulation for the number of plies $N1$ of the model under applied pressure in fig: 4.54a goes thus:

$$F = -\frac{\alpha}{2}EX - \frac{\alpha}{2}N1 + \frac{\beta}{2}SX + \frac{\beta}{2}EPTOX \qquad (190)$$

EX, N1, SX and *EPTOX* are Young's Modulus, Number of Plies, Maximum Stress and Maximum Strain respectively. These are the notations that were used in Ansys to define these parameters. In this case we have the details of the Ansys case and fig: 4.54a shows the model employed with pressure applied. These codes that follow are the initial set of definitions that has to be set out before all the others

```
N1=T1/0.0024999903     ! Number of Plies
EX=610500000000        ! Young's Modulus
T1=0.00999999614       ! Thickness of the Plies
SX= 398350000          ! Applied Load
```

```
EPTOX=0.006525        ! Strain
/UNITS, si, 1, 1, 1, 1, 0, 1, 1, 1
```
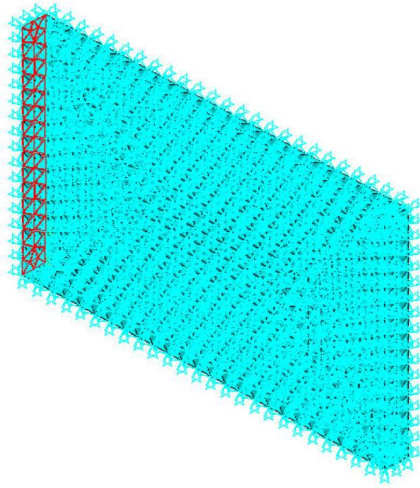

Fig: 4.54a. Employed model under applied pressure

Element Type

The Element type adopted in this analysis was Solid and the type is Solid-45.

Meshing

30862 Solid45 quadratic 10-nodes tetrahedral

1 Volume

60594 Nodes

7328 Elements

Element Edge Length: 1.0

Displacement

UX = 0.0001360 m

UY = 0

UZ = 0

Pressure

Pressure = 398.35 MPa   (Pressure of 398.35 MPa was applied in the X-direction on the side of the model in fig: 4.54a that is red.)

Material Properties

EX = 61049.6757 MPa

EY = 61037.2538 MPa

EZ = 61013.4909 MPa

PRXY = 0.3

PRYZ = 0.3

PRXZ = 0.3

GXY = 30572.2248 MPa

GYZ = 30566.0023 MPa

GXZ = 30554.1043 MPa

Optimization Variables

Objective (OBJ):

Initial Thickness of Plies (T1) = 0.999999614 mm

Design Variables (DV):

Maximum Number of Plies (N1) = 8

Minimum Number of Plies (N1) = 4

Maximum Young's Modulus (EX) = 61049.6757 MPa

Minimum Young's Modulus (EX) = 15252.4189 MPa

State Variables (SV):

Maximum Equivalent Stress (SX) = 398.35 MPa

Minimum Equivalent Stress (SX) = 100 MPa

Maximum Total Mechanical Strain (EPTOX) = 0.6525

Minimum Total Mechanical Strain (EPTOX) = 0.1525

The optimization analysis in Ansys was solved using Sub-problem Approximation iteration and it produced five sets of results as can be seen in table: 4.26a below:

```
                 SET 1         *SET 2*        SET 3         SET 4
                 (INFEASIBLE)  (FEASIBLE)    (FEASIBLE)    (FEASIBLE)
 SX      (SV)    0.39835E+09   0.39835E+09   0.39835E+09   0.39835E+09
 EPTOX   (SV)    0.65250E-02   0.65250E-02   0.65250E-02   0.65250E-02
 N1      (DV)    4             7(approx)     6(approx)     6(approx)
 EX      (DV)  > 0.61050E+11   0.36190E+11   0.46961E+11   0.43551E+11
 T1      (OBJ)   0.10000E-01   0.10000E-01   0.10000E-01   0.10000E-01

                 SET 5
                 (FEASIBLE)
 SX      (SV)    0.39835E+09
 EPTOX   (SV)    0.65250E-02
 N1      (DV)    5(approx)
 EX      (DV)    0.19521E+11
 T1      (OBJ)   0.10000E-01
```
Table: 4.26a. LIST OF OPTIMIZATION SETS FROM SET 1 TO SET 5 SHOWING ONLY OPTIMIZATION PARAMETERS. (A "*" SYMBOL IS USED TO INDICATE THE BEST LISTED SET)

Below in fig: 4.54b is a graph of the derived Young's Modulus values (EX) against Number of Plies (N1), tracing all the points will not produce a smooth curve as such a trendline was used, notice that all the points lie above the trendline apart from that of SET-5. This SET also accounts for the lowest EX value, though the result says its feasible it was also the most undesirable because if a laminate such composition is developed it will be a poor one relative to the other SETs.
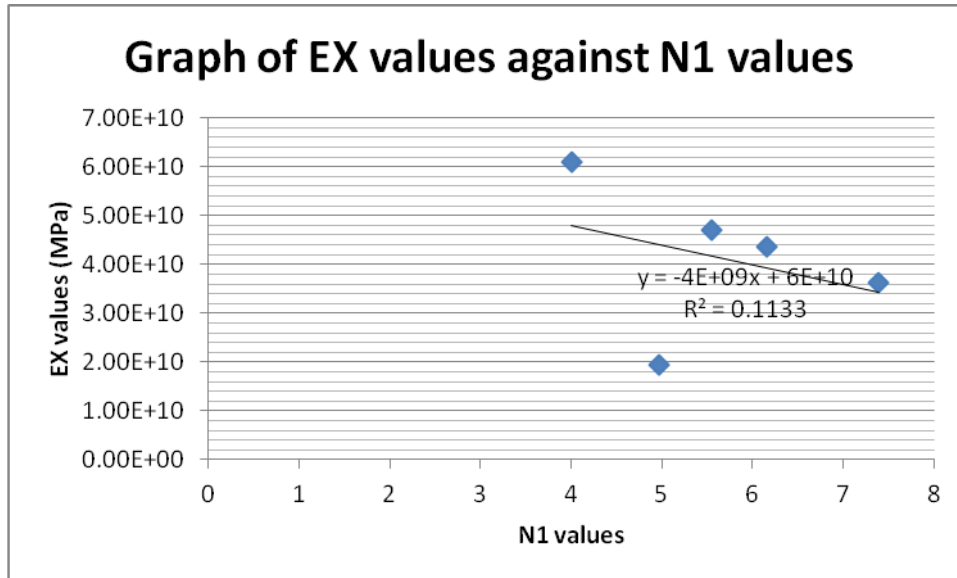
Fig: 4.54b. Graph of EX values against N1 values

4.9.2 Optimization with Young's Modulus as Objective Function

In this case we have the details of the Ansys case and fig: 4.54c shows the model employed with the load applied, the load was Pressure; this model was also the same model used in sub-section 4.9.1.
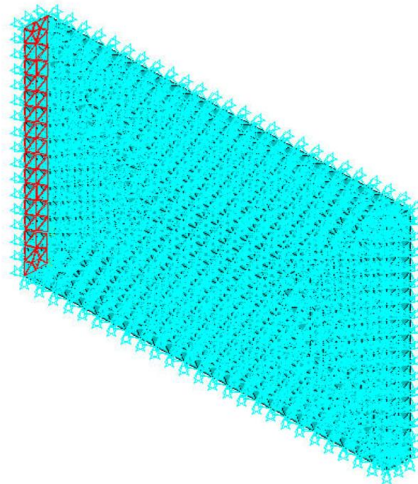

Fig: 4.54c. Employed model under applied load

```
N1=T1/0.0024999903    ! Number of Plies
EX=SX/EPTOX           ! Young's Modulus
T1=0.00999999614      ! Thickness of the Plies
SX= 398350000         ! Applied Load
EPTOX=0.006525        ! Strain
/UNITS, si, 1, 1, 1, 1, 0, 1, 1, 1
```

Element Type

The Element type adopted in this analysis was Solid and the type is Solid-45.

Meshing

30862 Solid45 quadratic 10-nodes tetrahedral

1 Volume

60594 Nodes

7328 Elements

Element Edge Length: 1.0

Displacement

UX = 0.0001360 m

UY = 0

UZ = 0

Pressure

Pressure = 398.35 MPa   (Pressure of 398.35 MPa was applied in the X-direction on the side of the model in fig: 4.54c that is red.)

Material Properties

EX = 61049.6757 MPa

EY = 61037.2538 MPa

EZ = 61013.4909 MPa

PRXY = 0.3

PRYZ = 0.3

PRXZ = 0.3

GXY = 30572.2248 MPa

GYZ = 30566.0023 MPa

GXZ = 30554.1043 MPa

Optimization Variables

Objective (OBJ):

Initial Thickness of Plies (T1) = 0.999999614 mm

Design Variables (DV):

Maximum Number of Plies (N1) = 8

Minimum Number of Plies (N1) = 4

Maximum Young's Modulus (EX) = 61049.6757 MPa

Minimum Young's Modulus (EX) = 15252.4189 MPa

State Variables (SV):

Maximum Equivalent Stress (SX) = 398.35 MPa

Minimum Equivalent Stress (SX) = 100 MPa

Maximum Total Mechanical Strain (EPTOX) = 0.6525

Minimum Total Mechanical Strain (EPTOX) = 0.1525

The optimization analysis in Ansys was solved using Sub-problem Approximation iteration
and it produced five sets of results as can be seen in table: 4.27b below:

```
LIST OF OPTIMIZATION SETS FROM SET 1 TO SET 5 AND SHOWS ONLY OPTIMIZATION
PARAMETERS (A "*" SYMBOL IS USED TO INDICATE THE BEST LISTED SET).

                    SET 1          *SET 2*         SET 3          SET 4
                    (INFEASIBLE)   (FEASIBLE)      (FEASIBLE)     (FEASIBLE)
SX      (SV)        0.39835E+09    0.39835E+09     0.39835E+09    0.39835E+09
EPTOX   (SV)        0.65250E-02    0.65250E-02     0.65250E-02    0.65250E-02
N1      (DV)        4.0000         7(approx)       6(approx)      6(approx)
T1      (DV)      > 0.10000E-01    0.14572E-02     0.16924E-02    0.16179E-02
EX      (OBJ)       0.61050E+11    0.61050E+11     0.61050E+11    0.61050E+11


                    SET 5
                    (FEASIBLE)
SX      (SV)        0.39835E+09
EPTOX   (SV)        0.65250E-02
N1      (DV)        8(approx)
T1      (DV)        0.18896E-02
EX      (OBJ)       0.61050E+11
```

Table: 4.27b. `LIST OF OPTIMIZATION SETS FROM SET 1 TO SET 5 AND SHOWS ONLY OPTIMIZATION PARAMETERS (A "*" SYMBOL IS USED TO INDICATE THE BEST LISTED SET).`

Just as in sub-section: 4.9.1, the Number of Plies for the Feasible SET was 7 as well. Notice that the Young's Modulus values (EX) were all the same as such the Maximum Equivalent Stress (SX) and the Strain (EPTOX) values were equally equal. Fig: 4.54d below is graph of Number of Plies (N1) against Thickness of Plies (T1).
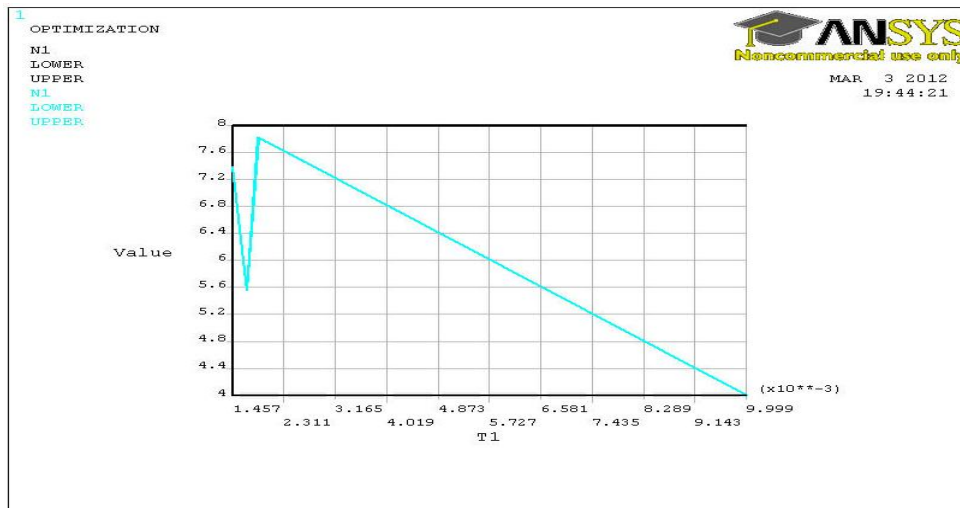

Fig: 4.54d: Graph of Number of Plies (N1) against Thickness of Plies (T1)

4.9.3. Optimization Progress Trend and Conclusion:

The Young's Modulus value (EX) from the feasible set-'SET 2' of the optimization results in sub-section 4.9.1. was used to carryout the same kind of numerical analysis described earlier in this section on the same model in fig: 4.54a and fig: 4.54c; the purpose of this was to show the progress or the application of the feasible optimization results the details follow below:

Element Type

The Element type adopted in this analysis was Solid and the type is Solid-45.

Meshing

30862 Solid45 quadratic 10-nodes tetrahedral

1 Volume

60594 Nodes

7328 Elements

Element Edge Length: 1.0

Displacement

UX = 0.0001360 m

UY = 0

UZ = 0

Pressure

Pressure = 398.35 MPa   (Pressure of 398.35 MPa was applied in the X-direction on the side of the model in fig: 4.54c that is red.)

Material Properties

EX = 36190 MPa

EY = 36168 MPa

EZ = 36154 MPa

PRXY = 0.3

PRYZ = 0.3

PRXZ = 0.3

GXY = 18123.0908 MPa

GYZ = 18112.0737 MPa

GXZ = 18105.0628 MPa

Below in fig: 4.54e-4.54h we have the element solution contour plots for deformations and stresses
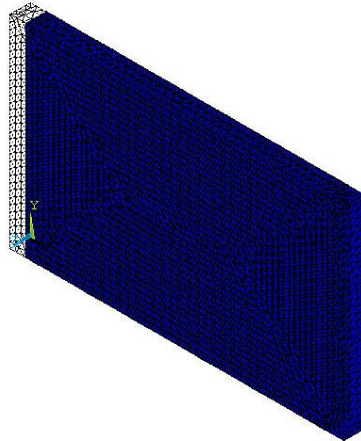
Fig: 4.54e. Deformed and Undeformed contour plot of the model
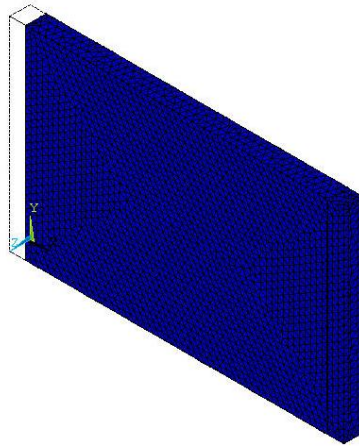
Fig: 4.54f. Deformed and Undeformed Edge contour plot of the model
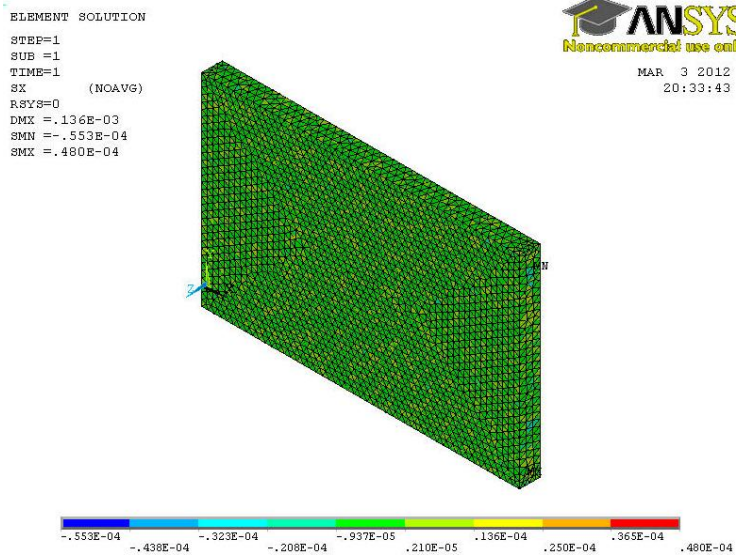
Fig: 4.54g. Maximum Stress in X-direction element solution contour plot of the model
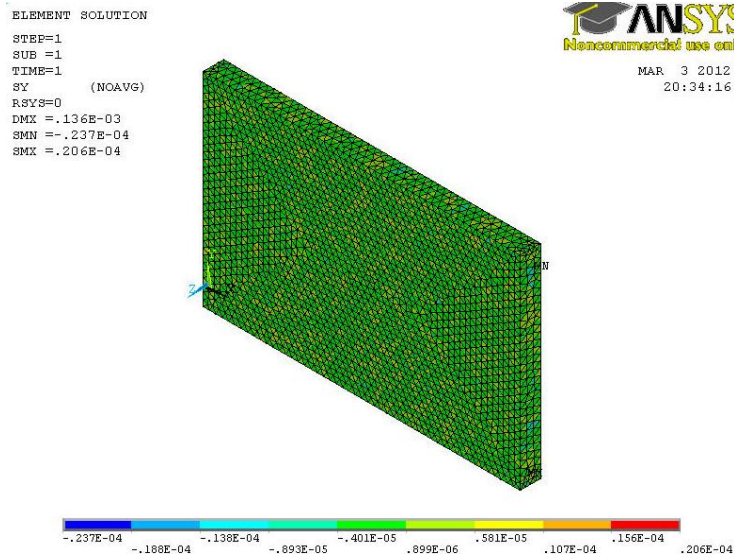
Fig: 4.54h. Maximum Stress in Y-direction element solution contour plot of the model

Optimization progress trend can be interpreted to mean among other interpretations the direction of the milestones accomplished during and after the optimization iteration or the outcome of the application the optimization results. In Fig: 4.54b and fig: 4.54d we have graphs of Young's Modulus (EX) values against Number of plies (N1) values and Graph of Number of Plies (N1) against Thickness of Plies (T1) respectively; as can be seen the curves in these graphs were point downwards implying a downward trend. At the same time some inconsistencies can be observed in the 5th SET of all the results in table: 4.26a and table: 4.27b; the EX value in the former going by the other values was not consistent this was also the case in the latter for the T1 value of the 5th SET of that table.

In conclusion the number of plies that was estimated to be the optimal figure was 7 but if applied to a Young's Modulus value of 36190 MPa; while 61050 MPa was the optimal value for the Young's Modulus with 7 as the desirable number of plies. These two sets of conclusions on the face of it of look inconsistent but were expected as they are different optimizations. Section 4.11 below is a form of optimization progress as the parameters in that analysis were derived from the Young's modulus optimization value that was obtained using Excel in this section.

4.10. Fatigue analysis of optimization outcomes

Using the obtained values above in (section 4.3.13) in a fatigue analysis one would expect that the outcomes will be worse than the previous ones in the fatigue section. Indeed that was the case; this was largely down to the fact that the sample in this case was a thicker one as such its cycles to failure and life would be relatively worse.

144

Cycles to Failure	Stress (MPa)			Endurance Limit (MPa)	Stress (MPa)			Life	Stress (MPa)
900000	84.86			42.3213	84.86			170000	84.86
890000	143.8			71.8206	143.8			120000	143.8
880000	152			75.9641	152			120000	152
880000	158.5			79.25	158.5			120000	158.5
910000	241			120.1141	241			79000	241
880000	246.9			123.3534	246.9			77000	246.9
940000	263.7			131.0183	263.7			72000	263.7
880000	290.2			145.0416	290.2			65000	290.2
820000	303.2			152.489	303.2			62000	303.2
*868060.5212	398.35			*199.2531	398.35			*10167.81	398.35

Table: 4.28. Values for the number of Cycles to failure, Endurance limit and Life all with respect to stress

In table: 4.28 we have values for the number of Cycles to failure, Endurance limit and Life all with respect to stress; the values at the bottom of the three sections are for the optimized case. Notice that the Life of this optimized case was significantly off the mark, the Endurance limit showed an improvement and the Cycles to failure also showed a relative improvement especially with the stress value it has.

To obtain these values the FORECAST and TREND functions in Microsoft Excel were used to extrapolate or interpolate the existing values as the case may be. Bear in mind that in the case of the Cycles to failure the existing values are not uniform and this had an influence on the interpolated case. So going by the interpolated Life value and even the number of Cycles to failure it can be said that increasing the number of Plies in itself is not exactly the way forward.

4.11. Optimization of the Piston Cap

In this optimization case the details used in the last numerical stress analysis was equally used. The objective was to reduce the volume of the cap, the variables were internal diameter, external diameter and depth; they were equally constraints as well. The other constraints were Z-, Y-, X- components of stress and the displacement.

Objective	Initial Values	Final Values
Volume (m^3)	0.000396403	0.000143278
Variables		
Internal Diameter (m)	0.0745	0.0765
External Diameter (m)	0.078	0.078
Depth (m)	0.083	0.03
Constraints		
Z-Component of Stress (MPa)	0.0036	0.0000189
Y-Component of Stress (MPa)	0.0066	0.000113
X-Component of Stress (MPa)	0.0015	0.0000248
Displacement (mm)	0.000372	0.000102

Table: 4.29. Table of the entries before the solution was solved for.

Below in fig: 4.55 we have the picture of the Solver Parameters tool for this optimization case and after that we also have the Answer report.
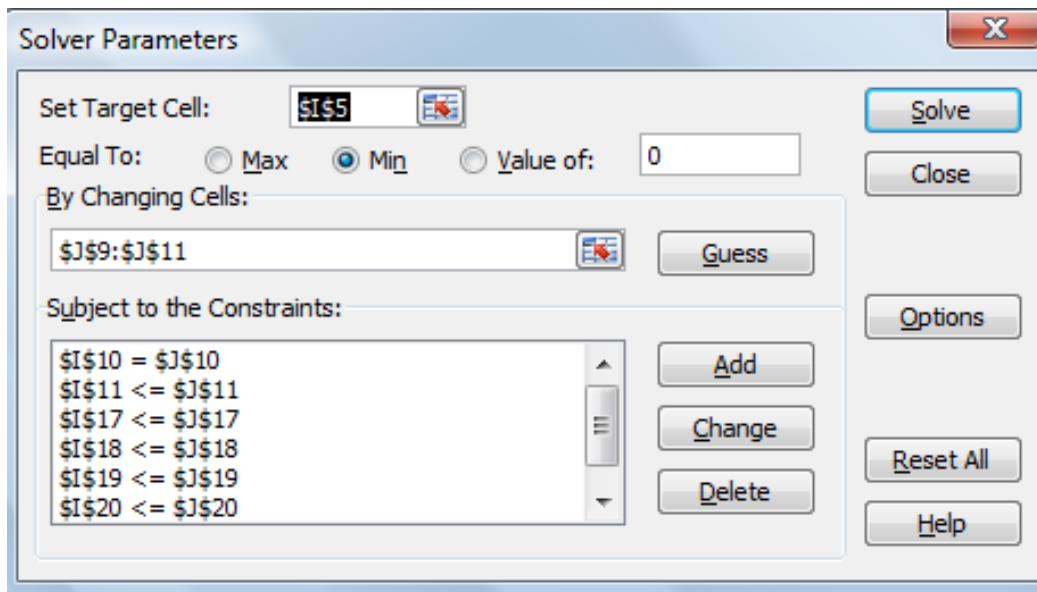
Fig: 4.55. Solver Parameter for optimizing the Volume of the Piston Cap

Target Cell (Min)

Cell	Name	Original Value	Final Value
$I$5	Volume (m³)	0.000396403	0.000143278

Adjustable Cells

Cell	Name	Original Value	Final Value
$J$9	Internal Diameter (m)	0.0765	0.0745
$J$10	External Diameter (m)	0.078	0.078
$J$11	Depth (m)	0.083	0.03

Constraints

Cell	Name	Cell Value	Formula	Status	Slack
$I$17	Z-comp stress Min (MPa)	0.0000189	$I$17<=$J$17	Not Binding	0.0035811
$I$18	Y-comp stress Min (MPa)	0.000113	$I$18<=$J$18	Not Binding	0.006487
$I$19	X-comp stress Min (MPa)	0.0000248	$I$19<=$J$19	Not Binding	0.0014752
$I$20	Displacement Min	0.000102	$I$20<=$J$20	Not	0.00027

	(MPa)			Binding	
$I$9	Internal Diameter (MPa)	0.0765	$I$9>=$J$9	Not Binding	0.002
$I$11	Depth (MPa)	0.03	$I$11<=$J$11	Binding	0
$I$10	External Diameter (MPa)	0.078	$I$10=$J$10	Not Binding	0

Table: 4.30. The Answer Report for the Optimization case.

In the Answer Report above of table: 4.30 the final value for the Volume was 0.000143278 m^3 and was achieved by minimising the depth of the cap otherwise known as the skirt. The minimum value for the piston skirt 0.03 m was chosen arbitrarily. This minimum value was also the final value for the depth. The other parameters were unaffected as can be seen from the Answer Report hence the reason their status says 'Not Binding'. Having optimized the piston cap, we can go ahead and determine the Stress, Strain and Displacement of this new piston cap based on the existing data from the original. This was done by extrapolating the data; which means that the load remained the same- 4.7KN. So we have below in table: 4.31 the results from the extrapolation:

Depth	0.03 m
Z- Direction Stress	1.5730 MPa
Z- Direction Strain	2.8171E-11
Displacement	0.1029 m

Table: 4.31. Results from the extrapolation

In the table: 4.32 below, we have the results from the extrapolation and the initial values for the purpose of comparison.

Depth	0.03 m	0.083 m

Z- Direction Stress	1.5730 MPa	0.00157 MPa
Z- Direction Strain	2.8171E-11	3.53E-14
Displacement	0.1029 m	0.000229 m

Table: 4.32. Comparing the optimized piston cap and the initial one

It can be seen that with the shorter cap we have a greatly increased stress in the Z-direction, more strain and displacement. These are all largely down to the fact that we now have a smaller volume and area as well. Going by that we can expect that stress would be greater in the optimized piston cap as area is a factor of stress; the less it is the greater the stress as the case may be. A decision as to which of the caps has to be adopted has to be made, and to do so the fatigue analysis of the piston caps has to be carried out as well as other analysis like the Monte Carlo simulation. This is because we are dealing with some uncertainties and in this case; the decision as to which piston cap that has to be adopted fatigue as such Monte Carlo simulations will help in estimating these uncertainties.

	Piston Cap
N_f (Life)	$2.3*10^5$
E (MPa)	61050
S_u (MPa)	137.6046
S_F'(MPa)	220.1674
B	-0.085
S_{FL}(MPa)	55.0424
S_{max} (MPa)	70
S_{min} (MPa)	1
N_{FL} Cycles	$1.2*10^7$
K_t	1

k_L	1
k_{size}	0.5695
k_{SF}	1
S_a (MPa)	34
S_m (MPa)	36
S_{eq}	46
Slope	-0.13

Table: 4.33. Fatigue results for the initial Piston cap

In the fatigue analysis whose results are above in table: 4.33 a cycle to failure of 12 million cycles was arrived at. Bear in mind that this piston cap has a depth of 0.083 mm, so in other to determine that of 0.03 mm case extrapolation was used again. This produced a cycle to failure of 65 million cycles, see table: 4.33a. This was of course what was expected not essentially the result but an improved number of cycles to failure.

Cycles	Displacement (mm)	Strain	Stress (MPa)	Depth (m)
1.20E+07	0.000229	3.53E-14	0.00157	0.083
1.21E+07	0.000372	6.80E-14	0.0036	0.0829
1.20E+07	0.00017	1.17E-14	0.000645	0.083
1.20E+07	0.000212	1.22E-14	0.000299	0.083
1.20E+07	0.000102	2.99E-16	1.89E-05	0.083
*65000000	0.10286575	2.82E-11	1.573023975	0.030

Table: 4.33a. Values from the extrapolation of the fatigue analysis
values of the initial piston cap

4.12. Verification of the piston cap optimization

In carrying out this verification normal random variables were used to verify the number of cycles that were obtained from the optimization. This verification with normal random variables or Monte Carlo simulation is necessary so as to ensure that there is some confidence in the number of cycles that were obtained from the optimization, since we are dealing with uncertain events it aids in estimating this uncertainty accurately. In doing so the random numbers were set out on Microsoft Excel; typing =RAND() in the desired cell will produce a value between 0 and 1. In this case what was at hand was far less discrete and more of a random case, so we take up 400 cases or iterations of this simulation. In doing so the Excel functions NORMINV(rand(), mu, sigma) and =RAND() were typed in adjacent cells. The rand() value refers to the cell containing the =RAND function, mu is the mean and sigma the standard deviation. The mean in this case was that of the two cycles to failure obtained for the two piston cap depths 1.2e7 and 6.5e7 respectively; this was also the case for the standard deviation. Since about 400 iterations or cases were used, these functions had to be copied from the initial cells and pasted in 399 cells below, see fig: 4.56 below.

Fig: 4.56. Picture showing some of the cells out of the 400 cells

The random numbers can be recalculated by pressing the F9 button on the computer keyboard; this actually recalculates the RAND() value which consequently affects the other values associated with it. In the picture above looking at cells B23 and C23 we have 51, 311, 029.75 cycles and a probability of 0.633764433; this means that at about 63% of the time the

number of cycles to failure is less than 51, 311, 029.75 cycles. In the case of the piston whose depth is 0.030m, at about 72% of the time it takes 65, 000, 000 cycles for the piston skirt made of the structure in this work to fail. When the mean value was changed to 65 million cycles there was equally not much of a difference; at about 75% to 76% of the time the number of cycles to failure of the 0.030m piston was less than 65 million cycles. This goes to tell that changing the mean value in this case to encompass only one piston cap case does not produce a very diverging outcome relative to the case where two cases were involved.

Table: 4.35 below facilitate the comparison of the two different piston caps through the information about them provided.

Number of cycles to failure	Probability	Piston Cap Height (mm)
12,000,000	0.24	83
65,000,000	0.76	30

Table: 4.35. Comparison of the two different piston caps

It can be seen that the longer piston cap spots a probability that says; 24% of the time the number of cycles to failure is less than the stated value which is 12 million. Though it is a relatively poor value it offers less window of uncertainty of what is established. The shorter one spots a probability that says that 76% of the time the number of cycles to failure is less than 65 million, this is a price normally incurred from optimizing parameters and their like. A decision has to be made as to which of the piston caps has to be adopted based on these probabilities. The decision was to go ahead with the one derived from the optimization which was the one that has the 30mm height. The reason was largely down to the fact that it will still deliver more number of cycles to failure regardless of how certain the latter is.

Using the IF function which goes thus IF(logical test, [value if true], [value if false]) in combination with the other functions mentioned above one can find out more about the data we have. One of such cases was establishing what number of cycles to failure was associated with a particular stress value. Random stress values can be setup by using the normal variable function NORMINV(rand(), mu, sigma). In this case the mean and standard deviation values were for the

stress values obtained from the numerical stress analysis in ANSYS; these stress values were stated in one of the tables above.

To go about doing this the functions goes thus:
=IF(M29>=0.00157,FORECAST(M29,M14:M19,P14:P19),0), see fig: 4.57 right below.

	f_x	=IF(M29>=0.00157,FORECAST(M29,M14:M19,P14:P19),0)									
	F	G	H	I	J	K	L	M	N	O	P	Q
	0.0745	0.0745						cycles	Displacement	Strain	Stress	Depth
	0.078	0.078						1.20E+07	0.000229	3.53E-14	0.00157	0.083
	0.083	0.083						1.21E+07	0.000372	6.80E-14	0.0036	0.0829
								1.20E+07	0.00017	1.17E-14	0.000645	0.083
								1.20E+07	0.000212	1.22E-14	0.000299	0.083
								1.20E+07	0.000102	2.99E-16	1.89E-05	0.083
	6.50E+07							65000000	0.10286575	2.82E-11	1.573023975	0.03
	37476659.4											
	Cycle	1.20E+07						0.069156047			0.64168491	
	Rand#	0.70577186			0	1.20E+07						
	Sim Cycle	48000000			0.25	2.40E+07						
	Depth1	0.03			0.5	4.80E+07						
	Depth2	0.083			0.75	6.00E+07						
		65000000			0.8	6.50E+07						
		32552912										
								0.610392111				

Fig: 4.57. A Picture from Excel showing the IF function used in detail

It says if cell M29 is greater than 0.00157 MPa; forecast the value of cell M29 based on the data available which are on cells M14 to M19 and cells P14 to P19 if it is true and zero if false. In order to do this the value for cell M29 has to be defined or determined, hence fig: 4.58 right below shows that.

	f_x	=NORMINV(G23,0.263192812,0.64168491)									
	F	G	H	I	J	K	L	M	N	O	P	Q
i	0.0745	0.0745						cycles	Displacement	Strain	Stress	Depth
	0.078	0.078						1.20E+07	0.000229	3.53E-14	0.00157	0.083
	0.083	0.083						1.21E+07	0.000372	6.80E-14	0.0036	0.0829
								1.20E+07	0.00017	1.17E-14	0.000645	0.083
								1.20E+07	0.000212	1.22E-14	0.000299	0.083
								1.20E+07	0.000102	2.99E-16	1.89E-05	0.083
	6.50E+07							65000000	0.10286575	2.82E-11	1.573023975	0.03
	37476659.4											
	Cycle	1.20E+07						0.057041878			0.64168491	
	Rand#	0.70921642			0	1.20E+07						
	Sim Cycle	48000000			0.25	2.40E+07						
	Depth1	0.03			0.5	4.80E+07						
	Depth2	0.083			0.75	6.00E+07						
		65000000			0.8	6.50E+07						
		32769690.9										
								0.616823458				

Fig: 4.58. Picture showing the function for simulating the M29 values.

In the function NORMINV(G23,0.263192812,0.64168491) above in fig: 4.58 the two values stated there are the mean and the standard deviation respectively of the stress values while cell G23 is the random value. With what is on the figures right above a stress of 0.6168 MPa was associated

with 32, 769, 690.9 cycles to failure. It must be noted that in this case the higher the stress value the higher the number of cycles to failure, and the less the volume. Indeed if a piston has less volume it will undergo greater stress based on the model used in this work and at the same time the number of cycles to failure would be high which was true in all cases. With less volume which may be due to less height as in this case stiffness strength may be increased and consequently the number of cycles to failure.

Chapter 5

5.0. Results and Discussion

In the previous chapter a significant amount of what was discussed there are pertinent to this chapter, as a result this chapter will be a little bit more of a review of such cases and more.

5.1. Crack propagation.

This is a continued bid to determine some kind of damage and all that's related to it. In this case a model was created in the CAD application Pro-engineer Wildfire. This model was saved as an IGES file as this is one of the few geometry file formats that Ansys can read. This model unlike that of Fig: 4.39 was created whole meaning two or more volumes were not glued together. The crack case was created by removing or subtracting a triangular solid from the bigger volume, see fig: 5.1 and fig: 5.1a below; for each radius case the desired value like 0.06 mm was entered while the model it is been created.
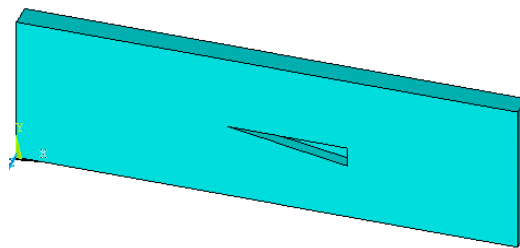
Fig: 5.1. Model with crack.

The simulations were carried out by applying uniform displacement on all the four crack areas. The loading was carried out using automatic time stepping feature in the solver. This feature will respond to plasticity when it occurs (which was after) by reducing the load step size subsequent to a load step in which a large number of equilibrium iterations takes place or a case where a plastic strain increment greater than 15% has occurred. The program uses a smaller step size if a very large step size was initial taken [21]. It must be noted that 'large deflections and large strain geometric nonlinearities' usually associated with plasticity do occur, because these are anticipated the feature in the solver that normally affects this was activated. In solving this kind of analysis in Ansys unspecified nonlinear behaviour might also occur along with plasticity. As such plastic material response may be associated with

large deflection and consequently large strain geometric nonlinearities [21]. The following GUI path will ensure that the effects are activated:

Main Menu> Solution> Analysis Type> Solution Control (: Basic Tab) or

Main Menu> Solution> Unabridged Menu> Analysis Type> Analysis Options

Below is the details used in the analysis:

Element Type

The Element type adopted in this analysis is Solid and the type is Solid-46 or layered 46-Node.

Meshing

32792 Solid46 quadratic 10-nodes tetrahedral

1 Volume

65604 Nodes

7848 Elements

Element Edge Length: 0.01

Displacement

UX = 3 mm

UY = 3 mm

UZ = 3 mm
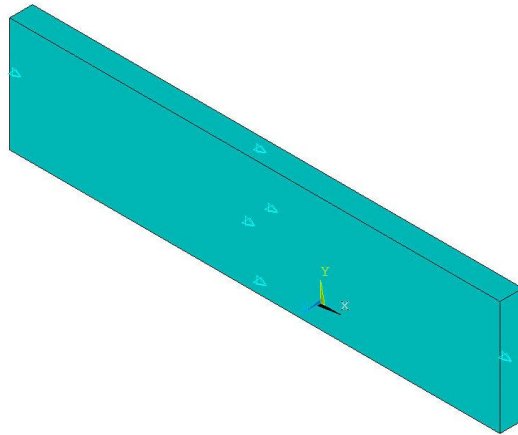
Fig: 5.1a. Model with boundary controls applied

Pressure and Temperature

Pressure = 16.4 MPa   (Pressure of 16.4 MPa was applied on all the four crack sides; also the combined stress in the top ring land. This is where the top most piston rig rests.)

Temperature = 210 ^{o}C (Temperature of 210 ^{o}C was applied on all the four crack sides; this is also the highest temperature that can be attained at the hottest part of the piston based on the design.)

Material Properties

EX = 0.615e14

EY = 0.614e14

EZ = 0.1433e14

PRXY = 0.039

PRYZ = 0.46

PRXZ = 0.46

GXY = 0.58e13

GYZ = 0.26e13

GXZ = 0.28e13

DENSITY = 1.55

ALPX = 0.00000123 (Coefficient of thermal expansion in X-direction)

ALPY = 0.00000184   (" " in Y-direction)

ALPZ = 0.0000407   (" " in Z-direction)

Table: 5.1 below contains some results from the element solution of the simulation:

Crack Radius (mm)	0.06	0.12	0.18	0.24	0.3
Maximum stress in X-component (MPa)	41.4	45	45	60.6	55.3
Minimum stress in X-component (MPa)		-115	-101	-116	-102
Maximum stress in Y-component (MPa)	41.4	41.3	49.6	35.6	35.6
Minimum stress in Y-component (MPa)		-95.7	-103	-97.6	-104
Maximum stress in Z-component (MPa)	51.6	46.6	54.2	43	48
Minimum stress in Z-component (MPa)		-111	-135	-140	-138
Maximum XY shear stress (MPa)	28.2	27.2	22.9	30.6	47.6
Minimum XY shear stress (MPa)		-28.4	-36	-34.3	-35.2

Maximum YZ shear stress(MPa)	33.8	36.9	29	31.7	36.1
Minimum YZ shear stress (MPa)		-31.3	-33.4	-38.4	-34.8
Maximum XZ shear stress (MPa)	33.2	36.8	28.4	61.4	59.3
Minimum XZ shear stress (MPa)		-30.7	-28.3	-26.1	-28.2
Max 1st Principal Stress (MPa)	62.1	64.8	57.7	64.1	76.5
Min 1st Principal stress (MPa)		-75.6	-73	-78.6	-80
Max 2nd Principal stress (MPa)	39.8	37	47.1	35.6	30.5
Min 2nd Principal stress (MPa)		-98.3	-98.5	-114	-119
Max 3rd Principal Stress (MPa)	26.6	27.7	25.6	20.2	18.7
Min 3rd Principal stress (MPa)		-139	-135	-145	-138
Energy release rate (J/m^2)					
Max Strain energy (J)	0.001343	0.001035	0.01101	0.007281	0.003034
Min Strain energy (J)		0.00086	0.000970	0.000828	0.000355
Time (Processing)	1hr 50mins	1hr 36mins	1hr 38mins	1hr 37mins	1hr 46mins

Table: 5.1. Array of element solution results from the simulations

Not much can be really said about the nature of the results in (table 5.1) above, there is almost no uniformity or consistency of stresses relative to the crack lengths. In the individual cases we will see below there was no case of deformation and plasticity.

5.1. 1. Crack Length: 0.06mm
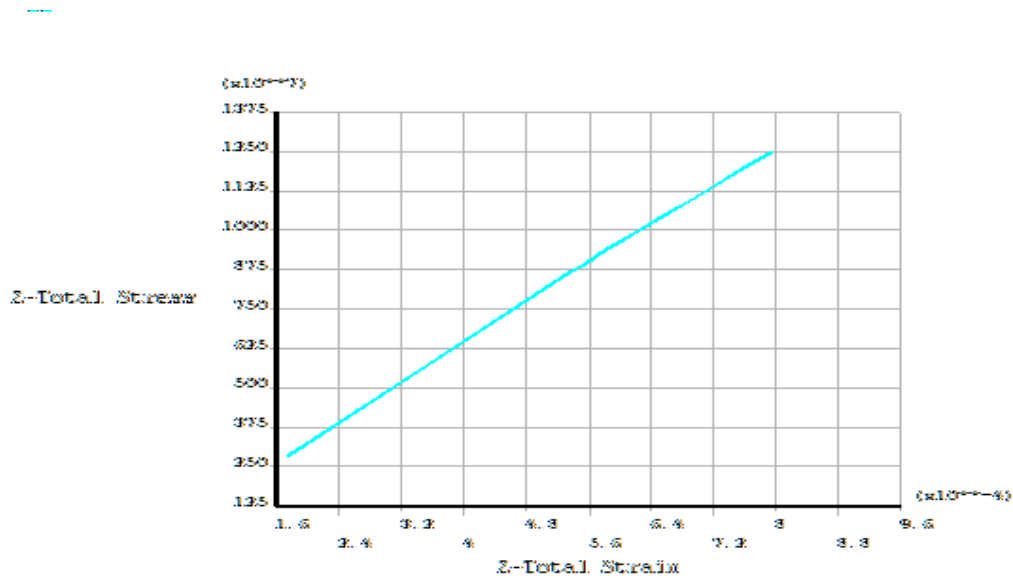
Fig: 5.2. Plot of Total Stress in Z-direction against Total strain in Z-direction
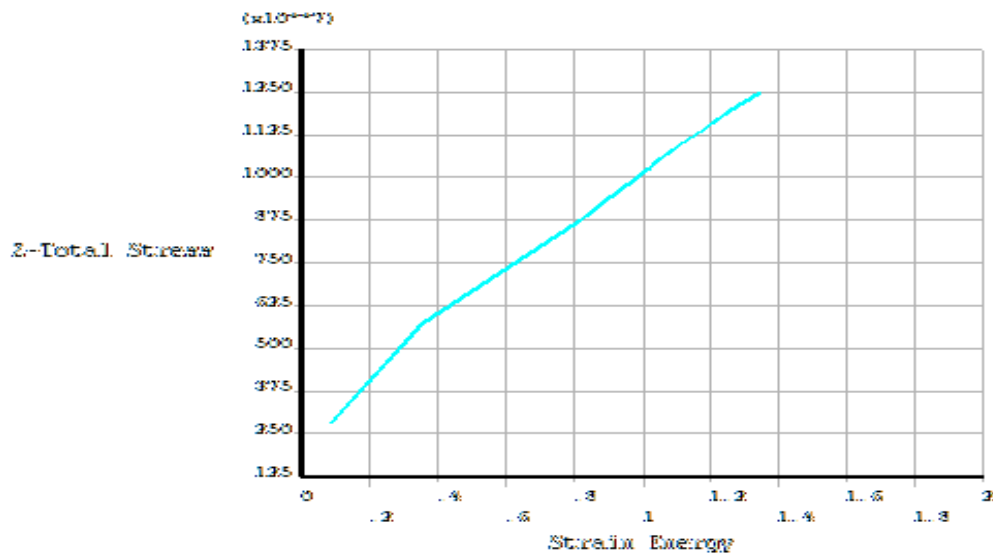
Fig: 5.3. Plot of Total Stress in Z-direction against Strain Energy
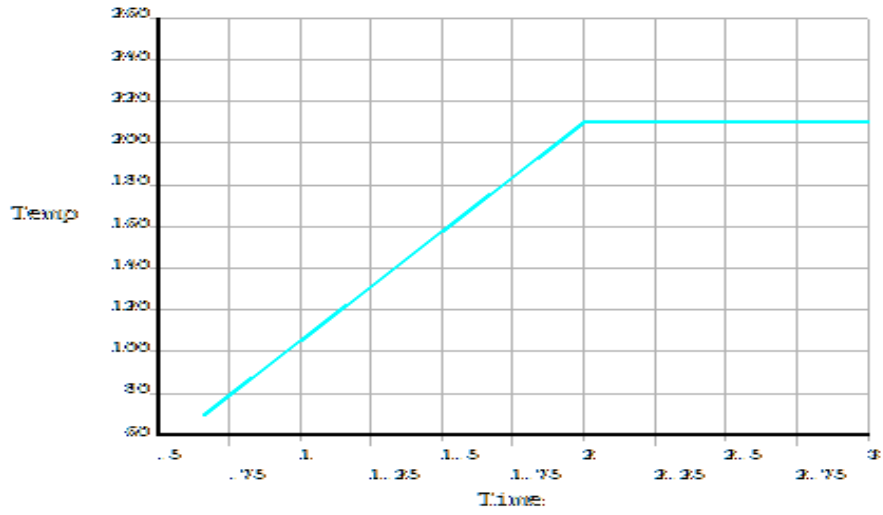
Fig: 5.4. Plot of Temperature against Time

## 5.1. 2. Crack Length: 0.12mm
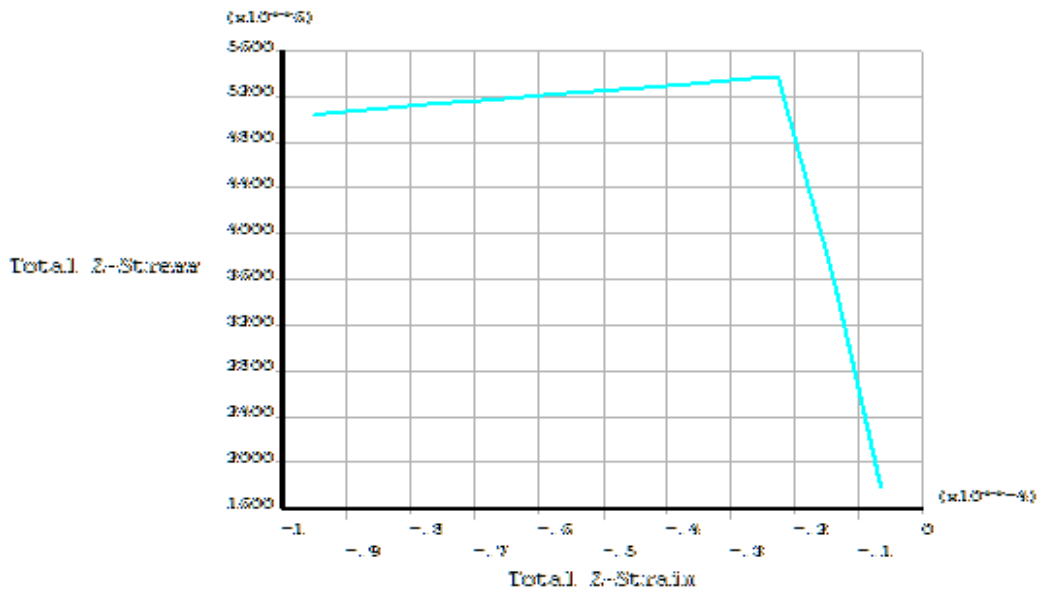
Fig: 5.5. Plot of Total Z-Stress against Total Z-Strain for crack length 0.12mm for node-11008 attached to element-15723.
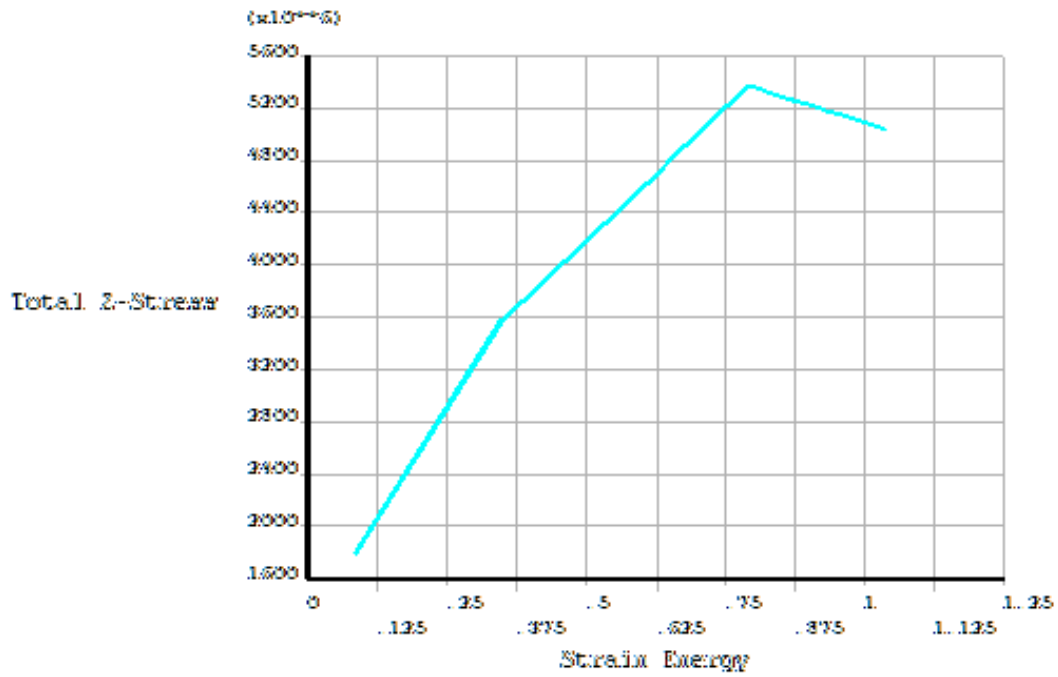
Fig: 5.6. Plot of Total Z-Stress against Strain Energy of crack tip node-11008 attached to element 15723.
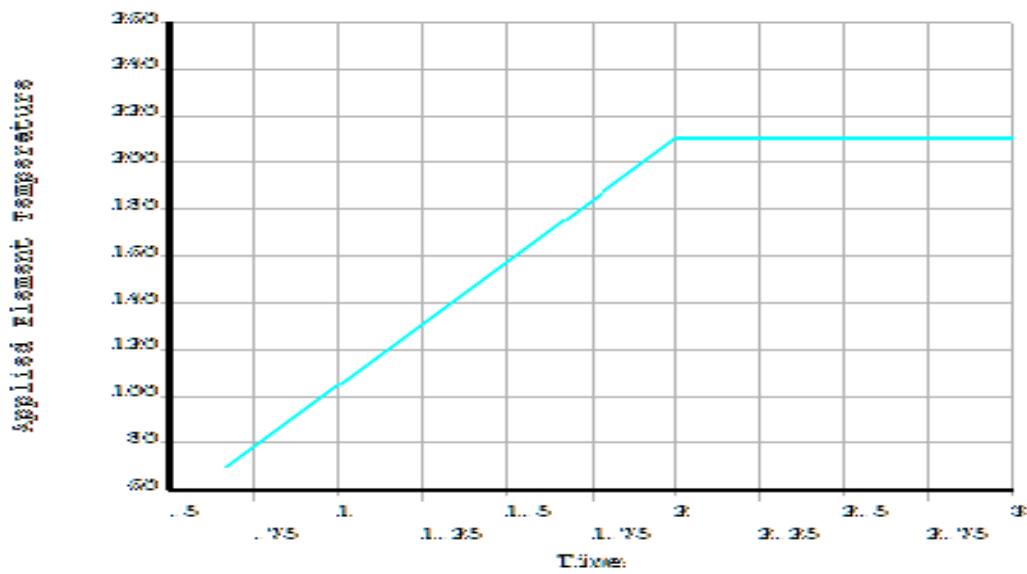
Fig: 5.7. Plot of Applied Element Temperature against Time of Node-2566 attached to element-3401. This was used because the former nodes and elements have zero temperature values. The latter were picked from areas where temperature values were not zero.

5.1. 3. Crack length 0.18mm
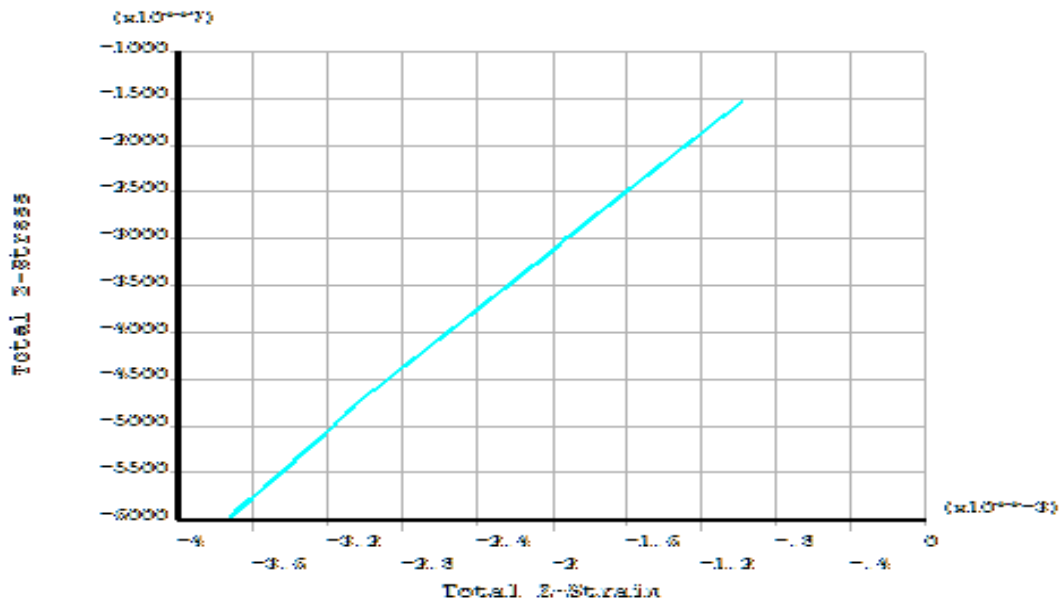
Fig: 5.8. Plot of Total Z-Stress against Total Z-Strain for crack length 0.18mm for node-867 attached to element-49142.
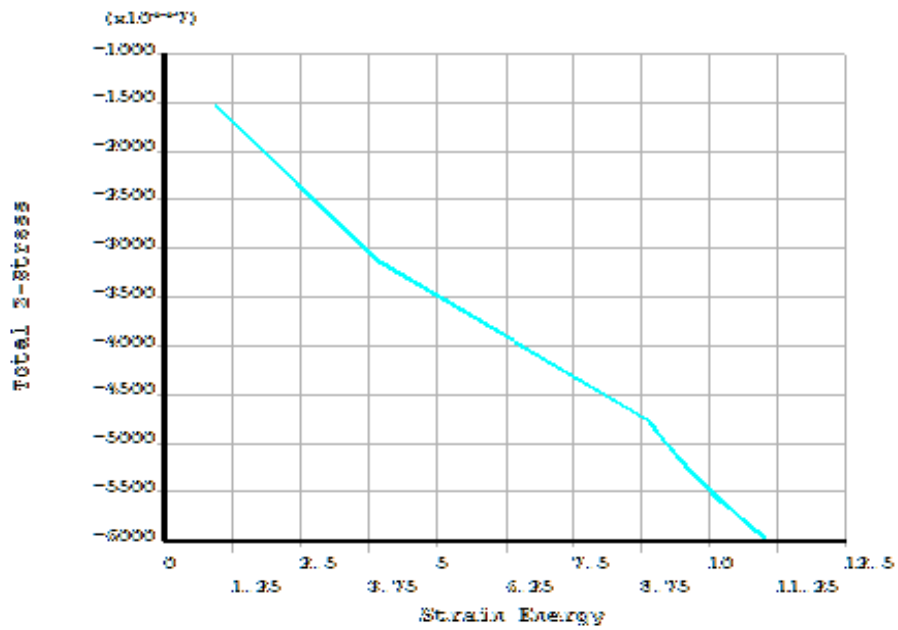
Fig: 5.9. Plot of Total Z-Stress against Strain Energy of crack tip node-867 attached to element 49142.
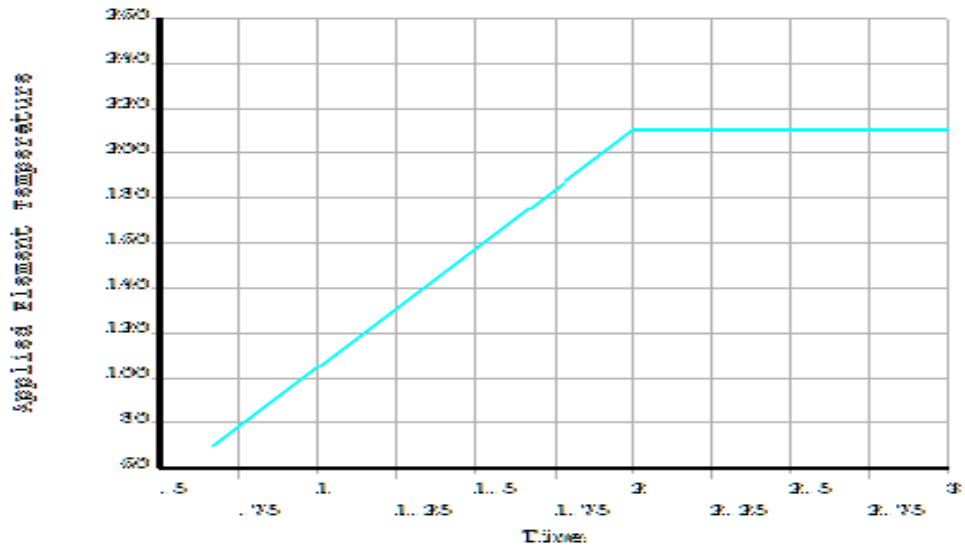
Fig: 5.10. Plot of Applied Element Temperature against Time of Node-867 attached to element-49142. In this case the node and the element it was attached to had real temperature values as against zero values obtained in the previous case.

## 5.1. 4. Crack length: 0.24mm
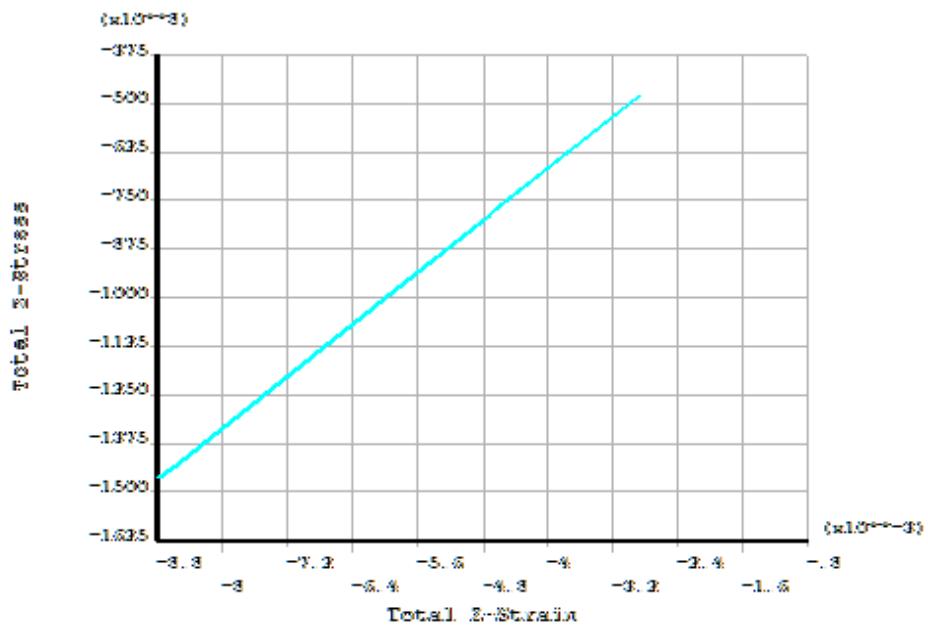
Fig: 5.11. Plot of Total Z-Stress against Total Z-Strain for crack length 0.24mm for node-867 attached to element-6246.
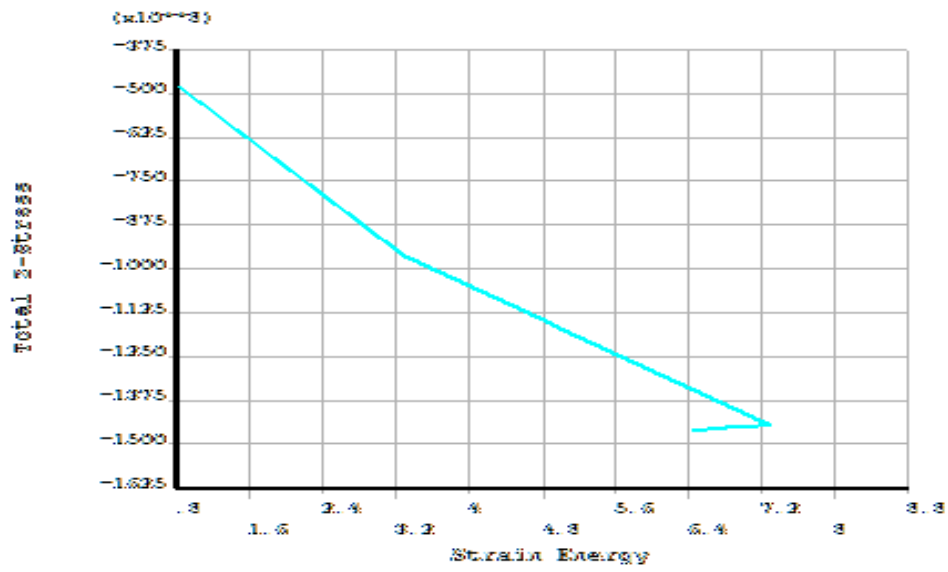
Fig: 5.12. Plot of Total Z-Stress against Strain Energy of crack tip node-867 attached to element 6246.
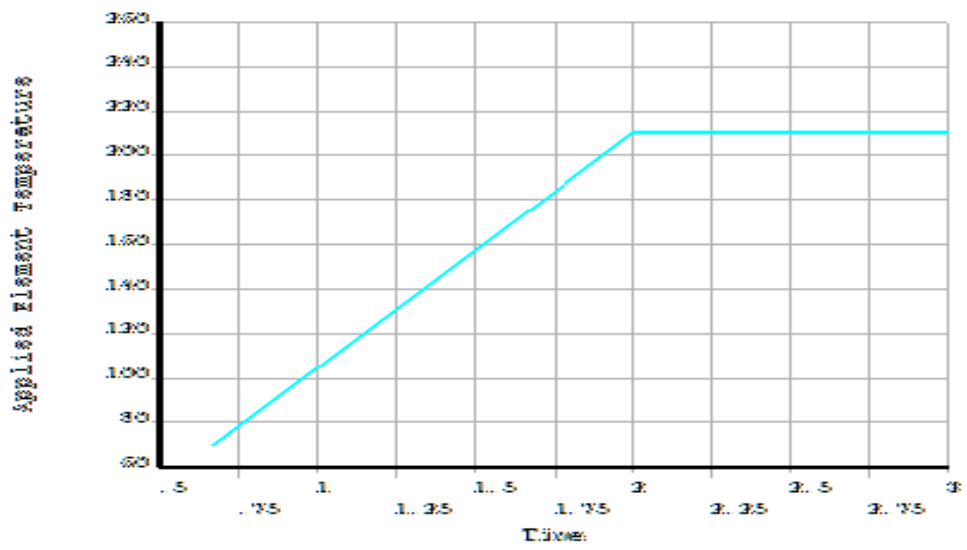
Fig: 5.13. Plot of Applied Element Temperature against Time of Node-867 attached to element-6246.

5.1. 5. Crack length: 0.30mm
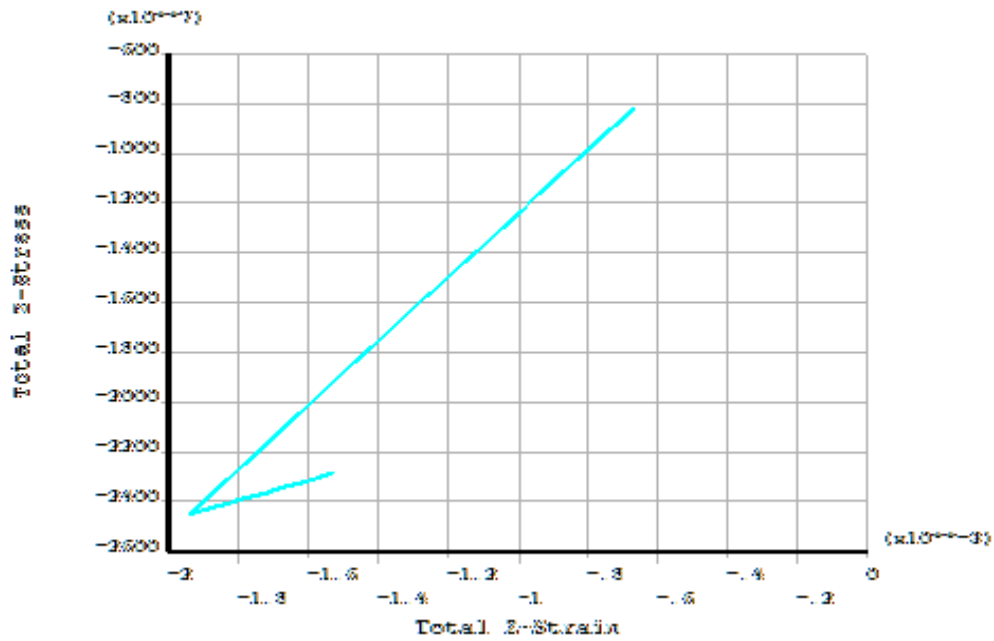
Fig: 5.14. Plot of Total Z-Stress against Total Z-Strain for crack length 0.30mm for node-867 attached to element-22338.
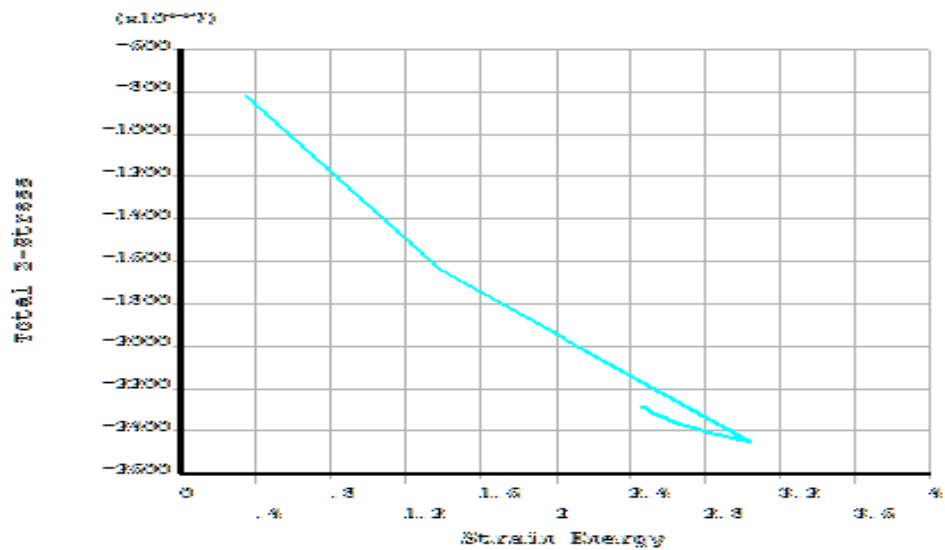

Fig: 5.15. Plot of Total Z-Stress against Strain Energy of crack tip node-867 attached to element 22338.
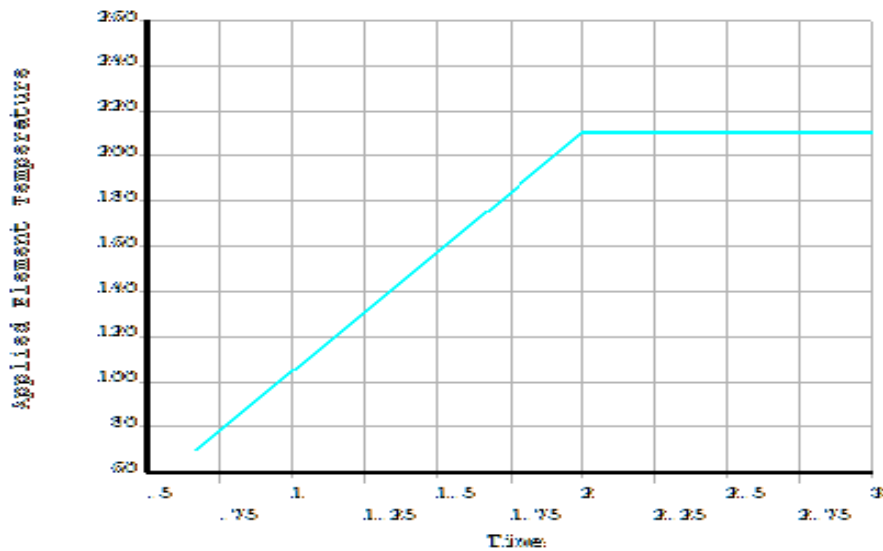
Fig: 5.16. Plot of Applied Element Temperature against Time of Node-867 attached to element-22338.

In figs: 5.2-5.16 above we have graphs of total stress against total strain, total stress against strain energy and applied element temperature against time for every crack length case. It turned out that the 0.12mm crack length case showed some inelasticity going by the total stress against total strain graph. This inelasticity can also be seen in the total stress against strain energy graph of the same 0.12mm crack length case. Every crack length analysis is different as such the same nodes and elements were not used for determining these strain and strain values, this is one of the reasons why the 0.12mm crack length case was showing some inelasticity and the others do not. Indeed inelasticity may have occurred on some of the other nodes that were not analysed, bear in that the nodes and elements that were analysed were those around the various crack tips.

5.2. Further crack propagation.

In the case below the same model was used this was all in a bid to achieve some significant if not visible damage, see fig: 5.17-5.19.
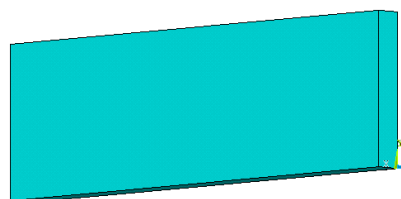
Fig: 5.17. This is the base of the model before the load was applied; notice that the crack doesn't extend to this side of the model.

Element Type

The Element type adopted in this analysis was Solid and the type is Solid-46 or layered 46-Node.

Meshing

Solid46 quadratic 3D 8-node tetrahedral

1 Volume

22028 Nodes

106429 Elements

Element Edge Length: 0.01

Displacement

All the Nodes were allowed to have 3mm displacement in all X, Y and Z directions except for all the nodes in the inner areas of the crack (ALL) (solid element nodes):

Ux, Uy, Uz = 3mm.

The nodes on the inner areas of the crack: *Ux, Uy, Uz = 0*. These nodes are located at the internal areas of the crack, it can be equally said that the model was supported at these points.

Loading

Loading of the finite-element models involved applying a force of 8MN on some nodes in the longitudinal direction the X-direction.
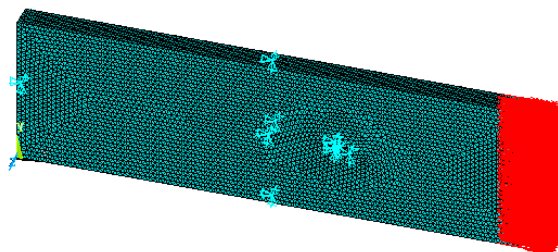

Fig: 5.18. The red arrows indicated applied force in the X-direction, notice the DOF indicators as well.

Fig: 5.19. A slightly magnified top view of the model, notice the crack has yielded on the flip side.

Crack Radius (mm)	0.06	0.12	0.18	0.24	0.3
Maximum stress in X-component (GPa)	18.5	17.3	14.1	13.3	16.6
Minimum stress in X-component (GPa)	-12.3	-11.9	-12.2	-10.7	-9.67
Maximum stress in Y-component (GPa)	14.6	17.3	17.3	21.1	17.6
Minimum stress in Y-component (MPa)	-19.4	-16	-19.5	-16.8	-20.4
Maximum stress in Z-component (GPa)	8.83	12.9	12.9	10.6	9.61
Minimum stress in Z-component (GPa)	-11.9	-11.3	-8.35	-12.4	-11.3
Maximum XY shear stress (GPa)	6.05	6.96	7.84	11.4	6.35
Minimum XY shear stress (GPa)	-6.89	-9.2	-8.41	-7.18	-11.4
Maximum YZ shear stress(GPa)	6.77	5.8	5.81	7.67	5.55

Minimum YZ shear stress (GPa)	-4.24	-4.78	-4.59	-5.44	-4.83
Maximum XZ shear stress (GPa)	10	9.63	6.46	4.8	10.8
Minimum XZ shear stress (GPa)	-5.17	-3.96	-4.03	-7.18	-5.75
Max 1st Principal Stress (GPa)	25	23.1	20.5	26.8	22.4
Min 1st Principal stress (GPa)	-7.04	-3.51	-4.09	-4.55	-3.38
Max 2nd Principal stress (GPa)	9.44	9.65	9.69	7.13	7.12
Min 2nd Principal stress (GPa)	-10.9	-6.31	-9.01	-7.21	-7.73
Max 3rd Principal Stress (GPa)	2.92	3.13	3.68	4.46	4.45
Min 3rd Principal stress (GPa)	-22.4	-22.2	-23.7	-20.7	-26.5

Table: 5.2. The nodal and elemental stress and strain values of the various crack lengths

The exercises that produced the values in table: 5.2 above were linear analyses as a result of these the nodal and elemental values of stresses and strains were just single values hence with these, graphs cannot exactly be produced. In the previous non-linear analyses that were carried out before these the elemental and nodal values of stresses and strains were not single. So attempts were made to make them run as a non-linear analysis to see if the elemental and nodal values for the stresses and strains will produce non single values. They still turned out as single values meaning that the minimum and maximum values were all the same or that there was no range of values for them.

5.3. Fracture Mechanics

In this case a time based numerical analysis was carried out on the same model described in section: 5.2 above, the model was initially subjected to a tensile load of 8 MN as the first load step; afterwards a pressure of 16.4MPa was applied for the subsequent load steps. The aim of this was to see if some time to failure can be obtained. As it were the analysis did not converge after a certain number of cycles. This was also the case with the work of Munoz et.al (2006) [33] where for the largest cycle at 46,000 no convergence was attained.

Table: 5.3 below shows times to failure obtained for the given crack diameters.

Crack Diameter	Number of cycles to failure
0.001	712.667
0.0015	466.66
0.002	649.685
0.0025	775.667
0.003	649.665
0.0035	725.5

Table: 5.3. Table of Crack diameter and number of cycles to failure

 Using the time history post-processor in Ansys the Stress and Strain data along the Z-direction were used to develop the graph in fig: 5.17 below.
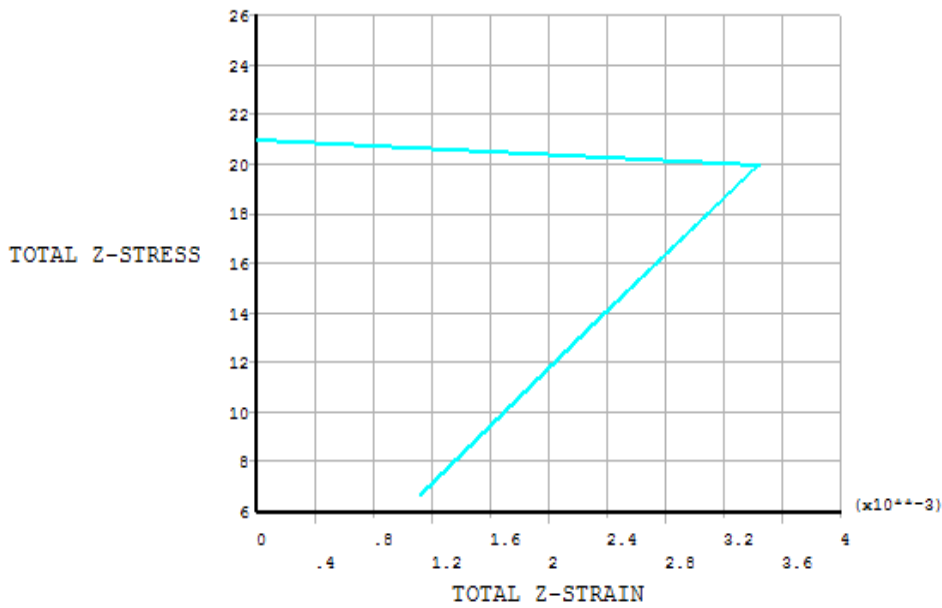
Fig: 5.17. Graph of Stress against Strain

On the face of it the curve above in fig: 5.17 may be indicative of an elastic-plastic deformation, see illustration figs: 5.18 and 5.19 below.


[35]

[35]
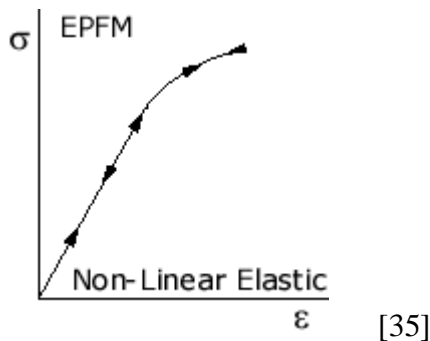
Fig: 5.18. A Non-Linear Elastic curve   Fig: 5.19. An Elastic-Plastic curve
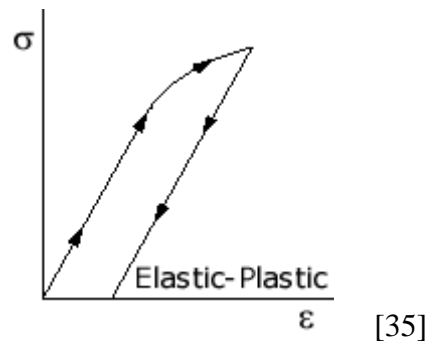
It must be noted that in some cases what is regarded as elastic-plastic behaviour is actually a non-linear elastic one. In essence it means that the unloading curve of what is thought to be an elastic-plastic behaviour of a material follows the original loading curve, as against a parallel line to the linear loading curve which is normally the case for true elastic-plastic behaviour. From (fig: 5.17) above it can be observed that the two parts of the curves are both linear, and stress decreases with respect to the increase in the strain in the first part of the curve which was the loading part of the curve-this is the upper curve. This was also the case

in the second part of the curve; the stress is decreasing and the strain is decreasing as well. This tends to be pointing towards elastic-plastic behaviour though the two curves were not parallel at any point. The curve is generally characteristic of elastic-plastic behaviour, but care must be taken to carefully review the data used for plotting the curve. It must be remembered that the curve above was a result of a combined load 8MN tensile force and 16.4MPa pressure. This goes to say that saying the two linear curves represent these two loads-that may not be absolutely true because such may occur when a simulation fails to converge which was the case. It can also be observed that what was thought to be the tensile part of the load had a gradually decreasing stress against an unusual increasing strain. Then what was thought to be the pressure part of the curve comes off sharply with decreasing stress and strain. One can imagine that if it were just one kind of load alone that was applied at some point it would begin to unload and possibly provide a more familiar curve. To get a better idea of what happened a look at a subsequent curve below in fig: 5.20 would help.
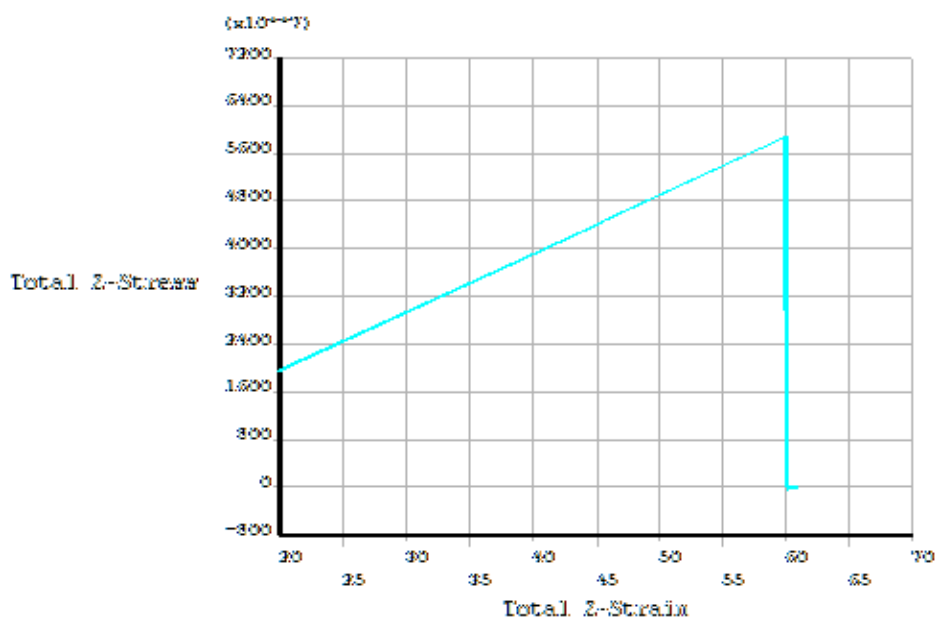
Fig: 5.20. Graph of Total Z-stress against Total Strain

The curve in fig: 5.20 above was quite a striking one making the case for an elastic-plastic deformation. As can be seen the stress begins with a progressive rise then ends up with a sharp continuous drop along the same strain value- this is also owing to the fact that the simulation converged. This really bears the hallmarks of an elastic-plastic deformation though the unloading curve is not parallel to the loading. What this simply means is that what

was available in the curve above is not exactly the true elastic-plastic behaviour. This is so because of the fact that the material used in the model is a composite. It must be mentioned that the lack of convergence may or may not mean that damage has occurred. It can really be taken to mean that damage has occurred in the cases in this work largely because same structures can attain damage at different number of cycles.

5.4. Comparing fibre directions from numerical analysis outcomes

	45° fibre direction for piston skirt. 45° direction per ply. Number of Plies = 4	45° fibre direction for block material (0.05 hexahedral element size). 45° direction per ply. Number of Plies = 4	0° fibre direction for piston skirt. 0° direction per ply. Number of Plies = 4	0° fibre direction for block material (0.05 hexahedral element size). 0° direction per ply. Number of Plies = 4	Aluminium piston skirt
Max-X-comp stress (MPa)	5.16	1680	8.15	1260	4.92
Max-Y-comp stress (MPa)	1.52	702	4.47	146	2.12
Max-Z-comp stress (MPa)	1.82	466	0.611	119	1.93
XY Shear Stress	3.34	11.1	5.53	240	2.53
YZ Shear Stress	0.0008305	0.965	0.45	5.30	0.697
XZ Shear Stress	0.00247	1100	0.878	305	1.68
1st Principal Stress	5.69	1680	8.76	1260	5.22
2nd Principal Stress	1.82	702	1.33	146	2.07
3rd Principal Stress	1.05	381	0.544	117	1.93

Table: 5.4. A Tensile force of 8MN was applied to the various materials in the table above.

	45° fibre direction for piston skirt. 45° direction per ply. Number of Plies = 4	45° fibre direction for block material (0.05 hexahedral element size). 45° direction per ply. Number of Plies = 4	0° fibre direction for piston skirt. 0° direction per ply. Number of Plies = 4	0° fibre direction for block material (0.05 hexahedral element size). 0° direction per ply. Number of Plies = 4	Aluminium piston skirt
Max-X-comp stress (MPa)	-0.00248	2.13E-7	0.00259	3.25E-7	-0.00116
Max-Y-comp stress (MPa)	-0.00247	4.02E-7	0.00320	7.27E-8	-0.000977
Max-Z-comp stress (MPa)	-0.00497	2.94E-7	0.000116	3.08E-7	-0.00101
XY Shear Stress	0.00835	0.000493	0.0108	2.33E-8	0.00508
YZ Shear Stress	0.0000175	0.000528	0.00176	3.65E-8	0.00478
XZ Shear Stress	0.0000196	1.25E-7	0.00168	5.36E-8	0.00518
1st Principal Stress	-0.00243	4.02E-7	0.00362	3.32E-7	0.00369
2nd Principal Stress	-0.00297	1.67E-7	0.000752	3.53E-8	-0.000999
3rd Principal Stress	-0.00497	1.47E-7	-0.00128	2.20E-8	-0.00503

Table: 5.5. A pressure of 16.4MPa was applied to the various structures in the table above. The pressure was applied on the curved external walls, while the rest of the walls had 3mm displacement in all directions.

In table: 5.4 above one can see that the 45° fibre direction piston skirts have less stress values compared to those of the block cases; this is also the case with the 0° stress values. This was not exactly the case in table: 5.5, in some cases the blocks cases had less stress values. One of the reasons why the piston skirt cases had less stress values was because of the curved nature of the model-they are likely to deal with stress better than the blocks as the latter have square edges. Square edges do not really deal with stress as good as curved ones. The other reason

was that in order to analyse the piston skirts as 45° fibre direction models their physical properties had to be determined and they were far less than those of the 0° fibre directions.

Chapter 6

6.0. Conclusion

In this research work beginning from the introduction and down to the discussion it was demonstrated that the composite Carbon fibre Phenolic composite was a suitable structure to be employed in a hybrid piston. The design of the piston was presented and this design took into account the fact that a composite was involved. A contact analysis was carried out to analyse the stresses arising from the interference of the composite piston skirt and the aluminium cap just in case interference fit were to be adopted as the method of assembly. Empirical analyses of tubular carbon fibre composite samples were carried out to determine the tensile, compressive and flexural capabilities of the material this though not very pertinent to this work was done as a precursor that prepared the ground for the empirical tests of the Carbon fibre Phenolic composite. In those analyses the load against displacement curves exhibited nonlinear-plastic and elastic-plastic tendencies in some cases and in the cases were notches were involved three phase curves were produced. Once again it was shown in this work that a structure with an unusually high Poisson's ratio can still pass as an engineering material just as some other authors have done in the work of Jones [42]. As a result of the high Poisson's ratio the stiffness of the structure turned out negative. The more pertinent empirical analysis was carried out on carbon fibre Phenolic composite samples and their load against displacement curves were largely elastic-plastic curves which was what was expected. In establishing the composite's constitutive model a finite element analysis was used to verify each test case and they were sufficiently verified. Following that was an elaborate analysis that led to the E_x value of 61049.6757 MPa and this is roughly about the same value of the Carbon fibre Phenolic composite that Lee and Lee [14] used in their work; the value they have as their E_x value was 61.5 GPa. This validation is a key point in this work as it brings it in line with related works. In section 4.4.3 a classical laminate theory for the material was presented based on the value stated above and it was established that its extensional stiffness matrix is satisfactory, the strain-curvature coupling stiffness matrix produced zero values and the bending stiffness matrix produced very low values relative to the design rupture stress of the piston. This is normally expected because composites normal do not have very good share and bending strengths. An experimental fatigue analysis was equally presented and cycles of up to 818181was attained and the sample did not fail. Suspecting that the material can possibly deliver more than that, the web tool www.fatiguecalculator.com was employed to

calculate the life and the cycles to failure using the data obtained from the fatigue experiments. The results from the tensile tests of the Carbon fibre Phenolic prepregs were also used to predict their respective fatigue parameters. The fatigue tests were carried out on a range of samples and they produced varying outcomes as a result of that the graphs of stress against number of cycles to failure or against life were largely scatter graphs at the same time confirming that stress is a factor of life. Presented in this work was what looked like fatigue resistance; see (fig: 4.49). In that graph the maximum stress remained the same over a varying number of cycles to failure. In the prediction of lifetimes of bundles under static fatigue load an equation was proposed incorporating creep and plasticity as well as time dependence. This was done by simply replacing some variables in the original equation F and F_m which are maximum load and fibre bundle. This led to maximum stress against failure time and strain against failure time graphs for the actual fatigue tests as well as for the tensile test cases. Their curves and general trend did indicate less failure times with respect to high stress respectively. Optimization of the Carbon fibre Phenolic samples was carried out as well as that of the piston cap. This led to further fatigue analysis of the optimized results and validations.

This work has been able to demonstrate that a hybrid piston employing Aluminium and Carbon fibre Phenolic composite is practicable as we already know. In the computation of the hybrid piston parameters care was taken to ensure that the composite part of the piston was sufficiently considered leading to the establishment of parameters like in-plane and out-of-plane diameter clearances in the hot state of the piston crown and skirt respectively.

As was seen in the laminate theory the shear modulus values are high relative to the rupture stress which has a value of 4.9 MPa, see table: 4.14. This rupture stress is associated with the rupture force and is expressed as:

$$\sigma_r = \frac{p_j}{F_{x-x}}$$

Where P_j is the rupture force and F_{x-x} the cross sectional area; the latter is where this rupture force and stress actually act. This is also where the piston crown ends and the skirt begins and this composite is expected to serve as the skirt of this hybrid piston, see (Fig 1.3). It must be noted that the samples in these simulations were 4 ply cases all having 90° fibre directions-

[90$^{\text{o}}$/90$^{\text{o}}$/90$^{\text{o}}$/90$^{\text{o}}$]. To obtain the fabric in this layout it has to be cut as such; it can equally be cut such that you will have a cross pattern or layout i.e. the fibres lying in the 45$^{\text{o}}$ direction and possibly other directions. The 45$^{\text{o}}$ directions as well as other directions were not tested as the resources human and material were no longer available.

References

[1]. FiberCote, *Resin Selector,* (no date) [Online]. [Cited 7th December 2005].

< http://www.parkelectro.com/parkelectro/images/nelcoteselector.pdf >.

[2]. Canada Commercial Vehicles, *Composites,* (2003) [Online]. [Cited 17th January 2006]. <http://www.ccvbc.com/composite-structure.html>.

[3]. C.S. Frame, Introduction to composite materials. In: (1989), pp. 1–12.

[4]. R. Kumar, G. Vinod, S. Renjith, G. Rajeev, M.K. Jana, R. Harikrishnan, Thermo-structural analysis of composite structures. *Materials Science and Engineering: A Volume 412, Issues 1-2,* (2005), *Pages 66-70.*

[5]. *Composite Structures* (2004) Special issue: World Wide Web Usability. Elsevier Science [cited 18th January 2006]. Accessed via <www.sciencedirect.com>.

 [6]. *Journal of Materials Processing Technology* (2004) Special issue: World Wide Web Usability. Elsevier Science [cited 18th January 2006]. Accessed via <www.sciencedirect.com>.

[7]. *Journal of Materials Processing Technology* (2004) Special issue: World Wide Web Usability. Elsevier Science, [cited 19th January 2006]. Accessed via <www.sciencedirect.com>.

[8]. *Composite Structures* (2005) Special issue: World Wide Web Usability. Elsevier Science, [cited 19th January 2006]. Accessed via <www.sciencedirect.com>.

[9]. The Focus, *Memory Usage Guidelines for Windows,* (2005) [Online]. [Cited 19th of January-2006]. <http://www.padtinc.com/epubs/focus/common/focus.asp?I=34&P=article2.htm>

[10]. *Journal of English for Academic Purposes* (2006) Special issue: World Wide Web Usability. Elsevier Science, [cited 20th January 2006]. Accessed via <www.sciencedirect.com>.

[11]. O. Attia, A. J. Kinloch and F. L. Matthews, Modelling the fatigue life of polymer–matrix fibre-composite components. *Composites Science and Technology, Volume 61, Issue 15, Nov-Dec* (2001) *pp 2273-2283.*

[12]. M. Hojo, K. Tanaka, C.G. Gustafson and R. Hayashi, Effect of stress ratio on near threshold propagation of delamination fatigue cracks. *Comp Science Technology 29* (1987), *pp. 273–292.*

[13]. Seong Su Kim, Dong Chang Park and Dai Gil Lee, Characteristics of carbon fibre Phenolic composite for journal bearing materials. *Composite Structures, Oct-Dec* (2004), *pp. 359-366.*

[14]. Seung Woo Lee and Dai Gil Lee, Composite hybrid valve lifter for automotive engines. *Composite Structures, Volume 71, Issue 1, Oct* (2005) *pp. 26-33.*

[15]. Byung Chul Kim, Dong Chang Park, Hak Sung Kim and Dai Gil Lee, Development of composite spherical bearing. *Composite Structures, Volume 75, Issue 1-4, Sept* (2006) *pp. 231-240.*

[16]. N.P. Suh, Tribophysics. , Prentice-Hall, Inc., New Jersey (1986).

[17]. Dong Chang Park, Seung Min Lee, Byung Chul Kim, Hak Sung Kim and Dai Gil Lee, Development of heavy-duty hybrid carbon–Phenolic hemispherical bearings. *Composite Structures, Volume 73, Issues 1, May* (2006) *pp 88-98.*

[18]. Dong Chang Park, Seong Su Kim, Byung Chul Kim, Seung Min Lee and Dai Gil Lee, Wear characteristics of carbon-Phenolic woven composites mixed with nano-particles. *Composite Structures, Volume 74, October* (2006) pp 89-98.

[19]. J. Flock, K. Friedrich, Q. Yuan, On the friction and wear behaviour of PAN- and pitch – carbon fibre reinforced PEEK composites. *Wear, Volume 225-229,* (2006) pp 304-311.

[20]. W. Sun, F. Lin, X. Hu, Computer-aided design and modelling of composite unit cells. *Composite Science and Technology, Volume 61, October* (2001) pp. 289-299.

[21]. Modelling Composites, Chapter 12, Ansys Release 9.0 Documentation.

[22]. Wen-Shyong Kuo, Tse-Hao Ko and Tzu-Sen Lo, Failure behaviour of three-axis woven carbon/carbon composites under compressive and transverse shear loads. *Composites Science and Technology*, *Volume 62, Issues 7-8*, *June* (2002) pp. 989-999.

[23]. Patrick Rosso and Károly Váradi, FE macro/micro analysis of thermal residual stresses and failure behaviour under transverse tensile load of VE/CF–fibre bundle composites. *Composites Science and Technology*, *Volume 66, Issue 16*, *December* (2006) pp. 3241-3253.

[24]. Siro Casolo, Macroscopic modelling of structured materials: Relationship between orthotropic Cosserat continuum and rigid elements. *International Journal of Solids and Structures*, *Volume 43, Issues 3-4*, *February* (2006), pp 475-496.

[25]. Pu Xue, Jian Cao and Julie Chen, Integrated micro/macro-mechanical model of woven fabric composites under large deformation. *Composite Structures*, *Volume 70, Issue 1*, *August* (2005), pp. 69-80.

[26]. Seth Nickerson, J. Steven Mayes and Jeffry S. Welsh, Multi-continuum analysis of thermally induced matrix cracking. *Engineering Fracture Mechanics*, *Volume 72, Issue 12*, *August* (2005), pp 1993-2008.

[27]. G. Pitarresi, M.S. Found and E.A. Patterson, An investigation of the influence of macroscopic heterogeneity on the thermo-elastic response of fibre reinforced plastics *Composites Science and Technology*, *Volume 65, Issue 2*, *February* (2005), pp. 269-280.

[28]. Antonio F. Avila and David T.S. Morais, A multiscale investigation based on variance analysis for hand lay-up composite manufacturing. *Composites Science and Technology*, *Volume 65, Issue 6*, *May* (2005), pp. 827-838.

[29]. M.J. King, P. Jearanaisilawong and S. Socrate, A continuum constitutive model for the mechanical behaviour of woven fabrics. *International Journal of Solids and Structures*, *Volume 42, Issue 13*, *June* (2005), pp. 3867-3896.

[30]. Bassem Zouari, Jean-Luc Daniel and Philippe Boisse, A woven reinforcement forming simulation method. Influence of the shear stiffness. *Computers & Structures*, *Volume 84, Issues 5-6*, *January* (2006), pp. 351-363.

[31]. Cédric Sauder, Jacques Lamon and René Pailler, The tensile behaviour of carbon fibres at high temperatures up to 2400 ℃. *Carbon*, *Volume 42, Issue 4*, (2004), pp. 715-725.

[32]. Kolchin A and Demidov V, 'Design of Automotive Engines', Mir Publishers, 1984.

[33]. J.J Munoz, U. Galvanetto, P. Robinson, On the numerical simulation of fatigue driven delamination with interface elements. *International Journal of Fatigue, Volume 28,* (2006), pp. 1136-1146.

[34]. Lukasz Figiel and Marcin Kaminski, Mechanical and thermal fatigue delamination of curved layered composites. *Computers and Structures, Volume 81,* (2003), pp. 1865-1873.

[35]. J. Wu and F. Ellyin, A study of fatigue crack closure by elastic plastic finite element analysis for constant amplitude loading. *International journal of fracture, vol. 82*, (1996), pp. 43-65.

[36]. K. H. Subramanian and A. J. Duncan, Tensile properties for application to type I and type II waste tank flaw stability analysis. [Cited 12th April 2008]. Accessed via online < http://www.ntis.gov/support/ordering.htm>.

[37]. G. M. Odegard, T. S. Gates, K. E. Wise, C. Park, E. J. Siochi, Constitutive modeling of nano-tube reinforced polymer composites. *Composites science and technology, vol. 63*, (2003), pp. 1671-1687.

[38]. R. M. Jones, Mechanics of Materials. Taylor and Francis; 1999.

[39]. Y.C. Wang and R. S. Lake, Extreme stiffness systems due to negative system elements, *American Journal of Physics, Vol. 72, No. 1,* (2004).

[40]. T. Jaglinski and R. S. Lake, Anelastic instability in composites with negative stiffness inclusions, *Philosophical Magazine Letters, Vol 84, No12*, (2004), pp. 803-810.

[41]. W. S Kuo and J. Fang, Processing and characterization of 3D woven and braided thermoplastic composites, *Composites science and technology*, *Vol 60,* (2000), pp. 643-656.

[42]. P. Xue, J. Cao and J. Chen, Integrated micro/macro-mechanical model of woven fabric composites under large deformation, *Composite structures, Vol 70,* (2005), pp. 69-80.

[43]. B. Harris, Fatigue in Composites. Woodhead Publishing; 2003.

[44]. OOFEM, *Boundary Conditions,* (2006) [Online]. [Cited 5th May 2006].

< http://www.oofem.org/resources/doc/programmer/node21.html>.

[45]. <www.fatiguecalculator.com/constamp/stresslife.htm>. [Online]. [Cited 17th May 2008].